Novel Uses of Spatial Light Modulators in Optical Tweezers

Daryl Preece

A thesis presented for the degree of

Doctor of Philosophy

Optics Research Group

Department of of Physics & Astronomy

University of Glasgow

Scotland

February 2011

Dedicated to

my loving parents Barry and Claudette.

Novel Uses of Spatial Light Modulators in Optical Tweezers

Daryl Preece

Submitted for the degree of Doctor of Philosophy

February 2011

Abstract

In recent years spatial light modulators (SLMs) have become an integral part of many optical trapping experiments. Yet their usefulness, which stems from their flexibility, is often under exploited. In this thesis I seek to demonstrate how it is possible to expand the range of optical trapping applications that may benefit from the use of spatial light modulators. From exploring the benefits of increased resolution to demonstrating novel applications like position clamping and polarization control, I show how SLMs are a resource which can benefit optical trapping in new and unconventional ways. The optical properties of liquid crystals have long been known however it is only recently that they have been applied to optical tweezers. The physics and operation of spatial light modulators are discussed in chapter 1, with specific attention paid to those aspects of operation which are of pertinent practical use to optical trapping. In chapter 2 it is shown how phase only modulation can be used to create effective holographic optical tweezers systems which are capable of manipulating micron scale particles and measuring pico-Newton forces. Chapter 3 charts the development and characterisation of a 4 Mega-pixel spatial light modulator which was created as an improvement on current SLM technology. The role of SLMs in utilising lights angular momentum as a tool for creating rotational torque is discussed in chapter 4. In chapter 5 describes how SLMs can be used to create torques based the application of spin angular momentum to birefringent particles. We show, in chapter 6 how with suitable software engineering it is possible to both move optical traps and track particles in real time. Since the use of SLMs has been previously been limited by their bandwidth constraints we discuss in chapter 7 the use spatial light modulators in closed loop systems. We finish with a discussion of the use of SLMs in a new technique that may be applied to microrheology.

7th March 2011

Declaration

I declare that, except where explicit reference is made to the contribution of others, that this dissertation is the result of my own work and has not been submitted for any other degree at the University of Glasgow or any other institution.

Acknowledgements

I would like to thank Professor Miles Padgett for his invaluable advice over the years, which has been both insightful and thought provoking. I would also like to thank him for his tolerance of the speed with which I understood that advice. I would like to thank Dr Sonja Franke-Arnold, Dr Johannes Courtial and Dr Jonathan Leach for the patience they showed in explaining certain abstract concepts of optics to me. Further thanks must go to Dr Manlio Tassieri for his explanations of the finer points of microrheology. I would also like to thank Dr Graham Gibson for showing me what can only be called the Tao of experimental physics. I must also acknowledge my all of my fellow students who make the Glasgow optics group a fun place to work. I particularly would like to thank Aline Vernier and Alasdair Hamilton for our many stimulating conversations. I would like to thank Halina Rubinstzein-Dunlop and group, for the understanding they have shown in allowing me to complete my thesis while starting a new job. I must also thank my partner Ai Katayama, for her understanding and support throughout the course of my PhD.

Publications

- Daryl Preece, Rebecca Warren, Manlio Tassieri, R.M.L. Evans, Graham M. Gibson, Miles J. Padgett and Jonathan M. Cooper, Optical tweezers: wideband microrheology, *(submitted Journal of Optics)*, arXiv:1005.1401v1.

- D. Preece, R. Bowman and M. Padgett, Increasing trap stiffness with position clamping in holographic optical tweezers, *Optics Express,* 17, 22718-22725 (2009).

- D. Preece, J. Leach, S. Keen, E. Botvinick, R. Bowman, M. Padgett, Independent polarisation control of multiple optical traps, *Optics Express* 16, 15897-15902 (2008).

- J. B. Götte, K. O'Holleran, D. Preece, F. Flossmann, S. Franke-Arnold, S. M. Barnett, and M. J. Padgett, Light beams with fractional orbital angular momentum and their vortex structure, *Optics Express,* 16, 993-1006 (2008).

- D. Preece, E. Yao, G. Gibson, R. Bowman, J. Leach, and M. Padgett, A spatial light phase modulator with an effective resolution of 4 mega-pixels, *Journal of Modern Optics*, 55, 2945-2951 (2008).

- D. Preece, R. Bowman, G. Gibson, and M. Padgett, A comprehensive software suite for optical trapping and manipulation, SPIE, *Optical Trapping and Optical Micromanipulation VI - 7400(1)*, 74001N (2009).

Conferences and Presentations

- April 11-16, 2010, ESF Conference "Trends in Optical Manipulation II", Obergurgl, Austria-Poster presentation on "Wideband Microrheology".

- August 2-6, 2009, SPIE Conference on Optical Trapping and Manipulation in San Diego, USA. Talked on "A Comprehensive Software Suite for Optical Trapping and Manipulation".

- May 6-8, 2009, COST Conference on Optical Micromanipulation by Nonlinear Nanophotonics Aberfoyle, UK. Talked on "High Speed Tracking and Control of Holographic Optical Tweezers".

- August 10-14, 2008, SPIE Conference on Optical trapping and Manipulation in San Diego, USA. Talked on "Independent Polarisation Control of Multiple Optical Traps".

- September 2-5, 2008, Attended COST Training School Optical Micro-Manipulation Ischia, Italy.

- August 26-29, 2008, Attended Photon 08 Conference. Edinburgh,UK.

- June 18, 2008, Awarded First place for presentation skills Glasgow University Graduate School Away Day.

- March 20-21, 2007, Attended EPSRC Grant Holders Workshop Leicester, UK. Took part in basic technology plenary seminar.

- August 26-30, 2007, SPIE Conference on Optical Trapping and Manipulation in San Diego, USA. Talked on " 4 Mega-pixel Spatial Light Modulator".

- February 4-9, 2007, ESF Conference "Trends in Optical Manipulation", Obergurgl, Austria- Poster presentation on "4 Mega-pixel Spatial Light Modulator".

7th March 2011

Contents

List of Figures

Chapter 1

Spatial Light Modulators

1.1 Introduction

Over the last two decades there has been be an increase in the use of and interest in holographic laser tweezers and optical trapping. These techniques provide a means by which scientists can perform experimental research into various areas such as cell structures, micro scale force measurements and micro machines. Currently this field of research has been benefiting from both an increased understanding of the underlying physics concerned in manipulating objects at the micro scale and increased development of technology. If further progress is to be made in this field it is imperative that this evolution brings with it practical advancements in the application of new ideas and technologies. Central to the operation of many holographic tweezers systems are spatial light modulators (SLMs) [3–5] these devices allow the complex interaction between a computer and the phase or intensity characteristics of a light beam. SLMs have not only been used in the optical trapping community they have also been beneficial in such diverse fields as: interference microscopy [6], optical switching [7], non-destructive testing [8] and wavefront control [9] as well as many others. Fundamentally a spatial light modulator is a device which allows the user to change the phase, intensity or polarisation of a light field in an arbitrary way. When used with optical tweezers spatial light modulators can be used to create controllable optical traps which may then be used to dynamically manipulate small particles.

1.2 Liquid Crystals

Although liquid crystals (LC) are often thought of as an exotic substance they are prolific in nature. Liquid crystals are defined as "a substance that flows like a liquid but has some degree of ordering in the arrangement of its molecules". Some examples of substances which may be classed as liquid crystals either by themselves or in solution include DNA, cellulose, and graphite [10–12]. There are many types of liquid crystal in common usage today which are used in both commercial and research sectors. Liquid crystals are often classified by their ordering and packing characteristics. Here we deal mainly with nematic liquid crystal, which has only one ordering parameter, the direction of orientation. Several other types exist such as: smectic A, smectic Ad , smectic B , and smectic C. Liquid crystals exhibit a number of different types of chemical structures and physical properties. Hence the type of liquid crystals used in an optical device will determine its optical characteristics. Due to optical anisotropy within the liquid crystal i.e. (different indices of refraction for different axes of the molecule) the liquid crystal my be used as phase, polarisation or intensity modulator. It is this behaviour that is exploited in spatial light modulators. Thought there are several types of liquid crystal used in SLM manufacture the most common are the ferroelectric and nematic devices.

1.2.1 Ferroelectric Liquid Crystals

Ferroelectric devices are smectic liquid crystals usually smectic C [13]. In a ferro-electric device molecules are always aligned perpendicular to the optical axis. The orientation of the liquid crystal couples to the direction of an externally applied electric field (see Fig.1.1) rotating the crystals about the optic axis. When the direction of the field is reversed the direction of the molecules undergoes a rotation, changing the polarisation characteristic's of the LC. Ferroelectric devices operate quickly with often only 50-100 micro seconds switching time but they often have a binary output they are also sensitive to shock and vibration. While nematic devices are slower, they have a greater dynamic range and better amplitude uniformity. They are thus more often used for applications where 2π phase only modulation is necessary.
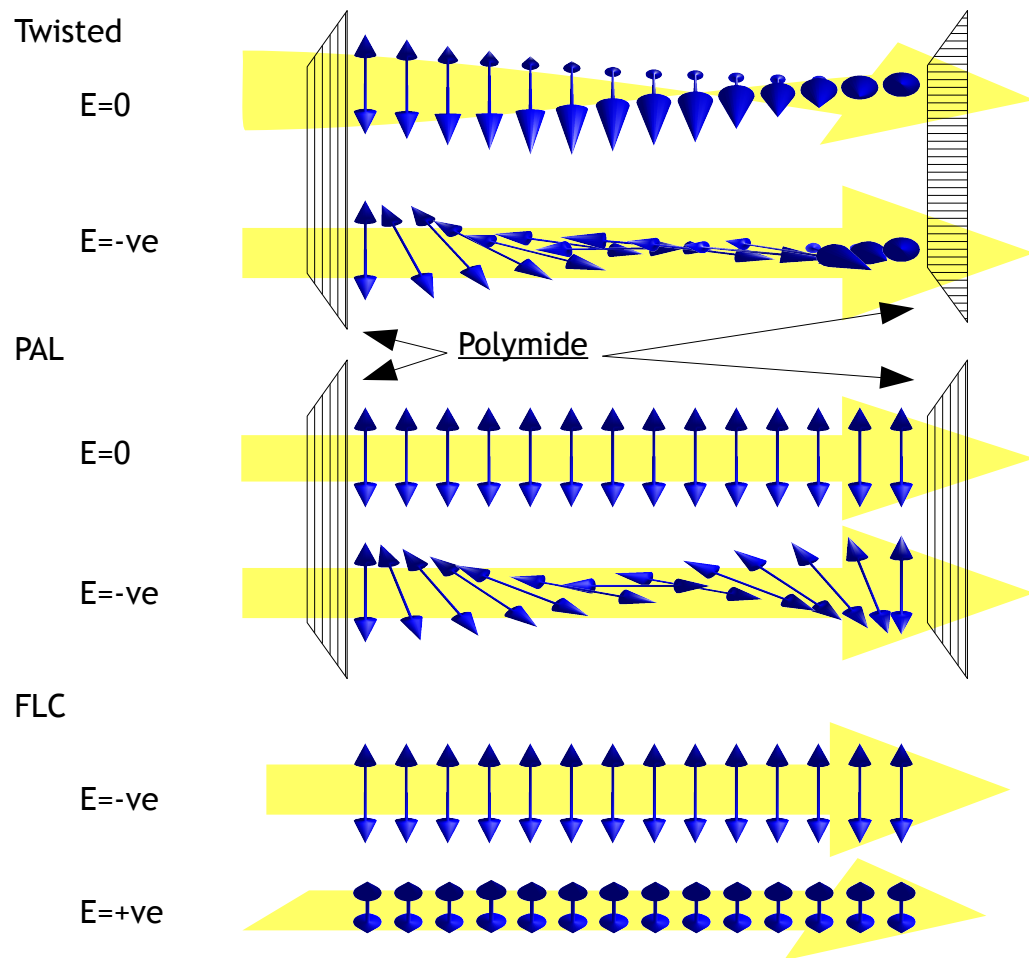
Figure 1.1: Molecular orientation for twisted, parallel aligned and ferroelectric liquid crystal. The orientation of individual liquid crystals and of the polyimide coatings for differing electric fields is shown.

1.2.2   Twisted Nematic Liquid Crystals

Twisted liquid crystals came out of LC display technology [14]. The liquid crystal molecules are initially aligned in a helix pattern across a cell this is often done by rubbing polyimide layers onto a glass substrate. When a voltage is applied the molecules quickly align with the field breaking the helix pattern. If the cell is sandwiched between cross polarisers the cell can act as an effective intensity modulator. Twisted nematic crystals increase the phase retardation as a function of voltage allowing quicker switching. Although they can be used as phase modulators they tend to have limited dynamic range and produce large polarisation changes. [15]

1.2.3   Parallel Aligned Liquid Crystals

Parallel Aligned liquid crystals (PAL LC) work in a similar fashion to the twisted case however the the initial alignment of the crystal layer is parallel through the SLM [16]. This decreases the polarisation effects present in the twisted nematic liquid crystal and increases the dynamic range but means that phase modulation only occurs parallel to the alignment direction of the liquid crystal. (see Fig.1.1). If the polarisation direction is tilted away from this, the phase modulation only occurs in the component which is parallel to the alignment direction and the output polarisation becomes, in general, elliptical. There is in essence almost no change in the effective refractive index other than in the alignment direction of the liquid crystal.

1.3   Principles of Operation

SLMs work in a variety of ways. Most however, rely on the application of an electric field to a liquid crystal substrate contained by optical flats. Many liquid crystal molecules are either permanent electric dipoles or induce electric dipoles on the application of an external field. By applying electric fields to the liquid crystal layer one may rotate the liquid crystal molecules resulting in a change to the effective refractive index of the liquid crystal. This manifests itself as a spatially dependent phase change to any light traveling through the liquid crystal. The electric fields

which address the nematic liquid crystal are commonly created in one of two ways. Firstly, they may be created by the use of local electrodes on a silicon wafer such as a CMOS chip. This is known a an electrically addressed SLM (ESLM). Secondly, the spatial light modulator may be optically addressed (OSLM). Incident light is focused on to a photo-sensitive material sandwiched in between two transparent electrodes. The local electric field then corresponds to the intensity of light which is incident on the optically addressed spatial light at modulator.

1.3.1   ESLMS

A number of companies produce ESLMs including Boulder Nonlinear Systems [17] and Holoeye [18]. As mentioned above, electrically addressed SLMs often use a silicon back plate such as a CMOS chip with liquid crystal on the front to produce a varying electric field across the SLM (see Fig.1.2). In practice these devices are often simply twisted nematic liquid crystal micro-displays manufactured without an intensity modulating sheet of plain polarized film. This is not always the case and a number of ESLMs are are on the market which use PAL LC [17].

As electrically addressed SLMS are closely linked to display technology they have fast update rates and high resolution. However they suffer from poor surface flatness and produce pixelation artifacts as well as often creating poor phase modulation due mainly to the type of liquid crystal used.

1.3.2   OSLMS

Optically addressed SLMs replace the direct electrical addressing from a silicon chip with optical optical modulation from an external light source. Rather than addressing the SLM via tiny individual electrodes an intensity pattern is projected onto the rear of the SLM (see Fig.1.3). The light hits a layer of photosensitive material typically amorphous silicon (a-Si:H) sandwiched between two large transparent electrodes. This material changes its dielectric properties with the amount of light incident on it. Therefore when a voltage is applied to the electrodes a spatially variant electric field is produced which is directly related to the intensity of the

CMOS
Chip

Liquid
Crystal

Cover
Glass

Pixel Electrodes

Dielectric Mirror

Transparent Electrode
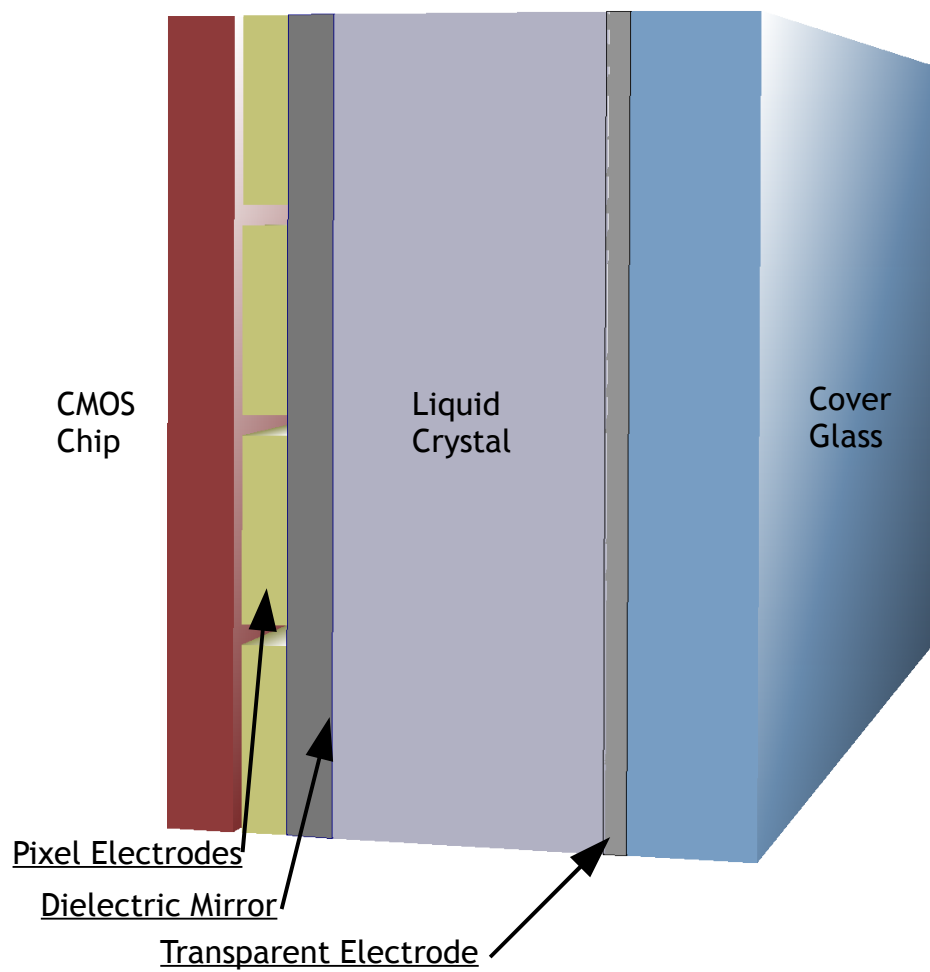
Figure 1.2: A cross-section through a typical typical reflective ESLM with a CMOS back plate. A variable electric field is created through the layer of liquid crystal which is sandwiched between the dielectric mirror and the cover glass.

Dielectric Mirror   a-Si:H   Transparent Electrodes

Write Light

Reflected
Readout Light

Glass Substrate

AR Coating

Liquid Crystal

Light Blocking Layer
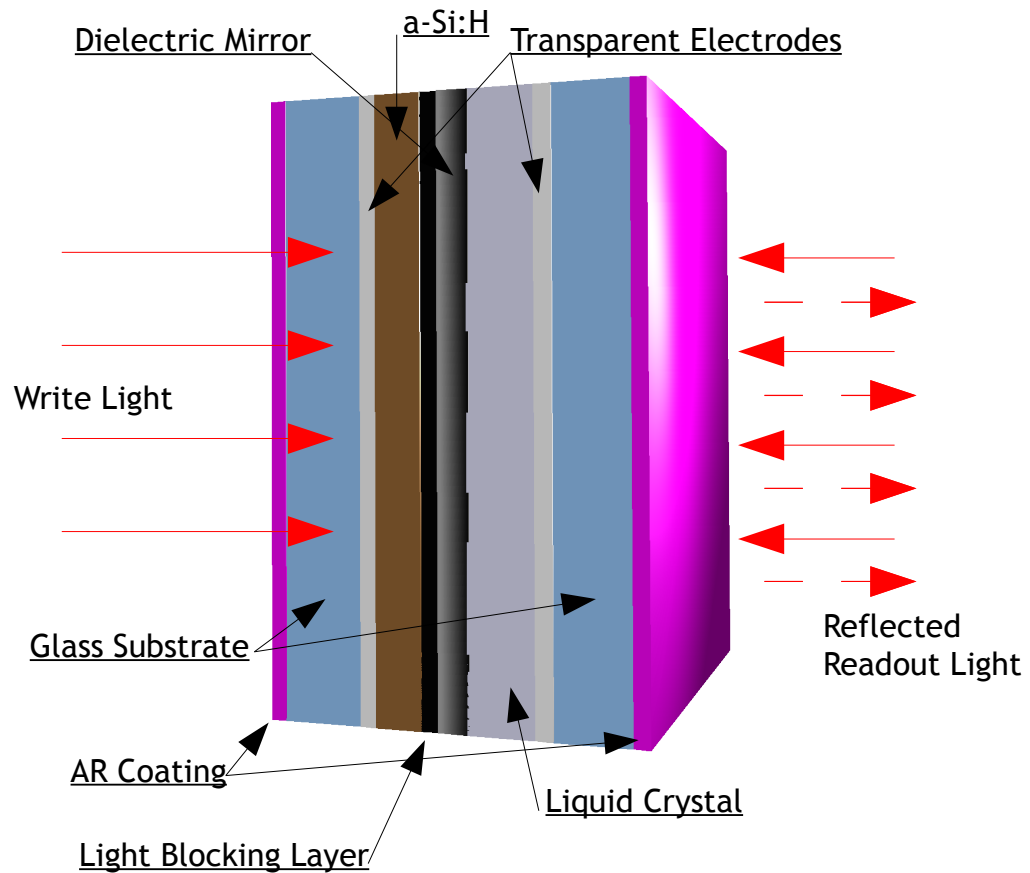
Figure 1.3: A basic OSLM. The diagram shows an incident "write light" illuminating the layer of amorphous silicon. The subsequent electric field determines the orientation of the liquid crystal.

aforementioned pattern. It is this electric field which acts on adjacent liquid crystals causing them to align accordingly. This means that OSLMs require a carrier signal of a few volts to be put across the electrodes in order to supply the the electric field necessary to turn the liquid crystal. OSLMs are primarily available from Hamamatsu [19] and generally use PAL LC.

Optically addressed SLMs have good optical flatness due to the lack of any electronics (flatness is only dependent on optical flats used) and can create more than 2π phase changes however, they are slower to update and require intensity modulation.

1.3.3 DC Balancing

Most nematic liquid crystals contain ionic impurities. In the presence of a strong DC field these impurities drift through the liquid crystal forming a charge depleted layer close to the surface resulting in a backwards electro-magnetic force and adversely affecting the liquid crystal response. Once this has happened it can be extremely detrimental to the SLM. In order to a stop long term drift of impurities SLMs routinely reverse the sign of the charge. In OSLMs this is done by means of a square wave voltage being applied to transparent electrodes within the OSLM. In the case of ESLMs pixel voltages are reversed on every up date. It should be noted that neither of these operations affect the resulting phase modulation since it is the amplitude of the field which is important and not the sign.

1.4 Factors Affecting the Efficiency of SLMs

Diffraction Efficiency

In an ideal SLM all light reflected by, or transmitted through the SLM undergoes a phase change commensurate to the phase displayed on the SLM. However this is not the case in practice. For most SLMs currently available a significant quantity of light either remains unchanged or is changed in way which is undesirable to the user. The proportion of light which may be usefully phase changed by the user is known as the diffraction efficiency. Although there are a number of definitions of diffraction efficiency in literature (particularly sales literature).

Here we define the diffraction efficiency (η) as the ratio of the power of the useful diffracted light (i.e. the light in the first order) to the power in the incoming beam.

$$\eta = \frac{P_{first\,order}}{P_{input\,beam}} \qquad (1.1)$$

A number of factors may be responsible for the diffraction efficiency of a an SLM.

Fill Factor

If gaps are left between charged pixels in an ESLM then the corresponding regions of zero electric field will create diffraction commensurate with the pixel spacing. This effect reduces the overall efficiency of the SLM by throwing a certain amount of reflected light into unwanted diffraction orders or even leaving some of the reflected light unaltered by the SLM [20, 21]. The effect of fill factor differs depending on the type of SLM, for instance some SLMs are composed of discreet cells while in others have continuous liquid crystal layer. For a simple grating the intensity of the first order spot is enveloped by sinc function of the ratio of the pixel size to the interpixel region.

Aliasing

Since most ESLMs are inherently pixelated devices it is necessary to consider the problem of aliasing. Aliasing happens when, due to the inherent pixelation of the device the shape to be represented on the SLM cannot be rendered accurately or artifacts are introduced which distort the rendering of the shape. Aliasing manifests itself as extra diffraction spots in the Fourier plane. Quantitatively the effects of aliasing are difficult to estimate since it dependent on the hologram displayed, the pixel shape and the fill factor.

Reflectivity

If a reflective SLM is used the efficiency of an SLM is also influenced by its overall reflectivity. Several factors affect this, most simply the reflectivity of the mirrored reflector within the SLM. However the diffusion characteristics of the liquid crystal also affects the overall reflectivity. As has been mentioned above liquid crystal is composed of layers of optically anisotropic molecules. Due to a certain amount of unavoidable inhomogeneity within the liquid crystal some scattering takes place thus reducing the overall reflectivity.

Many SLMs have anti-reflection coatings on the surface of the SLM. This increases the overall diffraction efficiency by not reflecting light which has not passed

through the liquid crystal layer and hence not undergone a phase change. Anti reflection coatings may as much as double the diffraction efficiency of the SLM in some cases. The overall reflectivity of an SLM has significant impact on the diffraction efficiency and good reflectivity is a prerequisite for high diffraction efficiency.

Angle of Incidence

As has been mentioned, due to the anisotropy of the liquid crystals, light hitting the liquid crystal at different angles experiences different effective refractive indices. This means that the angle of the incident light beam on the SLM also has an effect on the phase retardation of the SLM in effect changing the contrast of the SLM [22]. However for most nematic liquid crystal SLMs if light is incident at angles below 30 degrees from the normal the change in diffraction efficiency is less than 15% this figure is smaller still if anti-reflection coatings are used.

1.5 Factors Affecting the Speed of SLMs

Several factors effect the speed at which nematic liquid crystal SLMs can be driven. I neglect here computational speed, chip update rate or bandwidth limitations inherent in cable connections.

Liquid Crystal

Although the type of liquid crystal used has a major impact on the performance of the SLM (smectic LC often being far faster than nematic) the precise chemistry of the liquid crystal is a major factor in its response time.

Temperature

Increasing the temperature of the liquid crystal lowers its viscosity and allows a faster response. This may however have unpredictable effects on operational stability.

Voltage

The voltage applied to the liquid crystal also has major impacts on the speed of the SLM. Higher voltages create faster switching times. The direction of the voltage change also matters. For instance going from a high pixel value to a low pixel value is often faster than the reverse operation.

Boulder SLM XY series SLMs increase the pixel switching time by using an external transparent electrode to DC Balance the SLM rather than using the pixels. This gives increased speed by eliminating the need to update each pixel twice (positively and negatively). By setting a reference voltage appropriately it utilizes the full dynamic range of each pixel as well as increasing the maximum possible voltage, see "DC balancing skew white paper" [17]. However since it takes significantly longer to update the pixels than the electrode some pixels lead or lag the electrode leading to a skew effect.

Thickness

In general the thicker the liquid crystal layer the slower the response. This is a problem for applications which require longer wavelength light since a thicker liquid crystal layer is necessary for the same phase modulation as for shorter wavelengths. For this reason reflective SLMs are often more efficient than transmissive SLMs since the liquid crystal layer can be thinner as light takes a double pass through the LC layer.

Chapter 2

Optical Tweezers

2.1 Introduction

It is a truism to say that as our study and understanding of science evolves our interest takes us towards the very big and the very small. It is clear that our macroscopic world is not the only one in which interesting things are happening. It is the remit of this thesis to deal with the very small, specifically the 10's of microns regime. However to understand the physics at these extremes of scale we must learn to think differently, for fundamental physical concepts like momentum, force and electromagnetism often act counter intuitively at this small scale. In order to probe this micro world we require appropriate tools. Optical tweezers are one such tool. The concept of optical tweezers is at it core a simple one. To move small objects around, not by physical manipulation in the sense of a pushing one object against another, but rather optically utilizing the electro-motive forces present in a focused beam of light.

2.2 Early Work

The notion of light as a particle which has a momentum is an old one yet one which has been revised may times over the years. Ibn al-Haytham (965–1040) in his book "The Book of Optics" theorized that light was a particle which reflected or refracted based on its momentum. Johannes Kepler (1571 - 1630) also ascribes comet tails to

what we now call "radiation pressure" coming from light the sun. However radiation pressure as we know it today (the pressure exerted upon any surface exposed to electromagnetic radiation) came out of a theoretical tretise by Maxwell (1831 – 1879) [23] although much work was also done by Bartoli (1851 -1896) [24].

After the formulation of quantum mechanics in the 1930s and the discovery of the photo-electric effect, light was routinely thought of as being made up of small particles known as photons. Each photon carries a quantum of energy ($\hbar\omega$) where $\hbar$ is Plank's constant ($1.054571628 \times 10-34$ J·s) and ω is the angular frequency of the light. Furthermore, it is logical to assume that the photons may somehow impart their energy to matter with which they interact and indeed this seems to be the case. Each photon carries a linear momentum of ($\hbar k$) where $k = 2\pi/\lambda$ and is known as the wave number, which it may impart to an object. However in practice the momentum exerted on objects by light is very small. With the invention of the laser it became practical to focus high intensities of light onto small objects meaning that sufficient momentum could be transferred to move small micron sized particles as was first done by Arthur Ashkin while working at Bell Labs in 1970 [25]. Ashkin used a CW Argon laser to push transparent latex spheres of 0.59, 1.31 and 2.68 micrometers diameters suspended in water. However Ashkin also noticed that particles where not only pushed along in the direction of the beam propagation but were also pulled into the center of the beam. This force was christened the optical gradient force. Ashkin also managed to confine particles in a dual beam optical trap where two counter propagating beams were used to stably trap particles. In 1971 Ashkin published a further paper "Optical Levitation by Radiation Pressure " showing that particles could also be levitated by what he called an optical fountain [26]. In 1986 he published a paper exploiting the gradient force to create the single beam gradient trap [27].

Ashkin went on published papers investigating the trapping of bacteria, trapping in vacuum and trapping with feedback [28–30]. These papers perhaps represent what maybe called the birth of optical tweezers.

2.3 The Optical Gradient Force

Ashkin, with some degree of prescience in his early papers, proposed the use of the optical gradient force in a number of different fields and size regimes. Since we will not deal here with atom trapping we can loosely divide those particles which remain into particles which are smaller than a wavelength of the trapping light (those in the Raleigh regime) and those which are larger (those in the Mie regime). In the context of this thesis we will deal only with those in the Mie regime and more specifically only those between 1 and $10\mu m$ in diameter.

Though in recent years there has been much interest in computationally modeling the gradient force by various means such as the dipole approximation [31] for particles in the Mie regime it is convenient to use the ray optical approach as developed by Ashkin. Of course the validity of this approach is questionable particularly at the beam focus. It does however usualy give a good approximation for particles between 1 and $10\mu m$ in diameter [32,33].

We consider a spherical dielectric particle in the vicinity of a laser beam, that the refractive index of the particle is higher than the refractive index of the surrounding medium and that the laser beam is approximately Gaussian in intensity profile (see Fig.2.1). When light hits the particle some proportion of the rays will pass through the particle causing the particle to act as a lens. The rest of the rays which are incident on the particle will reflect from the surfaces of the particle imparting a momentum to the particle which is broadly along the axis of propagation. This is known as the scattering force. Those rays which pass through the particle however deliver a resultant force towards the center of intensity (see 2.2). Since in order for trapping to occur more light is transmitted than scattered the net result is a force pulling the particle towards the beam center. It should be noted the ratio of the gradient to scattering force depends in the size, refractive index of the particle and polarisation of the laser light [33].

If the trapping beam is tightly focused then the particle will also experience a force as consequence of its displacement from the beam waist. Since the convergence or divergence of the exiting light changes with the distance of the particle from the beam waist so does the axial momentum components of light exiting the particle.
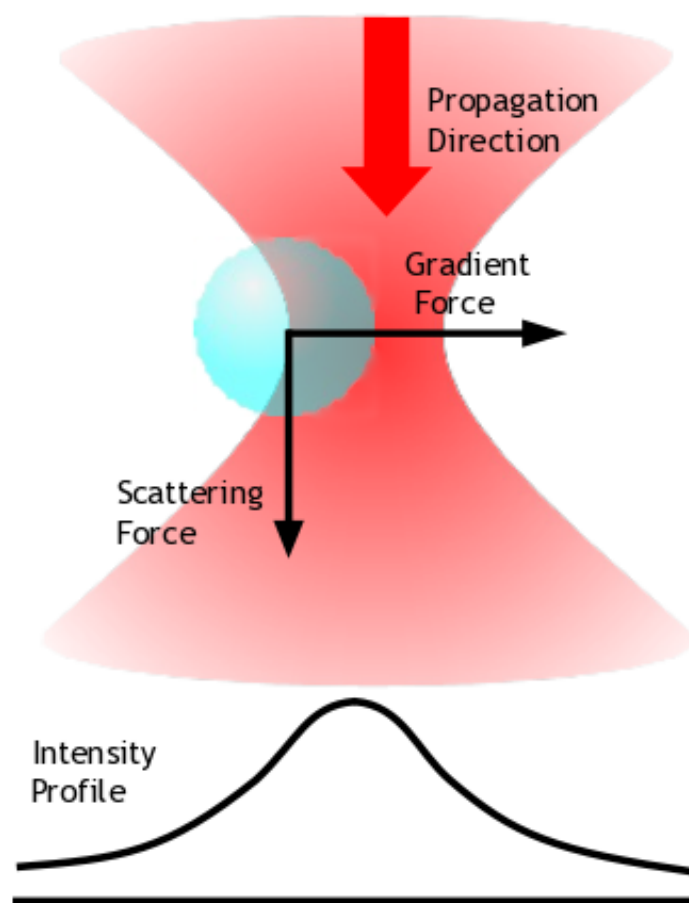
Figure 2.1: The focus of a laser beam with Gaussian intensity profile. The scattering force pushes the particle along in the propagation direction. While the gradient force pulls it towards the center of intensity.

This means that for a particle below the focus these components resolve to produce an upward force against the scattering force. Taking into account the force of gravity on the particle, the resultant force is minimized at a point slightly below the beam waist. Fig.2.2 a) and c) shows how axial displacement resolves to create a force towards the trap center, b) shows how lateral displacement also results in a force towards the beam axis [32].

2.4 Basic Optical Tweezers Setup

The most common type of optical tweezers set up is the single beam gradient force trap. It is fairly simple to construct a simple single beam gradient force trap (see Fig.2.3). Most simply a collimated laser beam is incident onto a beam steering mirror. The beam undergoes a 4f imaging into a standard microscope objective. 4f imaging; meaning imaging with four focal lengths otherwise expressed as using two lenses such as in a telescope. In the case of optical tweezers a telescope is placed between the beam steering mirror and the microscope objective (see 2.3). This allows a rotational tilt in the beam steering mirror to be translated into the a lateral shift in the trap position. Giving the user the ability to control the trap position by tilting the beam steering mirror. Without this system the trap would necessarily defocus from the trapping plane as the mirror was tilted.

Though most visible wavelengths are sufficient for optical trapping it is often preferable to use a infrared beam (λ =1064nm or 860nm) for biological systems as this is less likely to cause damage to biological systems [28, 34].

The objective lens should be of high numerical aperture (N.A.) to ensure that the gradient force outweighs both gravity and the scattering force. It should be noted that many tweezers systems tend to be inverted in order that the scattering force acts against gravity allowing lower laser powers to be used. For increased N.A. often water or oil immersion objectives are used [35]. The practical N.A. of the beam is fully exploited by over filling the back aperture of the objective lens.

The sample is usually held on a translation stage which may be moved to enable viewing of different parts of the sample. Illumination is provided by a strong light
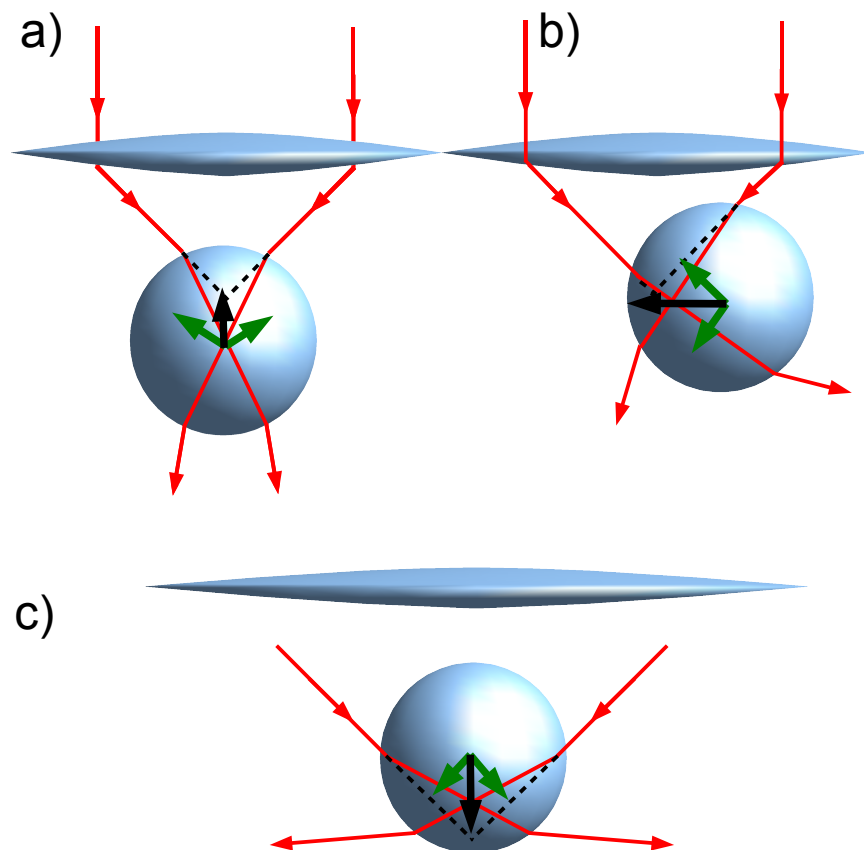
Figure 2.2: Gradient forces acting on a particle in different positions relative to the beam focus. Green arrows represent the force from a singe ray. Black arrows represent the resultant force. a) The particle is below the beam focus however the beam is more collimated on exiting the particle resulting in a net upward force. b) The particle displaced laterally from the beam focus this results in more light exiting the particle in the direction of the displacement pushing the particle towards the beam focus. c) The particle above the beam focus creates a net downward force as the particle spreads out the laser light exiting it.
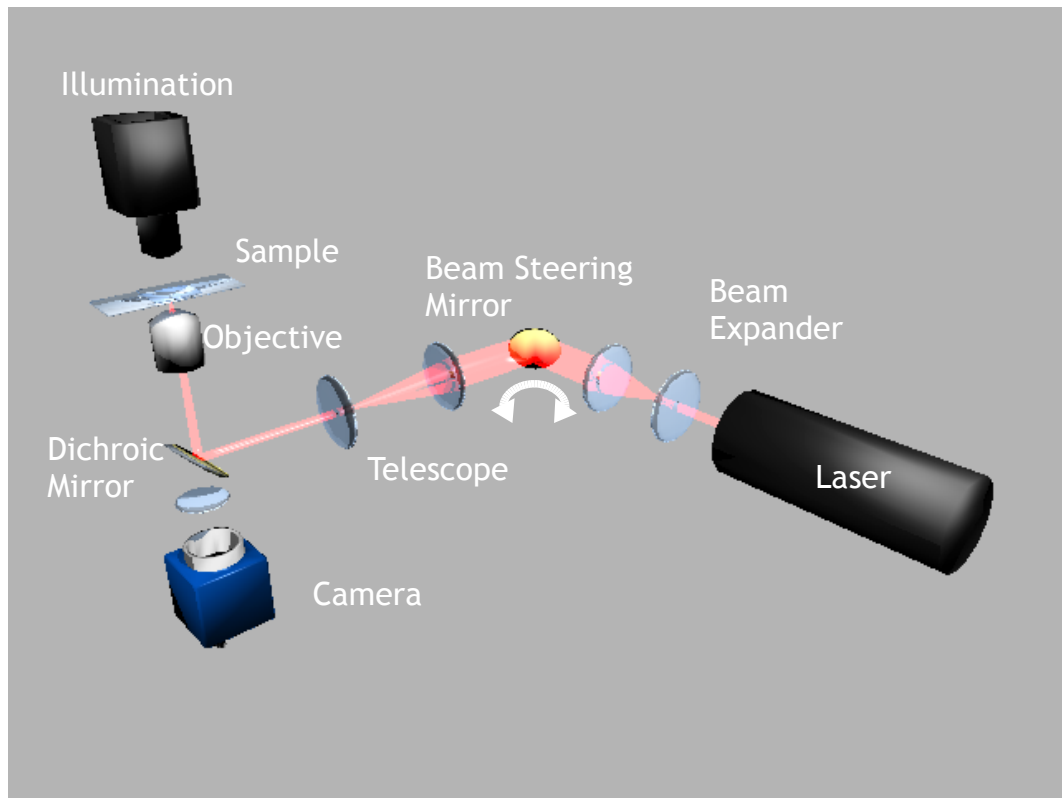
Figure 2.3: A simple optical tweezers setup.

source such as a 50W halogen bulb. A condenser lens is used to focus this onto the sample. The sample may be viewed by means of a camera although particle tracking may also be done by means of a quadrant photo diode. In the case of a camera system the laser light is separated from the illumination light by means of a dichroic mirror. Another option for splitting this light is a polarising beam splitter cube however this requires orientation of the beam polarisation with a $\lambda/2$ waveplate to work effectively. Filters may also be necessary to cancel out residual laser light.

2.5   Forces and Torques

2.5.1   Forces in Optical Traps

One of the major applications of optical tweezers are as a way of measuring or applying tiny forces. Forces have been calibrated down to 25fN [36] giving the technique unparalleled sensitivity. This put optical tweezers in a unique position for measure-

ment of forces applied to living cells [37] or the tensile strength of DNA [38] or even to conduct micro rheological measurements of viscosity [39]. In order to do this we must establish how optical tweezers react to an applied force. Ashkin calculated this ray optically [32]. Empirically it has been shown by Simmons et al. [40] that for small displacements from the center of the optical trap the particle behaves like a damped mass in a parabolic energy well. This is analogous to a mass attached to a spring as in Hooke's law $F = -\kappa x$ where F is the restoring force and k is the force constant (or spring stiffness). Though this is not the case for displacements of more than half a bead radii where the restoring force rapidly becomes nonlinear. Displacement can be measured in a number of ways most commonly by use of a calibrated photo-diode or a fast camera [38,41], such techniques allow measurement of displacements with a precision of better than 10s of nanometres. The force constant is proportional to the trap stiffness which depends on a number of factors such as the trapping geometry; particle size and refractive index; refractive index of the media and the overall laser power. If this can be calibrated it is possible to measure the overall force. However often such information is not easy to obtain therefore it is necessary to find alternative means to find the trap stiffness.

2.5.2 Stokes Drag

For a particle in an overdamped media where there is no turbulence (i.e. low Reynolds number, Re $<$ 1) the force due to fluid flow can be represented by the stokes drag [42].

$$F = 6\pi a\eta v \tag{2.1}$$

Where a is the radius of the particle, η is the dynamic viscosity and v is the velocity of the particle through the surrounding medium. Often this equation is expressed as $F = \gamma_0 v$ where $\gamma_0 = 6\pi a\eta$.

2.5.3 Determining the Trap Stiffness.

One method of determining the trap stiffness is to move the entire stage as was done by Simmons et al.. Such a movement creates an immediate stokes drag force which acts in opposition the gradient force.

$$\kappa x = 6\pi a \eta v \tag{2.2}$$

Thus the trap stiffness may be obtained by measurement of the stage velocity and particle displacement as long as the particle radius and fluid viscosity are known. Often the stage is moved in sine wave this allows the determination of trap stiffness from both the amplitude of the oscillation as well as the phase lag between the movement of the stage and the movement of the particle. Such an approach requires less bandwidth than many other methods since measurements can be taken relatively slowly.

2.5.3.1 Deflection Method

Though most methods for calibration of the trap stiffness are indirect. It is possible to measure the force directly. As has been mentioned earlier the force exerted on the particle is proportional to the deflection of the incident beam, thus if all of the light deflected by the bead could be measured by a photo-diode the momentum transfer to the trapped object could be directly calculated. This is the approach taken by Smith et al. [43]. However since such a technique requires full knowledge of all the scattered light and so is best suited to low N.A. systems.

2.5.3.2 Equipartition Method

The equipartition theorem states that in thermal equilibrium energy should be evenly distributed in all of its forms. The one dimensional kinetic energy of the particle given from kinetic theory as $\frac{1}{2}k_BT$, the potential energy held in the optical trap is given by $\frac{1}{2}\kappa\sigma^2$ where σ^2 is the variance in position. Setting the two equations as equal and rearranging we get:

$$\kappa = \frac{k_B T}{\sigma^2} \tag{2.3}$$

This allows the trap stiffness to be determined without any need for knowledge of the viscosity [41]. It should be noted though that in order for this technique to be valid a critical threshold of measurements is needed such that the variance and mean squared displacement of the particle converge to a constant ratio. Since this technique relies on accurate measurement of the variance, care must also be taken to avoid low frequency noise which would give the appearance of a lower apparent trap stiffness.

2.5.3.3 Langevin Method

A micron sized particle held in an optical trap in an overdamped media such as water is often subject to thermal excitation through continuous bombardment by fast moving molecules, just as was observed by Brown [44]. If the particle is weakly held in the optical trap the particles movement traces out constrained Brownian walk. The Brownian motion is easily noticeable and can be detected by cameras and photo-diodes. The thermal force takes the form.

$$F_T = \sqrt{2k_B T \gamma_0}\xi(t) \tag{2.4}$$

where k_B is the Boltzmann constant, T is the temperature, γ_0 is the Stokes constant and $\xi(t)$ is a random Gaussian process. The thermal force can be then balanced against the gradient force the stokes drag force and the inertial force to give the following Langevin equation.

$$m\ddot{x}(t) + 6\pi a\eta v(t) + \kappa x(t) = \sqrt{2k_B T \gamma_0}\xi(t) \tag{2.5}$$

The inertial term $m\ddot{x}(t)$ is dropped since we assume no inertia in a low Reynolds number media. Equations of this form have standard solutions. It can be shown that the time dependent auto-correlation function of such an equation is given by:

$$< x(t)x(0) >= \frac{k_B T}{\kappa} \exp(-\frac{\kappa}{\gamma_0}t) \tag{2.6}$$

This indicates the correlation between the position of a particle at an initial time and subsequent time t. Taking the Fourier transform of the auto correlation function one can the derive a expression for a power-spectrum of the particle movement. The power spectrum takes the form of a Lorenzian curve. Fitting such a function allows the determination of trap stiffness. The corner frequency f_c of such a curve is given by:

$$f_c = \frac{\kappa}{2\pi\gamma_0} \tag{2.7}$$

Furthermore from Parseval's theorem we can use the area under the graph to determine the trap stiffness using the equipartition theorem stated above.

It is not in the remit of this thesis to derive the equations of Brownian motion in detail. The body of literature around this field is both variable and extensive. A much more thorough explanation is given in [45] and [46].

2.6   Holographic Optical Tweezers

With the advent of optical tweezers there was an inevitable push towards multiple optical traps. Initial efforts were made to create two optical traps by means of a beam-splitter cube. However this was later extended by time sharing the optical traps using scanning mirrors [47–49]. In principal this can be quite reliable as long as the the trap switches faster than the resonance frequency of the trapped particle in other words the trap moves fast enough that the effect of is movement is compleatly damped by viscous drag forces in the surounding fluid. However the trap is limited to one focal plane. Other methods such as the use of multiple laser beams [50] have also been tried in order to get multiple optical traps. Another method for creating multiple optical traps is via acousto-optic Modulators (AOM's) these devices use a piezoelectric crystal to send compression waves in to a block of quartz. The variable refractive index in the quartz creates a diffraction effect. Since the center frequency

of the AOM is in the region of 100MHz the trap switching speed is extremely fast [51].

If a diffracting optical element is placed in the beam it is possible to create and array of diffraction orders. These orders may be re-imaged into the focal plane of the microscope in order to create multiple optical traps.

This approach was initially made first by [52] and then by Grier et al. [53]. However by replacing a single diffractive optical element with a spatial light modulator it is possible to create multiple movable arrays of computer controlled traps. Furthermore imparting a phase only modulation to the beam means that the efficiency of the process is improved. In fact this approach allows for much more flexibility since it means that arbitrarily constructed phase only patterns (kinoforms) can be displayed at frame rate of the order of 25 frames per second. This allows for the creation and control of multiple holographic optical traps in all three dimensions [54] [55]. The number of optical traps is largely only limited by the beam power and by the diffraction efficiency of the SLM. The SLM also opens up possibilities for beam shaping applications as well as in-line aberration correction.

Another novel method using an SLM is that used by Gluckstad et al. [56] where the SLM is placed in the conjugate plane to the trapping plane. A phase contrast method with a 4-f lens system [57] is used to convert phase modulated light at the SLM into intensity modulation at the focus. This technique has several advantages such as minimal computational calculation unlike the Fourier method and very efficient use of light. However unlike the Fourier approach its precision is limited to the pixel positions of the displayed image also the 3D manipulation of the particles is also more involved.

2.7 Basic Holographic Optical Tweezers

Fig.2.4 represents the type of experimental set up used in the majority of my work. These holographic optical tweezers (HOT) systems are implemented in a similar way to the single beam gradient trap. The beam steering mirror is replaced however by a diffractive optical element (SLM) which is imaged into the back aperture of the microscope objective. Optical traps are created by diffracted light in the sample
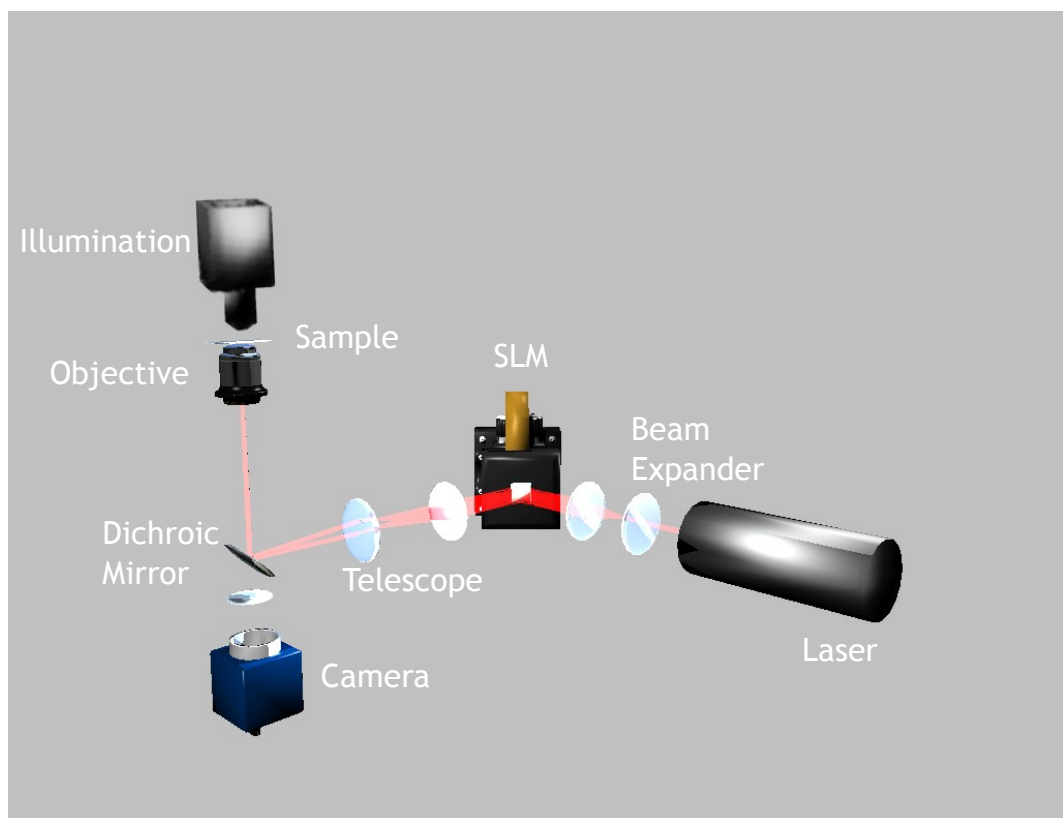
Figure 2.4: An illustration of a simple holographic optical tweezers setup.

plane. The type and number of traps generated depend on the kinoform used this will be discussed in more detail in further chapters. Typically such a system may generate tens of optical traps over the range of the field of view of the objective lens. Traps may be positioned to Angstrom precision [58] while maintaining a constant trap intensity [59] The trap strength is however limited by the laser power. The kinoform on the SLM may be controlled remotely by a computer. If a digital camera is used the user is able to both see the image of the sample under investigation and dynamically control the optical traps with the same computer. Calculation of kinoforms is often processor intensive however typically a refresh rate of 25 frames per second may be reached on a standard Pentium PC.

2.8   Uses of Holographic Optical Tweezers.

The ability to create holographic optical traps has been useful in a number of different areas. In colloid science [60] the ability to create multiple optical traps has been useful in probing crystal structures. Holographic optical traps have also been used to trap particles in air [61]. Biological experiments have also benefited HOT such as creating arrays of traps to hold cell assays [62].

As well as facilitating the simple manipulation of micro particles. The advent of holographic optical tweezers has also enabled the development of a number of other related technologies. For instance the inclusion of a spatial light modulator in the optical train has allowed for in-line aberration correction [63, 64] and the production of novel beams such as beams with angular momentum [65] and Bessel beam tweezers [66]. HOT have also been used to create optical potential landscapes for use in Brownian ratchets. [67]. Optical tweezers have also allowed the creation and manipulation of tiny polymerised structures. [68]

An overview of the basics of optical trapping and holographic optical tweezers has been outlined. We will deal with some of the above topics in more detail later in this thesis. For now though use full for the reader to appreciate the breath and scale of applications for holographic optical tweezers. We seek in further chapters to elaborate on the progress made towards improving this technology.

Chapter 3

4 Mega-pixel SLM

3.1 Introduction

Over the last 10 years interest has grown in the use of holographic optical tweezers and optical trapping [69]. Optical tweezers provide a means to conduct research into various areas such as cell biology [70], micro scale force measurements [40] and micro machines [71]. Currently this field of research has been benefiting from both an increased understanding of the underlying physics as well as the development of enabling technologies. However, if further progress is to be made in this field it is imperative that this evolution brings with it practical advancements in technology. In the field of optical trapping spatial light modulators are used to create diffraction spots which may then be used to manipulate small particles. Since holographic optical tweezers are an emerging technology there are certain difficulties which may hinder usage. One such problem is the drop off in trap strength as the diffraction orders move away from the optical axis. This is mainly due to the properties of the spatial light modulator (most notably its resolution). In this section I will outline attempts to overcome problems such as these by creating an SLM system which is capable of a 4 Mega-pixel resolution. This has been designed and built to take advantage of rapidly evolving display technology and to utilize bespoke software algorithms to augment the design of the system.

3.2 Performance Attributes of Spatial Light Modulators

Although there are many factors which contribute to optimizing an SLM for a particular application, in holographic optical tweezers high diffraction efficiency is a great advantage. It increases the amount of light available for optical trapping which in turn maximizes the number of optical traps. High diffraction efficiency is best achieved by phase only modulation as intensity modulation is inherently lossy. Furthermore the modulation should be ideally continuous and variable between 0 and at least 2π. Another problem in an SLM may be a lack of optical flatness which gives rise to aberrations in the modulated beam, thereby degrading significantly the reflected beam quality and in the case of optical tweezers creating optical traps with distorted beam profiles. Thus, the ideal SLM requires both high diffraction efficiency and high power handling capability, the later typically scaling with the area of the device. Since the trapping plane is in the far field (Fourier plane) of the SLM, the SLM is imaged to fill the rear aperture of the objective lens. The maximum lateral displacement of an optical trap from the beam axis is proportional to the maximum diffraction angle of the SLM. Hence, the field of view over which the traps can be positioned scales with the number of line pairs that can be reproduced by the SLM.

For commercially available units [17–19], when addressed at 532nm, and relayed to a tweezers system based on an x100, 1.3 N.A. objective lens, the resolution of the SLM gives a typical maximum trap displacement of order $50\mu m$ [72]. One aim of this work is to obtain an SLM capable of reproducing twice as many lines pairs (1000) so that the range over which the traps can be positioned better fills the field of view of the microscope, which for x100 can be as much as $190\mu m$ diameter. Another aspect of the design is that by increasing the physical aperture of the SLM, it is better able to cope with the higher incident laser powers that a large number of optical traps require.

3.3   Optical Design

The design chosen to satisfy the above problems was based on a wide-aperture, parallel-aligned nematic liquid crystal SLM. This SLM was specially ordered from Hamamatsu with an increased area active area. The device was originally a prototype and therefore is not part of their normal product range. Two ESLMs (LC-R 1080, 1920x1200 pixels) were used to produce a spatially varying intensity pattern on the write side of the OSLM with a resolution of 4 Mega-pixels. This was then converted to the corresponding phase hologram by the Hamamatsu device.

3.3.1   Holoeye (LC-R 1080) LCoS Display.

The Holoeye liquid crystal on silicon (LCoS) displays [18] consist of a CMOS chip with a reflective coating and a liquid crystal front. This means that it is possible to get very small pixels as well as a high fill factor at relatively low cost. Since the screen is reflective and the electronics are hidden a less pixelated image may be achieved. The contrast ratio is given by Holoeye as 2000:1 @ 633 nm and the reflectance as 63 %. The Holoeye LCoS displays have a 1920 x 1200 (WUXGA) screen giving them extremely high "2 Mega-pixel" resolution Fig.3.1. They work at a standard 60 Hz refresh rate and operate by creating a polarization change in the incoming light utilizing twisted liquid crystals which rotate according to the supplied electric field. Displays are small having a diagonal image array size of 18.34 mm.

3.3.2   Hamamatsu (X7665LA40) OSLM

The Hamamatsu OSLM (Fig. 3.2) is comprised of two transparent electrodes containing a layer of amorphous silicon separated by a mirror from a layer if parallel aligned nematic liquid crystal. This is enclosed by a two coated optical flats with optical flatness better than 3 wavelengths. The total active area of the OSLM is 40x40 mm. The SLM requires a drive signal to be applied across the transparent electrodes. A square wave at frequency 1kHz is used with a with a voltage amplitude $\pm 2.5V$ to $\pm 5.0V$. A higher drive voltage allows for a faster response speed but at the expense of phase modulation.

Figure 3.1: Bottom left:One of the Holoeye LCoS displays with a plane polarizer covering it in order to display an intensity modulated image.Top right: The image on the SLM.

The impedance of the amorphous silicon layer decreases approximately with the logarithm of the write light intensity falling on it. Thus the nematic liquid crystal experiences a voltage dependent alignment change due to electro-optic modulation. More than 2π Phase modulation can be achieved if the write light intensity is greater than $2mW/cm^2$ at 690nm. With a driving signal of 3.5 V the SLM responds temporally with 38ms rise time (black to white) and 63 ms fall time (white to black).

3.4   Setup

Figure 3.3 shows the layout of the optical system. The addressing light source was a 90mW laser diode (Thorlabs HL6515MG) at $\lambda = 690$nm. The diode was driven with a common cathode driver (Thorlabs LD1100). The laser light was projected through a quickly moving speckle plate to wash out the effect of laser speckle at the write plane of the SLM. The beam was polarized at 45° so that the light was split by the 50mm aperture polarizing beam splitter to equally illuminate the two LCoS displays. These two displays were tiled vertically, one corresponding to the top half of the intensity pattern and the other to the bottom. The LCoS displays are addressed with the blue and green channels of a three colour WUXGA display card, where the top and bottom halves of the pattern are encoded as blue and green respectively. The displays modify the polarization state of the light such that when
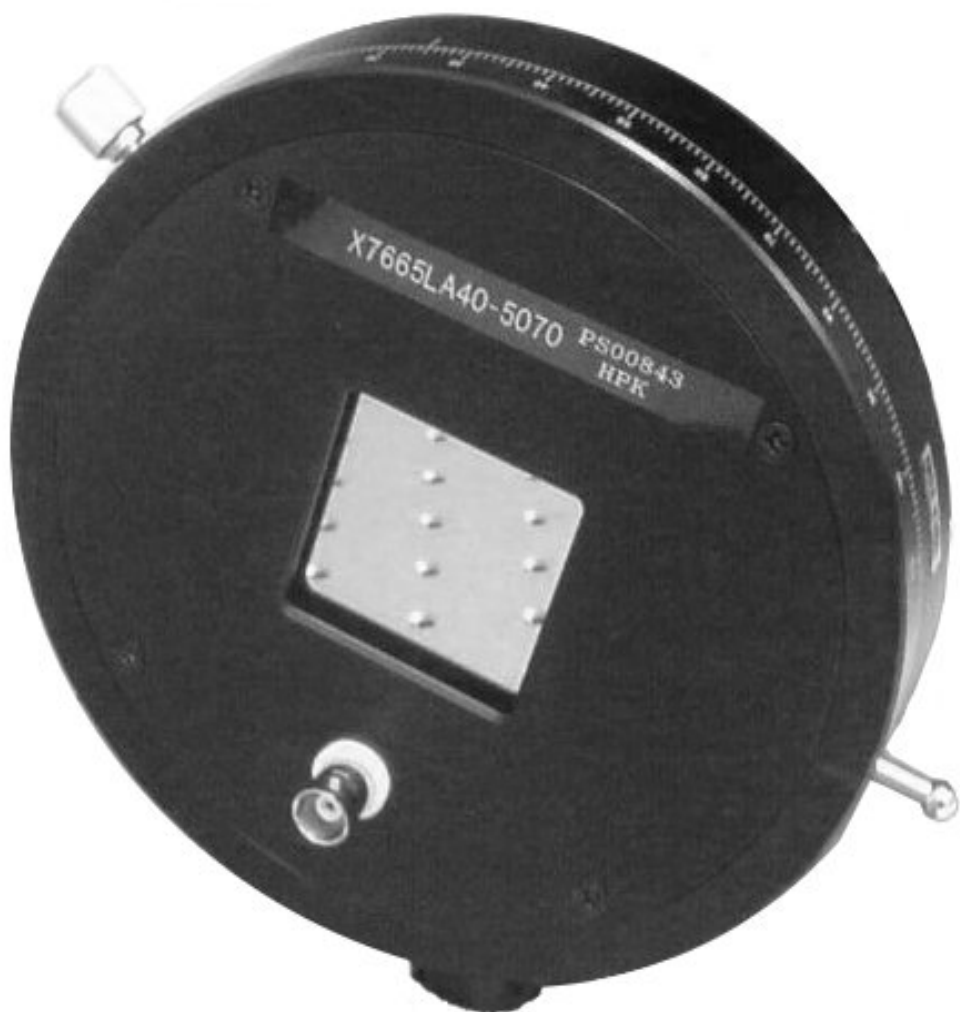
Figure 3.2: The Hamamatsu OSLM with 4cm by 4cm active area.
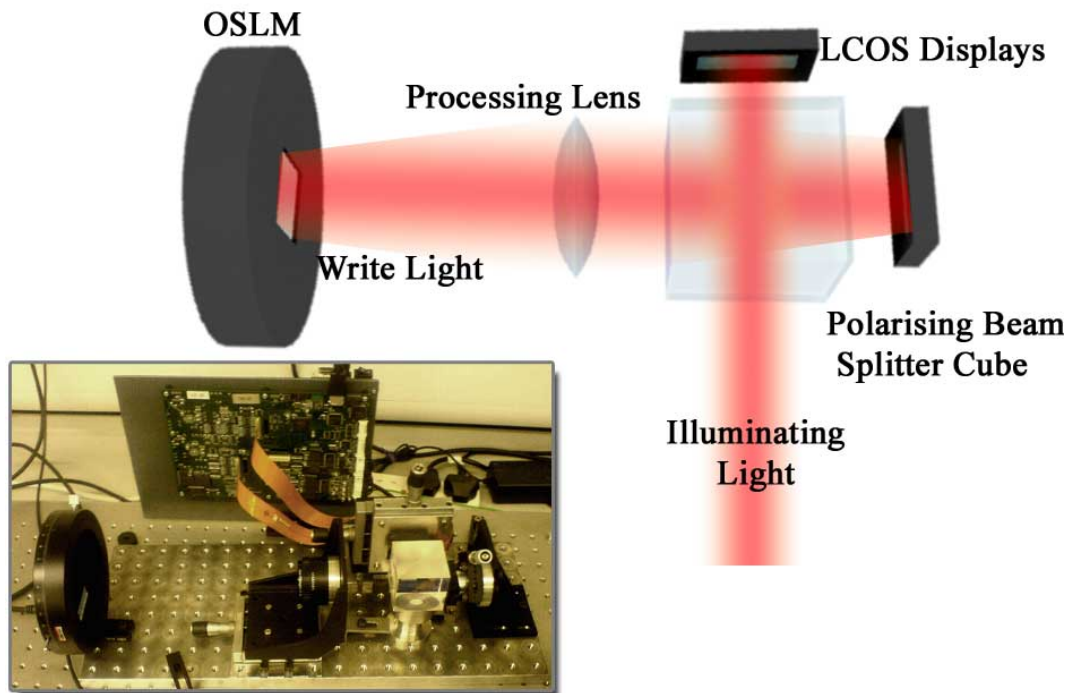
Figure 3.3: Layout of the optical system comprising, 2 Holoeye LCoS displays, polarizing beam splitter cube, processing lens and Hamamatsu OSLM. (Inset) A photo of the actual setup.

the light is transmitted or reflected by the polarizing beam splitter an intensity modulated image corresponding to the hologram was produced. A 75mm focal length process lens (Linos Rodagon D), optimized for low field distortion, imaged the planes of the LCoS displays to the write face of the 40 x 40mm OSLM. Though it would be possible to create the same effect as a high resolution SLM simply by tiling the two ESLMs alone this presents alignment issues associated with imaging a single beam onto two surfaces. In addition the surface of OSLMs tend to have less aberration compared to that of an ESLM as they are inherently non pixelated devices.

3.5 Calibration of the OSLM

The high diffraction efficiency of an SLM relies on the potential for a full 2π modulation and within that range a linearity of response. Using software the hologram is calculated at 256 levels within the 0-2π range. However, the linearity of the sys-

Phase against Pixel Value
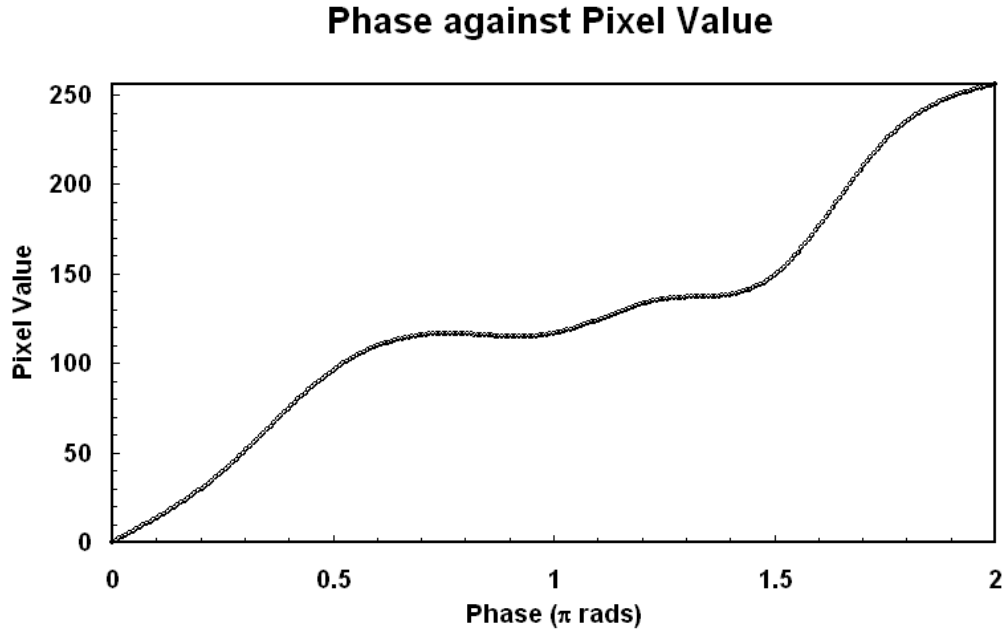
Figure 3.4: The optimized blazing function found to maximize the first order diffraction efficiency.

tem response depends upon the linearity of the LCoS display and the response of the photoconductor of the OSLM, both of which require calibration. A random search optimization algorithm was used to monotonically map the 0-2π range of the kinoform onto the 0-255 level of the LCoS display. The mapping function is a spline interpolation between 8 points defining the grey scale value at $\pi/4$ phase intervals. Whilst monitoring the light diffracted into the first order, the eight points are randomly adjusted, with the modification being kept if it leads to an improved efficiency and discarded if not. Eighty or so iterations are required to optimise the mapping function (see figure 3.4). The function can then be applied as a look up table (LUT) to all subsequent kinoforms.

One advantage of the OSLM is that the flatness of the device is determined by that of the optical flats. For standard units with 20x20mm this is better than $\lambda/2$, however, the larger aperture of the device means that this tolerance is relaxed. When used as a hologram, where the target beam is in the far field of the SLM, this residual aberration leads to a noticeable degradation in the fidelity of the diffracted beam. If the form of the aberration is known then it is a simple matter to add a correction to any subsequently calculated [73] kinoform.
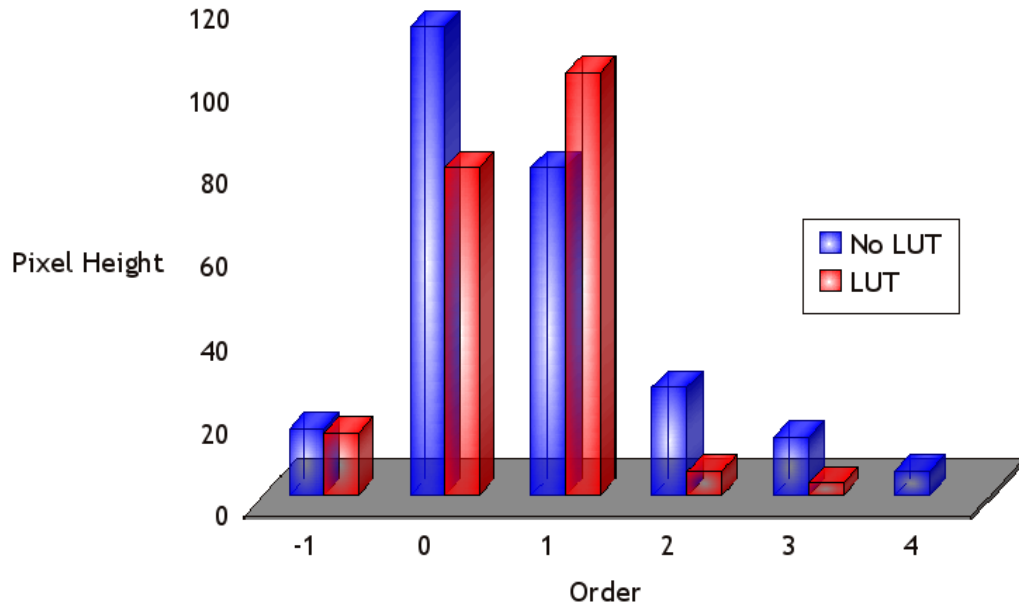
Figure 3.5: The power increase in the first order and decrease of the zeroth order due to use of an optimised phase response function, as measured by a CCD camera. The pixel height is assumed to be proportional to the intensity [1].

3.6   Linearised Intensity via a Multiplicative Mask

In addition to holograms which produce a laterally shifted beams, kinoforms can also be design to produce arbitrary distributions in the far field. The Gerchberg Saxton algorithm [74] is a powerful technique, converging from a random start to the final kinoform in a small number of iterations. This is discussed in more detail in Chapter 6. Fig.3.6 A) shows one such example. Note that whilst the target image is of uniform line intensity, the resulting diffraction pattern is not, the line intensity falling as a function of distance from the zero order in accordance with the diffraction efficiency of the SLM. Most simply this can be corrected by applying a multiplicative mask to the target image in effect multiplying the image intensity by the inverse of the diffraction efficiency, thus boosting the image intensity proportionally to the distance from the zero order. The result of this modification is shown in Fig.3.6 B).

7th March 2011
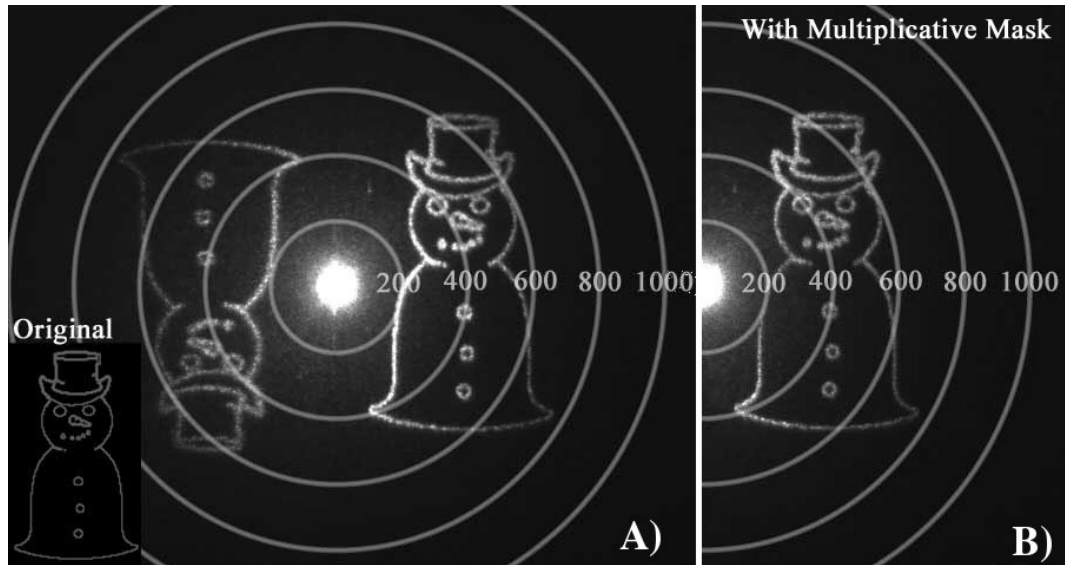
Figure 3.6: A) A far field representation of a snowman created by an iterative Gerchberg Saxton algorithm. The rings indicate the number of line pairs necessary to generate a first order diffraction spot at this point. The original image is shown inset in the corner. B) The corrected far field representation of a snowman with multiplicative mask applied.

3.6.1 Software Control

Having adopted an optical control technique first used by Lisener et al. [55] (see Chapter 6) consisting of the generation of kinoforms by the combination of gratings and Fresnel lenses, we are able to produce optical traps which may be both moved in three dimensions. The system was written in the LabVIEW programming environment and optimized for multiple-processor, desktop computers [75]. We found that for a given kinoform of 1920x1920 using a 3GHz, dual-core machine we can calculate at 2Hz. Although the resolution of the LCoS displays and the speed of the computer limit the update rate, this will be improved as computing power increases. Use of the graphics card for this application could also speed up the update rate of the kinoform. Some simple experiments were done using the CUDA programming language by Kevin O'Holleran and Graeme White to see if A Gerchberg Saxton algorithm could be implemented on the graphics card. The results seemed to indicate that holograms could be generated in real time at a maximum speed of frame rate of 40 FPS for 512 x 512 pixel hologram. Even though this is slow compared to other algorithims it has a major advantage in that optical traps generated this way

do not have to be a simple spot but instead could be made into squares, stars or any other shape. It is conceivable that a faster implementation of the GS algorithm could be made in openGL of DirectX. The snowman in Fig.3.6 was not done using the graphics card but created with a simple LabVIEW program.

Performance Evaluation

Examination of both the scientific and commercial literature reveals that the diffraction efficiency of SLMs have been defined in various ways. Within this work, we define the diffraction efficiency as the percentage of the light reflected from the SLM that can be diffracted into the first-order beam by a kinoform corresponding to a blazed diffraction grating. In this case since the grating is wedge shaped we define a line pair as one complete 2π cycle of phase. With zero line pairs, the hologram is blank and the SLM acts as a mirror. For higher numbers of line pairs, the power in the first order is divided by the sum of the power in all the orders, making the measurements insensitive to fluctuations in laser output power.

Figure 3.7 shows the measured diffraction efficiency of the SLM compared to various commercial optical and electrically addressed SLMs. These results are compared to the theoretical maximum diffraction efficiencies calculated by a Fourier decomposition of pixelated gratings used to simulate the OSLM. In all cases, the phase mapping function to maximize the first-order diffracted power was optimized. The diffraction efficiency was recorded up to the maximum line-pair value imposed by the Nyquist criteria (i.e. two pixels per line pair, 920 lines pairs for the SLM). We see that at low numbers of line pairs, the device is comparable to those commercial units, with no apparent disadvantage due to the tiling of the two halves of the kinoform. Obviously for line pairs above the Nyquist limit of the commercial devices the SLM still maintains a finite diffraction efficiency. However, it is also clear that even within the Nyquist limit, the increased aperture and pixel number of the device means that commercial efficiencies can be exceeded.

To test the SLMs capability to produce exotic beams [76, 77], which are sensitive to aberration, Laguerre Gaussian (LG) modes (see Chapter 4) were generated.
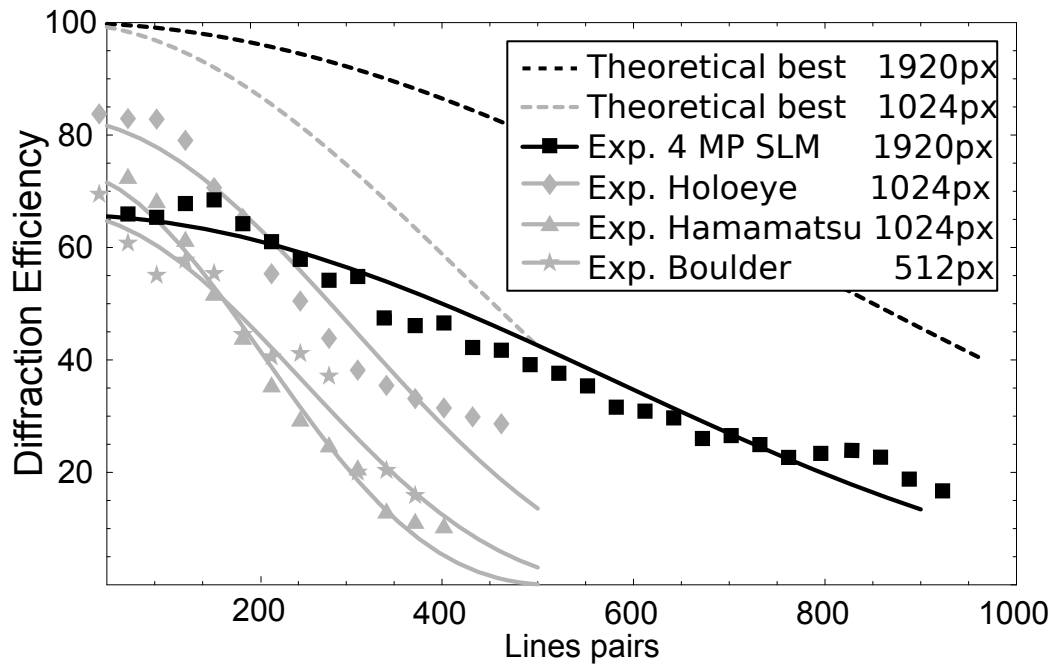
Figure 3.7: The measured diffraction efficiency of the 4 Mega-pixel SLM compared to various commercially obtained SLMs. Diffraction efficiency is shown as a function of line pairs displayed on the screen. The SLMs tested were a Holoeye (LC-R 2500), Hamamatsu (x8267 series) and a Boulder (prototype model). The width of each SLM in pixels is noted. The corresponding theoretical maximums based on Fourier decompositions of pixelated holograms are also shown.
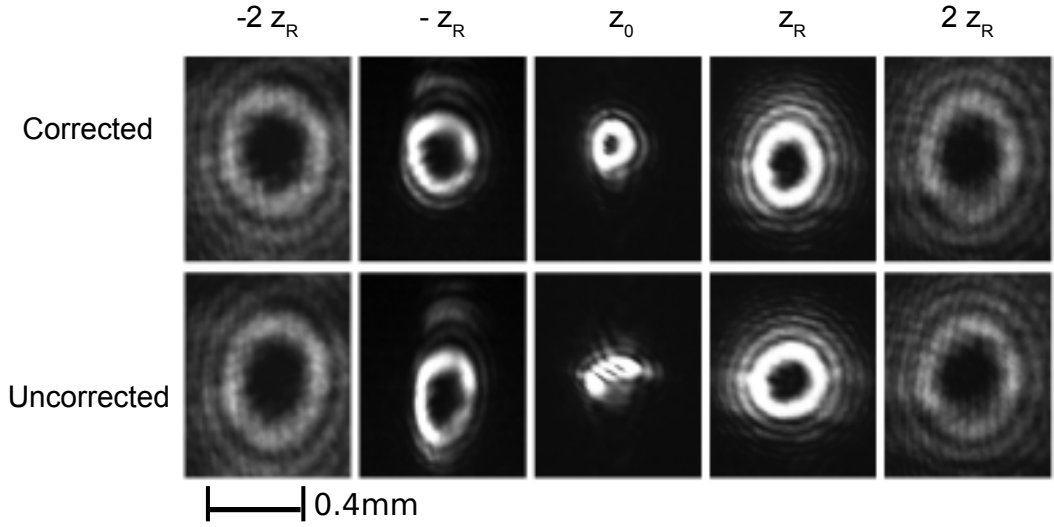
Figure 3.8: Series of images of a Laguerre Gaussian beam (L=4) as the camera is moved through the beam waist.

In collaboration with Richard Bowman an implementation of an algorithm first described by Jesacher et al. [63] was created in the LabVIEW programming environment. This algorithm can be used to correct aberrations caused by surface flatness by comparing the far-field intensity distribution of the generated LG beam to that predicted by theory. The SLM can be optimized via the use of standard Gerchberg Saxton algorithm [74]. Fig.3.8 shows a cross-sections of the resulting beam obtained in the far-field of the SLM. The displacement of the cross section from the beam waist is shown in terms of the Rayleigh range. We see that the fidelity of the beam produced by the corrected kinoform is significantly improved by use of Jesacher's algorithm [63]. It should be emphasized however that the beam quality is still superior to an LCoS Holoeye SLM.

3.7 Conclusions

As demand for spatial light modulators increases there will also be a demand for systems which have higher resolution. The design and construction of a 4 Mega-pixel spatial light modulator has been described above. In the context of holographic optical tweezers this higher resolution (960 line pairs) increases the available trapping range for a holographic optical tweezers system. With a bigger surface area the SLM

is at risk of creating increased aberrations. In this system however, these factors are accounted for by the use of an OSLM for phase modulation and by the adoption of aberration correction techniques. Computer calibration of the pixel to phase ratio of the system creates a well defined phase response. This leads to more intense optical traps (see Fig.3.5) [78]. The fall off of the intensity with radial displacement can be corrected by multiplicative masks. The systems size, optical flatness and resolution makes it ideal for the generation of exotic beams. Although the increased resolution of the system creates a computational challenge leading to bandwidth constraints faster hologram calculation will come with increased computing power and the adoption of graphics card technologies.

Chapter 4

Angular Momentum of Light

4.1 Introduction

Any discussion of optical tweezers experiments would be incomplete without reference to light's angular momentum. As discussed in the previous chapter light can carry $p = h/\lambda$ of linear momentum, where h is Planck's constant and λ is the wavelength of light. It is this momentum which enables optical tweezers to be used to trap microscopic particles. However it is possible for light to carry angular components which do not operate in the direction of the beam propagation. These components enable transfer of angular momentum to objects such as small particles, which may be optically trapped. The angular momentum (AM) of light exists in two forms. The first of these is known as orbital angular momentum (OAM) [79,80] and is produced through the helical phase structure of the light beam as a whole. The second, known as spin angular momentum (SAM) [81] is produced by circularly polarised light. In both cases light beams may carry an angular momentum component which is not co-linear to the lights propagation direction [82].

We seek in this chapter to familiarise the reader with the basics of angular momentum which will be useful in further chapters. Though light's angular momentum has been a constant thread through my work it is far too vast a subject to cover in totality. We seek here only to cover the basic concepts at play and not to get too involved in discussions about momentum which could easily become a thesis in itself (and no doubt has already). We confine ourselves to simple descriptions and avoid

excessively detailed mathematical models on which there is still disagreement particularly in the case of tightly focused beams of light. Explanation in greater detail may be obtained via several review papers and books which have been written on the subject such as [24, 83, 84].

4.2 Orbital Angular Momentum

In the case of orbital angular momentum the angular component of the light field is given by the divergence of the local phase gradient to the propagation direction of the beam. If the wave fronts of a beam are arranged such that there is an azimuthal shift in phase about the beam axis then the beam will have a net angular momentum which is proportional to the azimuthal displacement. This is best imagined as a "Fuselli" like helical structure in which the wave front twists around the central beam axis. Laguerre-Gaussian (LG) beams [85] have such a structure where the azimuthal phase is of the form $\exp^{i\ell\phi}$ where ℓ gives the number of 2π cycles in phase around the beam axis and ϕ is the phase. LG beams are often also expressed with a p number denoting the number of radial nodes in the mode profile. The equation of a Laguerre-Gaussian Beam is often described as:

$$E(LG_p^l) \propto \exp\left[\frac{-ikr^2z}{2(z_R + z^2)}\right] \exp\left[\frac{-r^2}{\omega(z)^2}\right] \exp\left[i(2p + |\ell| + 1)\arctan(\frac{z}{z_R})\right] \dots$$

$$\dots \times \exp\left[i\ell\phi\right] \times \left[\frac{r\sqrt{2}}{\omega(z)^2}\right]^{|\ell|} L_p^{|\ell|}\left(\frac{2r^2}{\omega(z)^2}\right) \quad (4.1)$$

Where z is the distance from the beam waist, z_R is the Rayleigh range, k is the wave number, $\omega(z)$ is the radius at which the Gaussian term falls to $1/e$ of its on-axis value, r is the radial position and L_p is the generalised Laguerre polynomial [86].

The far field intensity pattern generated by an LG_{01} beam forms a characteristic donut pattern with a dark central center surrounded by a bright ring, the size of this donut is determined by the ℓ number of the beam. The central dark region is called a phase singularity or optical vortex and comes about via the complete destructive interference of all parts of the light field at that point. The angular momentum imparted by such a beam is proportional to its ℓ number and is about the central

axis of the beam [87, 88]. Though such momentum is not an "intrinsic" property of the light as it requires an ensemble of photons. The momentum which can be transmitted to a particle in a linearly polarised beam may be expressed as $\ell\hbar$ per photon.

Beams with orbital angular momentum may be generated in a number of ways. Most simply LG beams can be produced with a spiral phase plate [89], here an optic with azimuthally varying thickness is used to create beams with OAM. Alternatively they can be produced in a laser resonator [90], a cylindrical lens mode converter [86, 91] or by the use of plate holograms [92, 93] where a diffraction pattern is used to create the appropriate phase retardation. More recently beams have also been created with the use of Q-plates which are liquid crystal cells confined with appropriate boundary conditions so as to create beams with OAM. [94]

The use of spatial light modulators for generation of beams with angular momentum has become quite popular due to the flexibility an SLM allows [95], not only for the generation of Laguerre-Gaussian beams but also for beams with more exotic phase structures. Furthermore the phase gradient at each point of a beam cross-section may be dynamically altered or reversed if an SLM is used. This temporal control not only makes experimentation easier but also allows for the center of rotation to be shifted or skewed dynamically, which can be useful for astigmatism correction. Beams may also be corrected in intensity by use of a shape phase mask [96]. Such masks send unwanted light into the zero order allowing a pseudo-intensity masked beam to be created which produces nicer donut beams in the far field.

OAM as Displayed on SLMs

Typically Laguerre-Gaussian beams are generated by displaying a spiral phase ramp on the SLM. Combining this with a diffraction grating produces a forked hologram and displaces the beam from the optic axis thus splitting it into different orders in the far field (see Fig. 4.1). Each order carries angular momentum which is commensurate with the order number and the charge of the original spiral phase pattern; thus in the case of an LG_{01} beam the positive first order is of charge 1 the
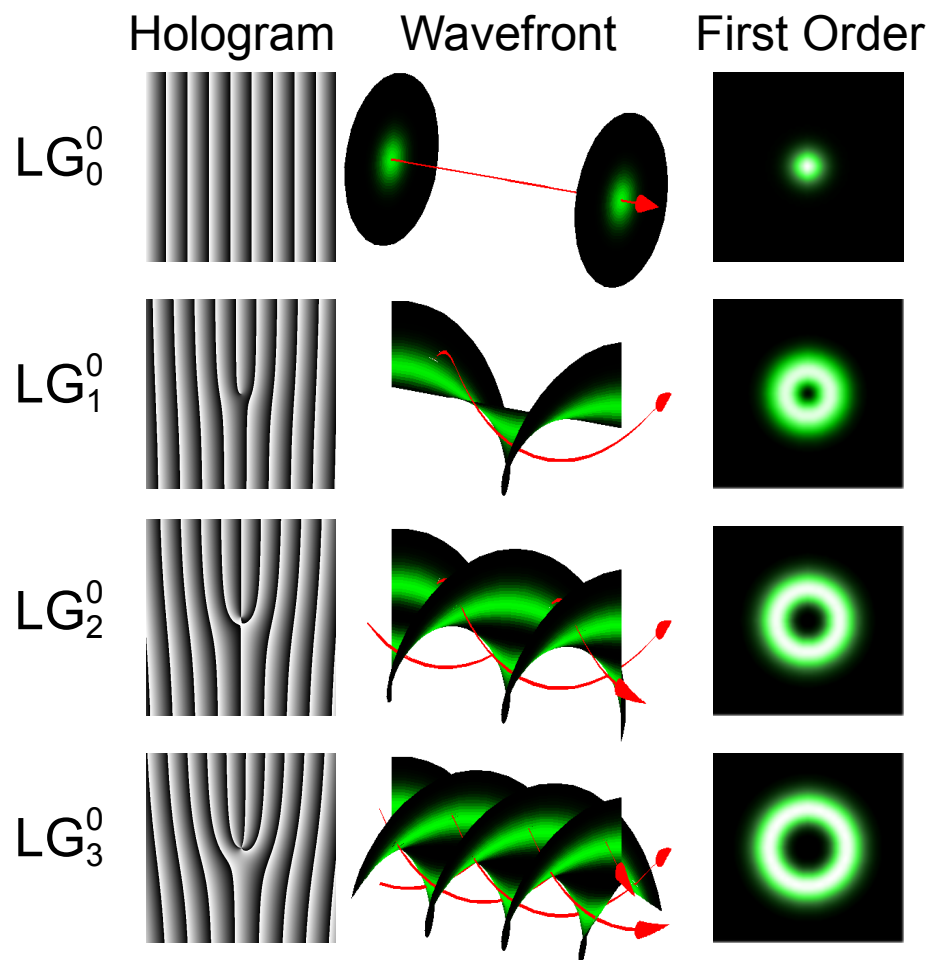
Figure 4.1: Some examples of Laguerre-Gaussian beams, Showing their hologram pattern, spiral phase structure and their far field "donut" shaped intensity pattern.

negative first order is of charge -1 and the positive second order is of charge 2 etc.. It is tempting to think that displaying spiral phase patterns which varies from 0 to 2π phase levels on an SLM with a limited diffraction efficiency of, for instance 1.2π would adversely affect the angular momentum of the beam generated. However this is not the case. In such circumstances the beam would only be attenuated in its diffraction orders. The pixelation of the SLM also has little affect on the quality of beams generated, as long as the SLM has resolution of greater than approximately (10x10) pixels.

4.3 Spin Angular Momentum

Unlike orbital angular momentum, spin angular momentum is not a property of an ensemble of photons but is rather an "intrinsic" property of light. The polarisation state of light may be looked at in terms of two orthogonal electric field components the relative phase of which dictates the polarisation state of the light. This can most easily be seen in terms of Jones' vectors or Stokes' parameters. When circularly polarized light with spin angular momentum is incident on a birefringent object there will be an exchange of angular momentum. The birefringence of the material may be considered to create a phase retardation of the light which is greater along one axis than the other, thus changing the polarisation state of the beam. As early as 1936 Beth [81] used a circularly polarized light beam to turn a quartz wave plate suspended from a fine quartz fiber. Since materials like calcite and quartz are highly birefringent the incident circularly polarised light is turned from circular to liner polarisation resulting in a momentum transfer from the beam to the object (see Fig.4.2). Halina Rubinsztein-Dunlop and colleagues have repeated Beth's experiment, using optical tweezers to rotate crushed fragments of birefringent material using the same mechanism [97]. Along with birefringent materials, "form birefringence" can also cause particle rotation; here the polarisation state of the light beam may be altered by the shape of the particle. Bishop et. al. [98] trapped long glass rods with birefringence and demonstrated rotation. For spin angular momentum the transverse momentum component is provided by the gradient of the
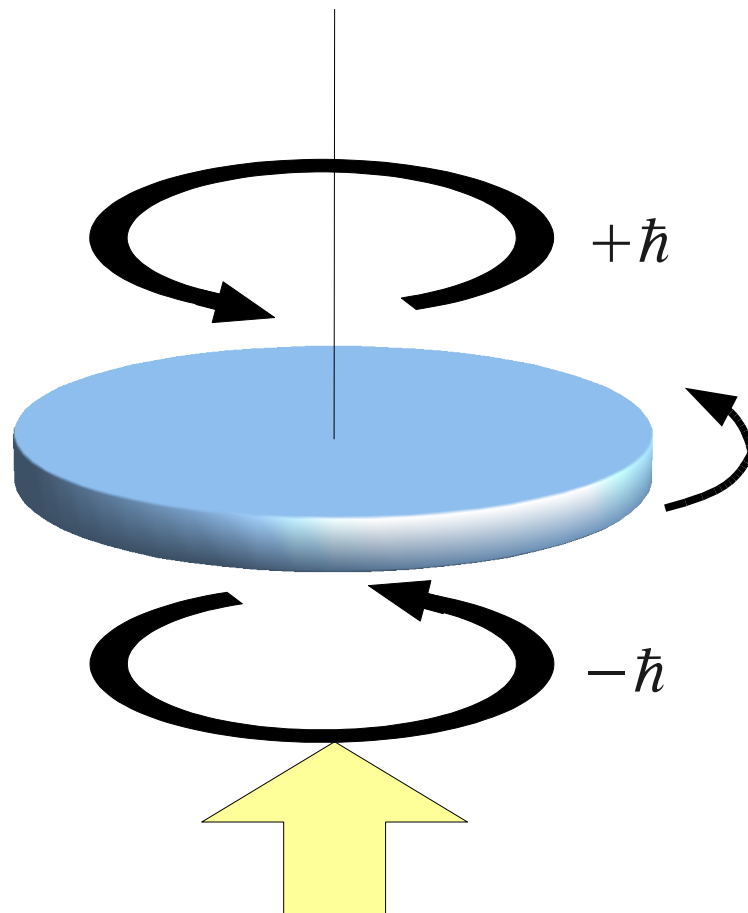
Figure 4.2: Beth's experiment; in which the handedness of the circular polarisation is reversed and $2\hbar$ per photon of angular momentum is transmitted into the calcite plate.

field intensity. An usefull explanation of this is found in Fig.4.3. This can lead to non intuitive results if, for instance, one realises that the field gradient may be negative as well as positive. This does not however mean that an optically trapped particle can have a reverse spin since for a dielectric particle to be trapped requires the gradient to be such that the particle is pulled towards the field maximum.
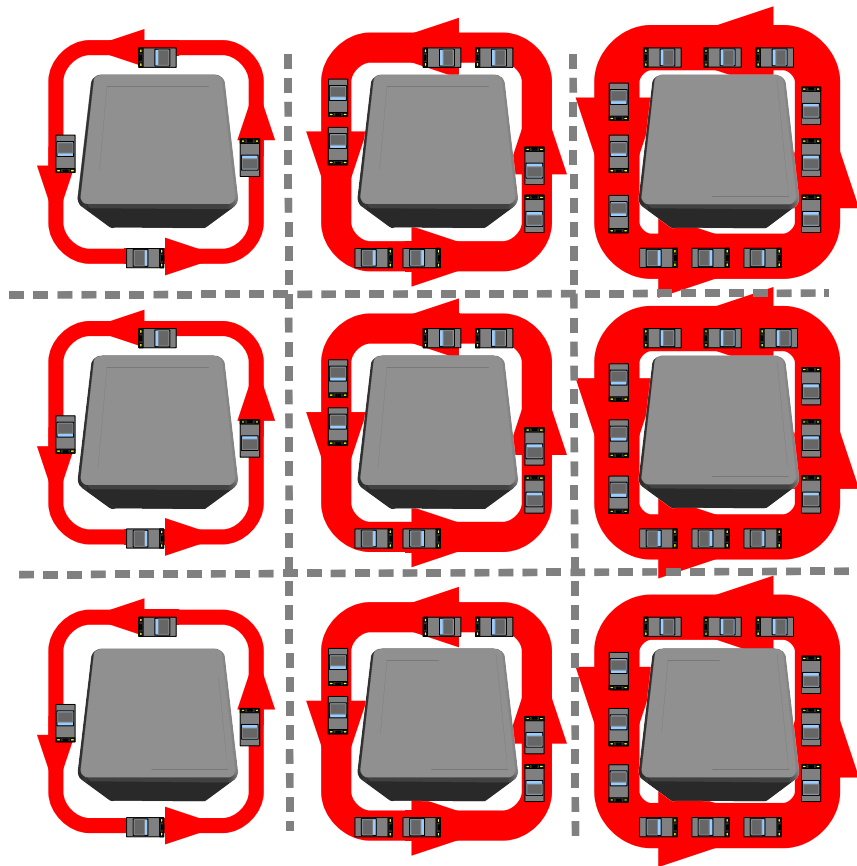
Taken from D.E. Soper, *Classical field theory*, Wiley 1976 (Dover 2008)

Figure 4.3: Traffic flow in London. A metaphor for the forces acting on individual dipoles in a lattice in the presence of a beam with spin angular momentum, taken from *Classical field theory by D.E, Soaper.* Horizontal forces cancel while those in the vertical direction do not, due to the presence of a field gradient.

4.4 Vaterite Crystals

Vaterite is a crystalline polymorph of calcium carbonate [99]. Spherical particles of vaterite can be synthesized to be between 1 and $10\mu m$ in size. Its sphericity and birefringence make it useful for optical trapping experiments. Vaterite is a positive uni-axial crystal which has strong birefringence $n_e = 1.65$, $n_o = 1.55$. This is most likely caused by its internal structure which grows from a liner arrangement of small crystals into a wheat sheaf like structure before forming a spherulite. When these small vaterite particles are optically trapped with circularly polarised light a strong torque is exhibited. Rotation speeds of 100s of Hz can be achieved [100]. During the course of my studies I was lucky enough to visit Halina Rubinsztein-Dunlop's group at the University of Queensland in Australia to learn how to make these vaterite particles for experiments in optical trapping. A recipe for the production of such particles is included in the appendices.

4.5 Torques in Optical Tweezers

By measuring the change in the polarisation of the trapping light extremely accurate measurements of torques can be achieved. The overall torque exerted on such a particle is given by:

$$\tau_s = \frac{\Delta\sigma P}{\omega} \tag{4.2}$$

Where $\Delta\sigma$ is the change in polarisation between light entering and exiting the birefringent object, P is the total power of the beam and ω is the frequency of the light [98]. Measurement of the torque enables the measurement of the local viscosity through relation to the stokes drag force.

$$\tau_D = 8\pi\eta a^3\Omega \tag{4.3}$$

Here τ_D is the drag torque, a is the radius of the sphere, η is the viscosity of a low Reynolds number liquid and Ω is the angular frequency. It is worth making explicit at this point that the torque exerted by a beam with OAM is around the

central axis of the beam, while that exerted by a beam with SAM is around its own axis. Of course it is possible to have a beam with both types of angular momentum. If a small birefringent particle is then trapped in a donut beam a sort of planetary motion is observed with both spin and orbital components rotating the particle. The vortex structure of LG beams has also been exploited for trapping particles. He et al. [101] demonstrated that black or reflective particles can be trapped in the central minimum of an LG laser beam which was produced using a high efficiency computer generated hologram. If the particle size is chosen such that beam and particle are coaxial, when the particle is trapped then the two momenta may be played off against each other [102].

In the paraxial limit, the torque on an absorbing particle due to both the polarization and the helical Poynting vector is given by

$$\tau_{(s+o)} = \frac{(\sigma_z + l)P}{\omega} \tag{4.4}$$

where σ_z is ± 1 for circularly polarized light and 0 for plane-polarized light. The non paraxial case of this equation has been derived by Barnett et al [80] to be:

$$\tau_{(s+o)} = \frac{P}{\omega} \left\{ (\sigma_z + l) + \sigma_z \left(\frac{2kz_R}{2p + |l| + 1} + 1 \right)^{-1} \right\} \tag{4.5}$$

where k is the wave number, and z_R is a length term, which in the paraxial limit is the Rayleigh range. Though strong torques are created by both spin and orbital momentum, it is worth noting that as the size of the trapped particle increases its associated moment of inertia and drag force rapidly increases [103]. Increasing the azimuthal mode index of the OAM beam does not necessarily help matters since the corresponding size increase of the beam decreases the per photon efficiency. The coupling optics and numerical aperture of the system may also decrease a beam's OAM due to the restriction of the beam's skew angle. Optical rotation of particles is therefore only practical up to a radius of not much more than tens of microns.

4.6   Novel Beam Generation

Along with the generation of beams such as LG beams SLMs have enabled the generation of many novel beam types which are difficult to produce in other ways.

One example of such beams is the the generation of beams with fractional orbital angular momentum (FOAM). Such beams have an azimuthal phase gradient which is not a multiple of 2π; as such these beams exhibit a dislocation in the far field intensity pattern. This dislocation is characterized by a chain of alternating vortices which form in a dark line associated with the edge dislocation of the azimuthal phase. A number of studies have taken place around these beams [104] which have applications in quantum information experiments. I was lucky enough to have been able to take part in an experiment with Jorg Götte in which a new type of beam with fractional orbital angular momentum was generated. It is possible as has been mentioned, to generate such beams with fraction orbital angular momentum by simply using hologram of a spiral phase plate with a non-integer azimuthal phase gradient (i.e. not a multiple of 2π). However the experimental beam, which was generated using an SLM, was a superposition of LG beams arranged to create a beam which has fractional angular momentum but which is stable on propagation. This stability is generated by arranging for the minimum number of Gouy phase changes to take place during the propagation of the beam. More details can be found in [105].

Along with beams that have FOAM a variety of other beam types can be generated with varying degrees of angular momentum. It is not possible within the context of this thesis to make reference to all of them but some examples of beams which have been useful in optical trapping experiments are: Leopard beams [106], Bessel beam [66], spiral beams [107, 108] and Airy beams [109]. Though they do not all carry angular momentum, it is true to say that they do carry transverse momentum components and it is the recognition of this fact which has enabled their use in optical trapping.

4.7 Conclusions

The recognition of light's angular momentum has sparked a blossoming in the study of light beams as mechanical actuators, sensors and information encoding devices. Spatial light modulators are integral to the development of these fields which require phase structures to be encoded onto coherent light beams. Using SLMs for this purpose not only provides a useful way of prototyping these beams but also provides a re-adjustable and dynamic way of interfacing with light. Future development of this field will almost certainly be helped by spatial light modulators. Although not dependent on extrinsic phase structures SAM also can benefit from SLMs which enable both control over multiple optical traps where tweezers experiments are concerned (as we shall see in future chapters), and inherent polarisation and intensity modulating abilities.

Chapter 5

Holographic Control of Spin Angular Momentum

5.1 Introduction

As we have mentioned in the previous chapter the ability to rotate particles in optical tweezers is one which is highly desirable for a number of applications such as microrheology [110] and optically driven micro-machines. Holographic Optical Tweezers (HOT) have been widely used to manipulate particles in three dimensions. However, using them to rotate particles is a more specialized application.

Several methods have been used to create optical traps which exert a rotational force on a trapped particle. To induce rotation, one must transfer angular momentum to the trapped object. In 1991 Sato et. al. [111] rotated a red blood cell using high-order Hermite-Gaussian modes in optical tweezers to trap and rotate it. Another method is to use a rotating aperture in the beam path [112]. Rotation can also be achieved via a rotating interference pattern [113]. Luo et. al. [114] used partially silvered beads to create rotation. While optical rotators have been constructed by two photon polymerization in order to scatter light asymmetrically and thereby rotate microstructures [71]. Spatial light modulators have been used to produce multiple optical traps revolving around each other [115].

One very appealing option then is the use spin or orbital angular momentum. In the case of beams with orbital angular momentum these create a "donut" shaped

intensity distribution in the trapping plane with rotation taking place about the central vortex. Another option for creating rotation is spin angular momentum. This is caused by circularly polarised light being transmitted through a birefringent particle. However the rotational control of multiple particles is a more complex operation than simple rotation. It is possible to generate multiple optical traps and control the orbital angular momentum of the individual traps by use of holographic optical tweezers with an appropriately designed hologram [116,117]. It has also been possible to generate multiple optical traps with spin angular momentum by means of polarizing beam splitters [75], but controlling the polarisation state of each trap independently is far more difficult. In this chapter we discuss the use of spatial light modulators as a control mechanism whereby the polarisation state of multiple optical traps can be controlled. A "split-screen" method has been introduced in order to create and control the spin angular momentum of multiple optical traps.

5.2 Polarisation Control of Multiple Optical Traps

The polarisation state of a beam of light can be expressed mathematically in terms of Jones vectors. Here the instantaneous electric field of a monochromatic wave is written as a column vector with each element being one part of an orthogonal set. We may then write each part in its complex form.

$$\mathbf{E} = \left[\begin{array}{c} E_x \mathrm{e}^{i\phi_x} \\ E_y \mathrm{e}^{i\phi_y} \end{array} \right] = \mathrm{e}^{i\phi_x} \left[\begin{array}{c} E_x \\ E_y \mathrm{e}^{i\delta} \end{array} \right]. \tag{5.1}$$

Equating $\phi_x = \phi_y - \delta$ it is evident that the polarisation state of a monochromatic beam is determined by the phase difference δ between each of the orthogonal components.

As we have mentioned in the previous chapter a wave plate with appropriate birefringence is enough to alter the phase difference between each component thereby changing the polarisation of the exiting beam. However spatial light modulators are also capable of making the phase changes. Furthermore such changes can be made both to the beam as whole and to individual pixels.

7th March 2011

In order to generate a particular beam type a phase pattern is applied to the SLM changing the beam characteristics to give the desired far field pattern. In order to simply generate multiple focused beams Liseners algorithm [55] is used to simulate a combination of gratings and lenses which enable the creation of multiple optical traps which are movable in three dimensions. This is discussed in detail in Chapter 6.

In addition, the phase of the reflected light can be controlled by multiplying the hologram by a constant phase factor $\exp(i\delta)$. This technique for controlling the phase of the reflected light was used by, Maurer *et. al.* [118] who used a spatial light modulator in a "split-screen" configuration to generate a number of different vector beams. Importantly the size of phase pattern displayed on the SLM does not in itself affect the shape of the far field pattern generated. Thus the SLM screen can be split into two halves, both displaying the same phase pattern but differing by a constant phase factor. The two halves of the spatial light modulator can then be illuminated with similar beams of orthogonal polarisation which can be subsequently combined but with a well defined phase difference δ between them. Adjusting the phase difference between the beams allows control over the polarisation state of the resulting superposition. Furthermore, since multiple traps may be produced by combining differing gratings if we adjust the phase difference between the individual gratings on each side of the SLM we can then control the polarisation of individual traps independently.

Even with a phase only SLM it is possible to have some degree of intensity modulation. This is done by applying a restriction to the range of phase values used in the holograms generated by the SLM. Doing so artificially decreases the efficiency of the SLM. It is possible to dynamically control the power coming from each side of the SLM by this method thus giving precise control not only of the polarisation state but also of beam power from each side of the SLM and hence the orientation of linear polarisation.

Experimentally each half of the SLM can be combined with a polarizing beam splitter cube. It is then possible to generate multiple optical traps with independent polarizations through a combination of a gratings and lenses algorithm [55] and the
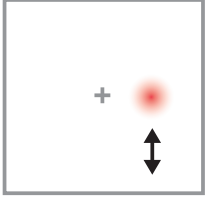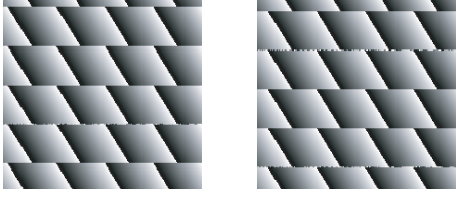
|	Holograms displayed on SLM	Intensity and polarization in trapping plane
One trap linear polarization	Phase difference = 0	
One trap circular polarization	Phase difference = π/2	
Two traps, linear and circular polarization		

Figure 5.1: Illustration of the holograms used to generate beams with independent polarisation control. To produce a single, linearly polarised trap the phase difference between the two holograms on the SLM is 0. To produce a single, circularly polarised trap the phase difference between the two holograms on the SLM is $\pi/2$.

use of the split a screen SLM technique described above, in order to control the polarisation state of each trap (see Fig. 5.1).

5.3 Experimental Setup

In order to create two similar spots with orthogonal polarizations a 532nm laser (Laser Quantum, Opus) was expanded and split onto a spatial light modulator (Holoeye, LCR 3000). A $\lambda/2$ wave plate was used in order to adjust the polarisation direction such as to get maximum diffraction efficiency from the SLM. The wide screen SLM was split into two halves with one beam exactly centered on each. The two reflected beams where then recombined via a polarizing beam splitter. A $\lambda/2$ wave plate was used to optimize the polarisation state of each beam before recombination. The recombined beam was then fed into a conventional laser tweezers setup. The system uses a beam steering mirror 160mm focusing lenses and an
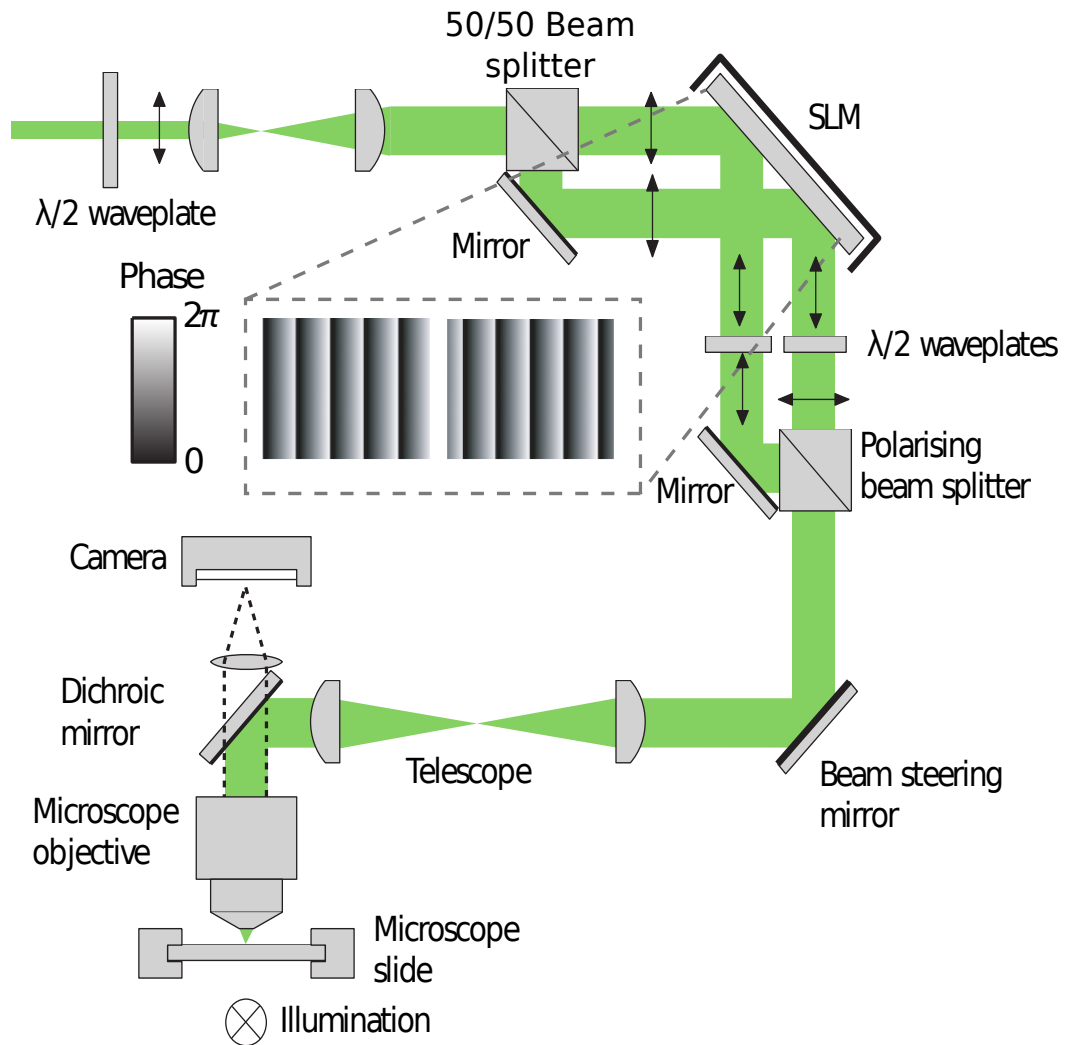
Figure 5.2: Experimental set up showing the addition of kinoforms of different gratings to produce variously polarised diffraction orders.

infinity corrected microscope objective (Zeiss, 100x 1.3 NA). A standard halogen lamp (50W) with appropriate condensing optics was used for illumination . A CMOS camera (Prosilica, EC1280) was used to image the sample. A dichroic mirror was used to separate laser light from the illumination light. The experimental setup is shown in Fig. 5.2.

A custom version of the Blue Tweezers suite was built in order to control the split holograms displayed on the SLM screen. The Blue tweezer suite was developed by Graeme White in order to amalgamate a number of preexisting subroutines being used in the Glasgow optics group into one coherent package. The system can be used to generate holograms which can be displayed on an SLM. It encompasses a number

of other useful functions and does not require a graphics card to display holograms. It is still available from the Glasgow optics group website. All programming was done in the LabVIEW programming environment. Mouse actions were used in order to create, destroy and move optical traps. The algorithm first reported by Liesener [55] was used to calculate the optical traps, 8-bit gray scale images were produced and displayed via an extended desktop directly onto the SLM where they were converted into phase holograms.

In order test the usefulness of such a system birefringent Vaterite crystals were produced (see Appendices) which could be rotated when optically trapped with circularly polarised light [110]. Under plain linear polarised light such crystals align to the polarisation direction.

5.4 Calibration of the System

Since each diffracted order from our split screen system is created by multiple holograms the phase difference between the two holograms is of critical importance. For this reason a single SLM was used rather than two separate ones. However as a diffracted spot is moved away from the central maximum a phase difference between the two sides is introduced due to the change in optical path length between the spot and each of the two holograms. This change is minimized due to the proximity of the SLM to the recombining beam splitter cube. However some residual phase difference remains. In order to correct this a raster scan of the trapping area was done with a single diffracted order and the intensity of the trap reflected from the cover slip of the microscope slide was observed (see Fig.5.3). It was then possible to construct a phase look up table which could be used to correct the δ phase change between each of the two sides based on the trap position. Further calibration was then done by scanning a trapped Vaterite crystal and observing its motion at different points. After the system had been calibrated such that the Vaterite crystal maintained a single orientation (some crystals are non-spherical) without rotation across the field of view. It was then possible to rotate the particle arbitrarily by adding a constant phase of $\delta = \pi/2, 3\pi/2$, or π to one half of the SLM thus allowed
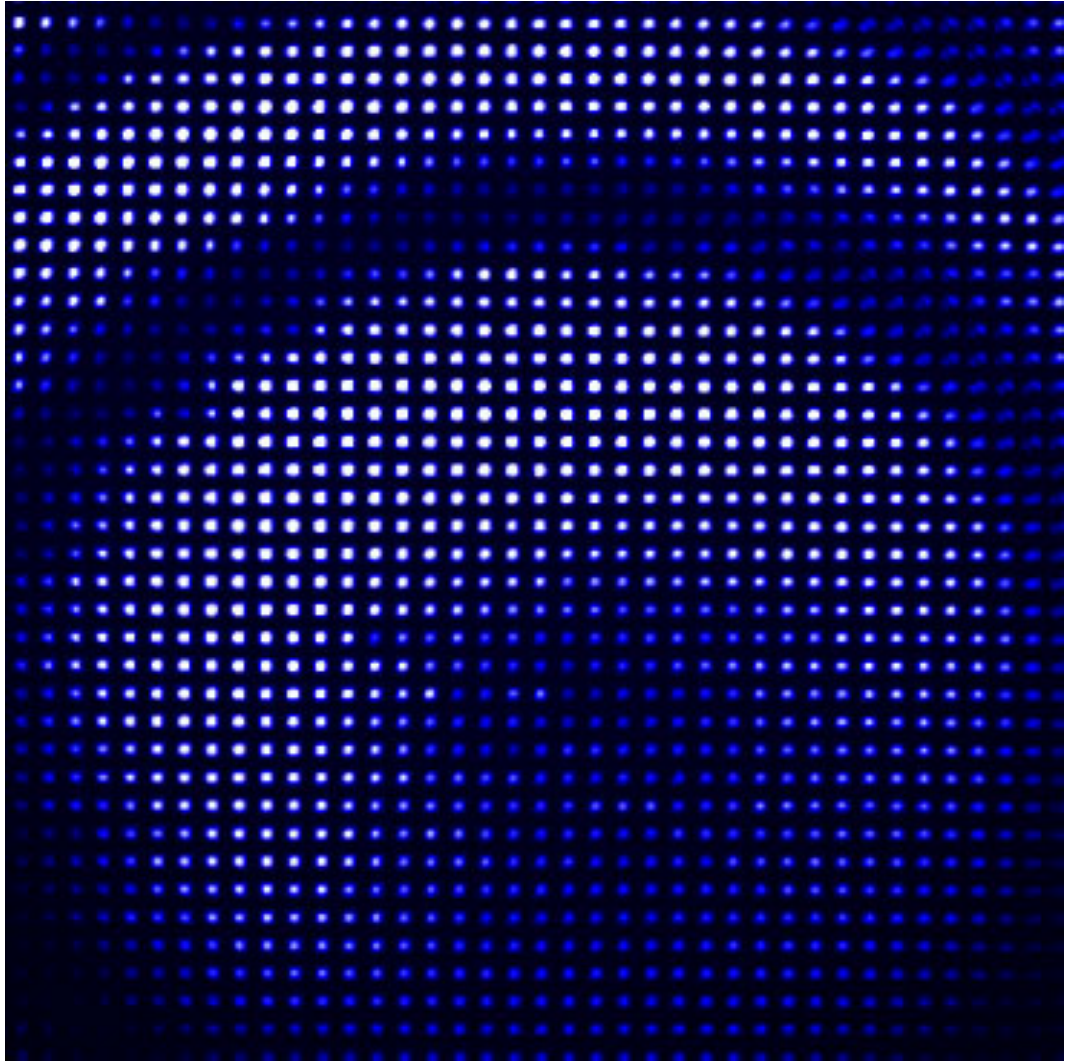
Figure 5.3: A raster scan image of the first order diffraction spot as seen through a polariser. The image shows how the polarisation changes with radial position.

us to generate either a circular polarisation state or an orthogonal linear state. The system was also calibrated such that each side of the SLM contributed equal beam power to the trapping beam. This was necessary so that circular rather than elliptical polarizations could be produced.

5.5   Results

In order to test the functionality of the system multiple vaterite crystals were trapped and rotated. The rotational speed was dependent on laser power and the crystals used. Since the vaterite created varied in size and shape a significant variation in

the rotational properties of the vaterite was experienced. Often cubic and saucer shaped particles were produced accidentally. However in the case of the saucer shaped particles good birefringence was discovered which lent itself to easy control using the holographic optical tweezers system.

When a particle with arbitrary birefringence is illuminated by circularly polarised light the exiting light will in general no longer have the same circular polarisation thus even if elliptically polarised light exits the particle some amount of momentum transfer will have taken place. A torque of some magnitude will thus be generated which is dependent on the handedness of the incident light. However when linear polarised light is incident on such a particle the torque may be changed in both magnitude and sign based on the properties of the particle. The particle will thus align itself to the orientation which best minimises the momentum exchange. It is therefore possible not only to rotate or stop particles based on the incident polarisation but also to precisely control the orientation of these particles by varying the power on each side of the SLM. Since this technique allows both the position, orientation and rotation direction of the multiple particle to be set independently of each other, it has significantly more flexibility than techniques previously reported in literature. Fig.5.4(A) shows frames of a movie illustrating the changing position and orientation of two vaterite particles being controlled with the system. At various times in the image sequence each of the particles is set into either clockwise or anticlockwise rotation, by trapping with circularly polarised light, or fixed in orientation by linearly polarised light. Fig.5.4(B) shows a non spherical vaterite particle being finely rotated. This is done by altering the power given to each side of the SLM thereby changing the polarisation direction of the light.

5.6 Conclusions

The split screen method can be used to independently control the polarisation state of multiple optical traps allowing the simultaneous movement and rotation of multiple particles. Vaterite crystals can be fabricated and rotated by means of the spin angular momentum created in such traps. Multiple particles could also be moved
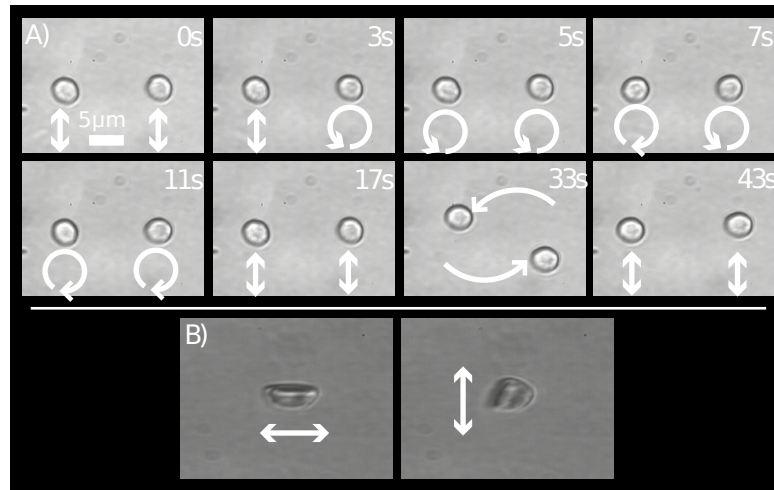
Figure 5.4: (A) Image sequence of two birefringent Vaterite crystals independently rotated in a holographic optical tweezers. Showing the current polarisation state of the incident light and the translation of the optical traps. (B) Change in particle orientation due to the change in polarization state. The movie can be found online with [2].

trapped and rotated. The speed of rotation was power dependent [119, 120] however, we were regularly able to reach rotation speeds of >30 Hz. One use for the system is the generation of complex flow patterns, which could not otherwise be created on such a scale. Microrheological experiments may also be possible in systems where simultaneous measurement at multiple points is necessary. Furthermore the technology may find application in the rotation of multiple micro-machines [121].

Chapter 6

Software for SLMs

6.1   Introduction

The use of spatial light modulators by necessity requires computer control, both to
generate an appropriate phase pattern and to analyse data produced by the function-
ing of the SLM. Since the SLM is a device which inherently requires communication
with a computer its proper functioning is premised on correct calculation of patterns
to be displayed as holograms. One of the benefits of holographic optical tweezers
systems is the ability to control multiple optical traps. This means however that
if particle tracking is to be implemented it is best done with a fast camera system
which has a wide field of view. In order to exploit the abilities of these fast cameras
a significant degree of software development is also required. Over the course of
my PhD a large amount of software has been developed for use with holographic
optical tweezers systems. Two full versions of integrated optical trapping software
currently exist on the Glasgow website developed by Graeme Whyte, Richard Bow-
man and myself. I have also developed camera software and analysis software which
is also available on-line. Along with generic tweezers software, bespoke software for
microrheology and position clamping has been developed. On reflection I could not
hope to cover all the code created in the course of this volume. I will therefore
constrain myself in this chapter to deal with only those algorithms which may be
considered as fundamental to the development of my holographic optical tweezers
systems. Most algorithms were written in the LabVIEW programming environment
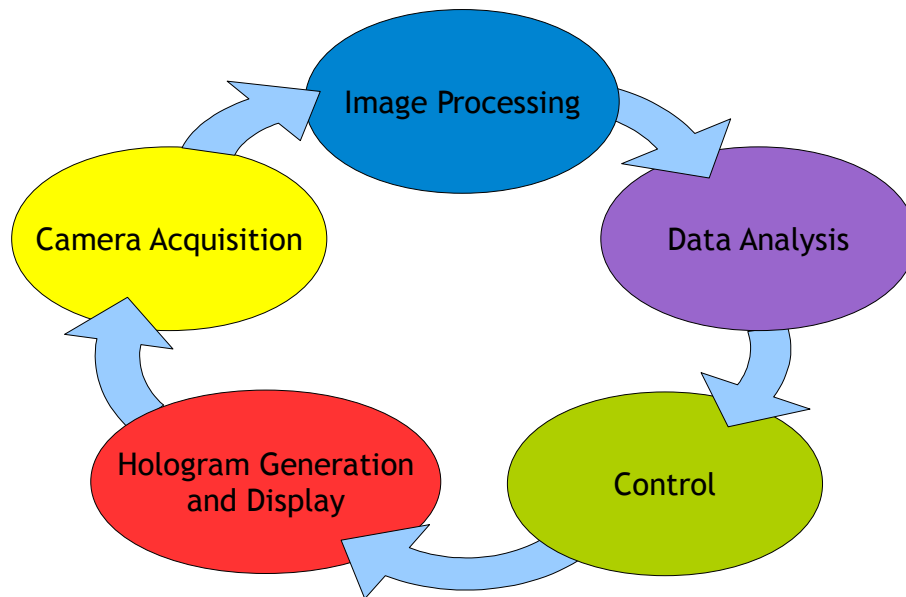
Figure 6.1: In general and specifically in the case of position clamping, the design structure of optical tweezers systems can be regarded as a cycle of several different tasks. Holograms are generated, camera images of the affect of those algorithms on particles are taken in by a fast camera. Those images must be then processed and analysed before control logic decides how to generate the next hologram.

(National Instruments) and experiments were conducted on a Dell Intel Xenon computer.

6.2 Hologram Control Algorithms

Holographic optical tweezers rely on the ability of SLMs to dynamically generate multiple optical traps which can be moved in three dimensions. A number of algorithms have been used to generate such optical traps. We concentrate here on the gratings and lenses algorithm proposed by Liesener [55] and the Gerchberg Saxton algorithm [122] although a number of other algorithms exist and have been looked at in detail in [78, 123].

Gratings and Lenses

As has has been mentioned it is possible to transform a beam through phase only modulation into a series of optical traps. Naively one might assume this could be done by simply taking the inverse Fourier transform of the desired intensity pattern however this would lead not only to phase but also intensity modulation. The hologram would thus be highly inefficient. In practice there are a number of different ways to create a phase holograms which will give the desired optical traps. In 2000 Liesener et al. [55] came up with an effective method for producing multiple optical traps with phase only holograms. The Fourier transform of a regular grating will, in the Fourier plane yield a diffraction pattern of constantly spaced spots the period of which is inversely proportional to the spacing of the grating and the intensity of which is enveloped by a sinc function. A similar sawtooth grating will give the same result but with the maximum intensity now in the first order rather than the zero. An optical trap can thus be constructed by modulating the phase on the spatial light modulator such that

$$\Phi(x,y) = (\frac{2\pi}{\Lambda_x}x + \frac{2\pi}{\Lambda_y}y) \bmod (2\pi) \tag{6.1}$$

where Λ_x and Λ_y are the fringe periods in the x and y directions. By varying the grating spacing and orientation the trap may be steered. Multiple optical traps can be constructed simply by summing the complex gratings and extracting the phase.

$$\Phi(x,y) = \arg(\sum_j \exp^{i\Phi_j(x,y)}) \tag{6.2}$$

Furthermore, the focal points of optical traps can be displaced by the addition of a Fresnel lens hologram to each optical trap.

$$\Phi(x,y) = (\frac{2\pi}{\Lambda_x}x + \frac{2\pi}{\Lambda_y}y + \Gamma(x^2 + y^2)) \bmod (2\pi) \tag{6.3}$$

Here $\Gamma = Cf$ where C is an experimentally determined constant based on the pixel size of the SLM and f is the focal length of the Fresnel lens thus controlling the axial position of the optical trap. This method allows the creation of multiple

holographic optical traps which can be moved in 3 dimensions. This method is quite computationally efficient however there are some drawbacks. The hologram produces multiple other orders (Ghost orders) which can interfere with other objects in the trapping plane though the likelihood of this is much reduced if the phase response curves (see Chapter 3) of the SLM are properly set and the SLM has a high spatial resolution. Another problem is that the other orders also limit the efficiency of the system. For a small numbers of traps this is not a major problem however if the number of traps is large significant amounts of light go into other orders.

Gerchberg Saxton Algorithm

The Gerchberg Saxton (GS) algorithm is an iterative phase retrieval algorithm, which given the intensity distribution in the object and Fourier planes calculates an appropriate phase patterns to generate such intensity distributions. The algorithm was originally developed by R.W. Gerchberg and W.O. Saxton [74, 122] to infer the phase distribution in electron beams. The GS algorithm is useful in optical trapping since it can be used to create arbitrary intensity distributions in the Fourier plane of a spatial light modulator. The Gerchberg Saxton algorithm is an error reduction algorithm. The algorithm works as follows: A random phase distribution and the known object intensity distribution are combined into a 2 dimensional complex function. This is then Fourier transformed and then separated again into its phase and intensity components. The intensity is discarded and replaced with the desired Fourier plane intensity. The complex function is then inverse Fourier transformed back into the object plane. The phase and intensity are once again separated and the intensity is replaced with the object plane intensity. The process is then repeated iteratively (see Fig.6.3). The algorithm usually converges on a solution within only a few iterations and the result can be then displayed on the SLM.

The advantage of iterative algorithms such as the Gerchberg Saxton algorithm [122] is that it allows good homogeneity between optical traps furthermore other unnecessary diffraction orders can be eliminated. Another advantage is that traps may be of any intensity distribution hence bespoke optical traps and novel beams can be created. It is also possible to extend the GS algorithm to create 3 dimensional
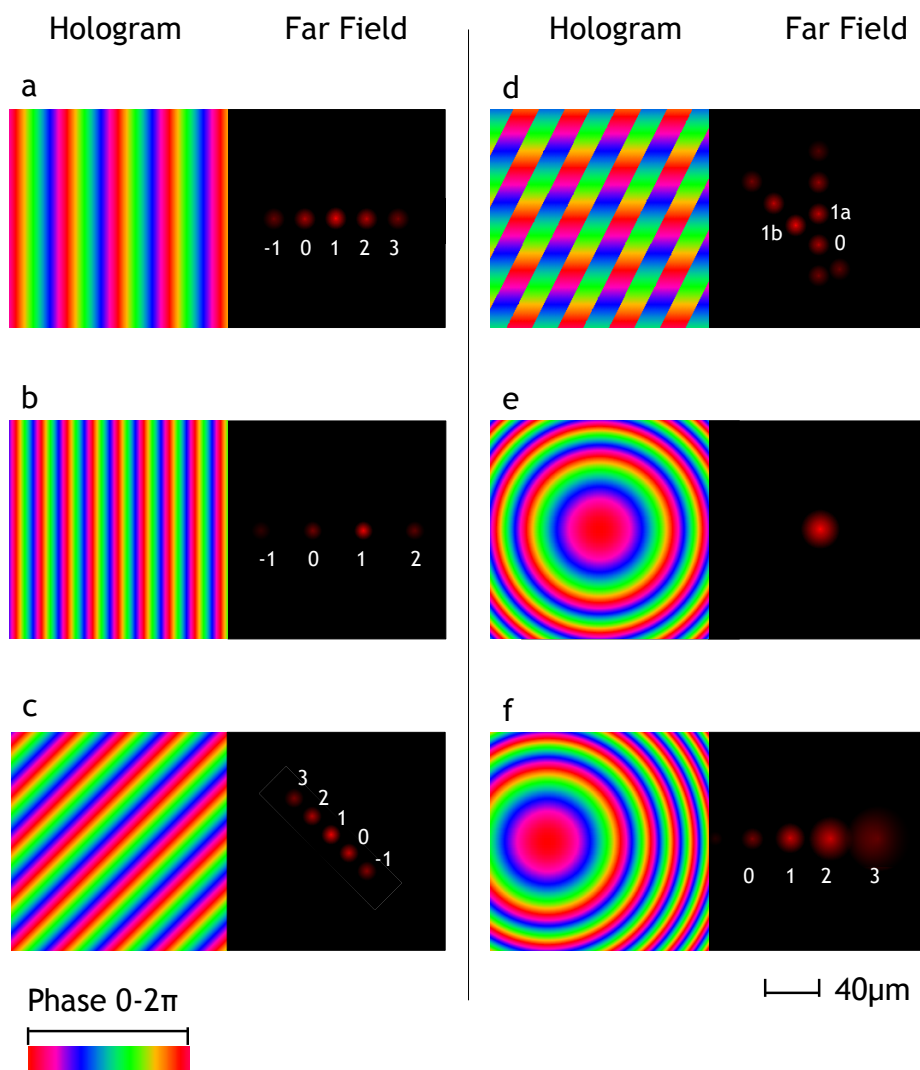
Figure 6.2: A series of phase patterns displayed on the SLM and a representation of the corresponding far field diffraction patterns produced. a) A simple blazed diffraction grating. b) A smaller period grating corresponding to a more widely spaced diffraction pattern. c) A rotated grating corresponding to a rotated pattern. d) The complex sum of two gratings. e) A single Fresnel lens phase pattern. f) The sum of a blazed grating and a lens.

Figure 6.3: Schematic drawing of the Gerchberg Saxton algorithm

intensity fields [124]. However, iterative algorithms are comparatively slow especially for large screen sizes or when used in 3 dimensions. As a consequence these algorithms tend to be used only for applications where high speed is not needed (though with increasing computing power this may change). A number of hybrid algorithms have been proposed in order to make iterative algorithms more suitable for optical trapping [125].

6.3   Image Acquisition and Particle Tracking

As has been mentioned previously much of the work done with optical tweezers has involved tracking the movements of particles. Although particle tracking in optical tweezers is most commonly done with photodiodes my work has centered around the use of fast cameras for the purposes of measuring particle position. Most often CMOS or CCD cameras were used such as those manufactured by Prosilica (GC640 Gigabit Ethernet camera and EC1280 Firewire camera). I designed and built a program for image processing in the hope of making a fast and easy to use system for acquiring experimental data. It is perhaps easiest to break this topic up into two parts. Firstly, the acquisition of data from the camera and secondly, the processing of that data to reveal the particle position.

Image Acquisition

Before processing of the data can occur, the data must be grabbed from the camera. This is made relatively easy due to the the LabVIEW Vision software which uses a standard API to access a variety of different makes of camera. In order to increase the functionality of the software a software wrapper was put over the standard LabVIEW functions to allow simple access to both Gigabit Ethernet and Firewire cameras. This subroutine dramatically simplifies the operation of the software. Since the Prosilica GC640 Gigabit Ethernet camera can run at up to 2000 FPS, in order for the camera to run in a closed loop all processing must take place within 0.5 ms. This puts bandwidth constraints on the acquisition and means that the user interface must be shut down during data acquisition. The image acquisition software therefore

runs in two modes. The standard mode allows the user all reasonable functionality but constrains the speed to be below $\approx 1500FPS$. The data acquisition mode allows the camera to take data at its full speed but does not allow the user to perform operations during this time.

In order to speed the acquisition process further, most fast cameras allow the user to reduce the portion of the chip which is accessed to retrieve pixel information. This decreases the number of pixels to be read and increases the frame rate. Prosilica cameras allow this to be done via a user specified region of interest (ROI). This functionality is integrated into the camera software to allow the user to select one or many regions of interest.

Particle Tracking

Much of the available particle tracking software for optical tweezers requires post processing of the acquired data. In such systems images are saved directly to disk for processing at a later date. Although this allows for more complex analysis of image data it precludes feedback and on-the-fly analysis of data which would be beneficial to many tweezers based applications. For this reason all image processing in my camera software was done in a way which is "real time" i.e. each image taken by the camera is processed into x,y and sometimes z coordinates (in microns) before the next frame is taken. Although subsequent buffering of data may take place this is simplified as it is only necessary to store coordinate data rather than image data. The speed constraint that this imposes means that only a few particle tracking algorithms are suitable.

In order to track a moving object most object tracking algorithms rely on some type of invariance such as shape or colour invariance. The more simply an object can be defined the simpler it is to reduce the search space which is necessary to find it. In the case of optical tweezers the object of interest is most often a silica or latex bead which are both rotationally symmetric and size and shape invariant. Furthermore, the behavior of the image obeys easily generalizable behavior as it moves through the focal plane of the microscope. Other objects of interest include cells bacteria and a variety of biological species. Tracking biological organisms is far

more challenging due to the vast array of different morphology present in biological species.

The camera software utilizes several imaging algorithms making it suitable for a variety of situations.

Centre of Mass (COM) This algorithm thresholds the image with user set values to eliminate background pixels. The center of intensity of each particle is then found using the formula:

$$x_{centroid} = \frac{\sum(x_i P_i)}{\sum(P_i)} \tag{6.4}$$

$$y_{centroid} = \frac{\sum(y_i P_i)}{\sum(P_i)} \tag{6.5}$$

Where P_i is the pixel value and x_i and y_i are the distances in pixels from the top left hand corner of the image. It relies on the focusing effect of the transparent particles to create a bright central region which may be separated from the rest of the image. This works extremely well for silica and latex spheres as long as background is of constant pixel value. Furthermore information about the z displacement through the imaging plane may also be gained. Since for small displacements of a particle through the image plane the intensity of the central region is linear with the displacement [60] a relative displacement may be obtained via the comparison of the background intensity to the thresholded intensity. Although the resulting displacement must be precalibrated, an accurate estimate of the displacement may be achieved.

Dark COM The dark COM algorithm is a variation COM algorithm as above however the pixel values are first inverted to yield a negative of the image. The algorithm gives good accuracy when the illumination or focus is such that is is easier to see the dark edges of the particle rather than a central bright spot.

Fourier Truncated COM First used by Crocker and Grier [60]. The algorithm performs center of mass tracking on an image which has been bandpass filtered by a user specified Fourier filter. Such filtering eliminates undesirable

pixel noise which may influence the SNR of the centroided position data. Furthermore it also eliminates intensity gradients which are often present in the background image. These are often caused due to illumination problems but may also be caused by the sample under study. Due to the computational complexity of this algorithm it can slow the data acquisition process for large regions of interest. Since high pass filtering is useful only over larger regions the region size must be chosen carefully.

Cross-Correlation An effective technique for tracking of a variety of shapes which are rotationally invariant is cross-correlation. A user specified "Ideal Image" is taken and stored in memory. The algorithm then compares all incoming images to the stored image by performing a 2D cross-correlation. Though the technique is effective at giving the position of a particles with more complex shapes such as cells, the computational weight when large regions of interest are specified means that it can be slow. The search space can be reduced however by limiting the correlation area to a region smaller than the object size so long as a good correlation can be still be achieved.

Circle Recognition Using the vision image processing library a native LabVIEW sub VI (Imaq detect circles) can be used to detect circular shapes through rotation invariant pattern matching within a specified region of interest. The algorithm is particularly effective when multiple rings are found as is often the case when Mie diffraction from a circular object is apparent in an image.

Radius Estimation The radius estimation algorithm uses the Dark COM Algorithm to invert the image and apply a threshold. The thresholded image along with the central (x,y) pixel coordinates are then fed into the LabVIEW (Find Circular Edges)sub VI. This algorithm works by taking radial spokes of pixels outwards from the center position. The edges are then detected on each spoke giving the radius of the particle as well as an alternate value for the center of the circle.

Multiparticle Tracking Most of the above algorithms require the user to specify a region of interest around the particle which is to be tracked. However, for

some applications where particles move across the screen a different technique is needed. Thus a multiparticle center of mass algorithm has been implemented via LabVIEW's native IMAQ Particle Analysis Vi. This allows tracking of many particles without selection of a region of interest.

After particle tracking has taken place the coordinates of detected particles must be either saved to disk or fed out to other applications. In an experimental context it is often fastest and more desirable to save the data directly to disk. This avoids detrimental effects in the performance of the software by avoiding a conflict with calls to other functions made by the operating system. It also is often necessary when large amounts of data is generated so that data does not exceed the system's active memory. In a multi-core machine it is possible to accomplish this in parallel with image acquisition and processing, with comparatively little disruption. However, for real time and feedback applications it is desirable to process the data directly. In order to make the data accessible to the programs with the least disruption, data is sent via a Transmission Control Protocol (TCP) connection to another application or computer or is made available via a standard queuing operation.

6.4 Analysis

It is often useful in optical tweezers experiments to directly observe data as it is being taken, both in order to adjust experimental parameters and to allow for immediate interpretation of results. In order to satisfy this demand a LabVIEW data analysis package was constructed to allow data to be simultaneously processed by the camera and displayed to the user.

The analysis software works by extracting data from the camera either from a LabVIEW data queue structure or via a TCP connection. The data can then immediately put into a buffer. The buffered data is then read out into a number of various basic useful mathematical functions the results of which can be displayed to the user. Several basic metrics have been implemented:

- Time dependent auto correlation of particle position

- Power spectra of particle position

- Mean squared displacement of the particle

- Cross-Correlation between X and Y data which reveals rotational movement

- Allan variance which gives information about the time evolution of the data.

Although these metrics do not satisfy all possible user requirements for an optical tweezers program they have been found to be sufficient for monitoring of trapped particles, allowing the user to get information about particle behaviour in a matter of seconds.

6.5 Conclusions

The use of high quality software is crucial to the successful application of SLMs. Software can make or break the success of an experimental procedure. Many algorithms have previously been created for use with spatial light modulators. This gives the experimentalist a large resource on which to draw. Though research in this area is ongoing it is currently possible to gain access to a wide variety of SLM software. This enables SLMs to be used for a variety of interesting applications.

The tracking of particles in real time is a novel twist on previous tracking software and enables SLMs to be further integrated into a cohesive optical tweezers software suite. It is hoped that this software may be useful for further experiments which involve multi-particle position tracking of particles in 3 dimensions.

7th March 2011

Chapter 7

Position Clamping

7.1   Introduction

Although holographic optical tweezers have been widely used for experiments where control over multiple optical traps is crucial they have often been neglected in applications which are time critical as discussed earlier. Conventionally, most SLMs have been limited to a frame rate of 60Hz, which is commensurate with standard video frame rates though some exceptions exist such as the Holoeye LC-R 720. These SLMs originally taken from projector systems are addressed by red, green and blue lights in succession with a frame rate of 180 Hz. However, since each frame is not independently addressable they are not capable of dynamically addressing faster than 60Hz. Recently Boulder Nonlinear (BNS) [17] released a SLM capable of a 203Hz frame rate. Although such speed is modest in comparison with faster control systems like acousto-optic deflectors (AODs) it creates the possibility that SLMs could be used in closed loop control systems for multiple particles. Such closed loop control has been used previously to achieve both position and force clamping of particles in optical traps. Position clamping reduces the effect of Brownian motion on the position of a trapped particle by dynamically moving the the optical trap in the opposite direction of the particle's instantaneous displacement from a fixed point. This makes the system extremely sensitive to disturbance. Force clamping however regulates the forces exerted by the particle on other objects surrounding the particle thus preventing damage to biological specimens [126]. A number of papers have been

previously published on this subject, commonly using either galvanometer-driven mirrors or AODs to provide the movement of the optical traps and photo-diodes to provide feedback based on particle position [127, 128]. However feed back control is not limited to this as piezeo stage control [126] and intensity modulation [38] have also been used. These techniques have have been useful particularly in biological experiments such as [129] where the increased sensitivity can be useful in precise force measurement.

A holographic approach has rarely been used with the exception of [37]. Since a 60 Hz Holoeye (HEO 1080P) SLM was used in this case, the feedback loop time was comparatively slow (0.26 seconds). However, with increased SLM refresh rate and high speed cameras [130, 131] a SLM based closed loop feedback system begins to look more viable. In collaboration with Richard Bowman a theoretical model and OpenGL software was developed which was used to facilitate the goal of creating a system which was capable of clamping particles effectively with an SLM.

7.2 Theory

As mentioned in chapter 2 the motion of a particle in an optical trap can be described as a Langevin equation [45]. If this equation is modified such that the restoring force is given by $k\left(x - x_{\text{trap}}(t)\right)$ the equation can be modified to:

$$m\ddot{x} + \gamma\dot{x} + k\left(x - x_{\text{trap}}(t)\right) = \zeta(t) \tag{7.1}$$

Here $m\ddot{x}$ is the inertial term, x is the position of the particle, $\gamma\dot{x}$ is the Stokes' drag force and $\zeta(t)$ represents the force exerted on the bead by the thermal motion of the liquid molecules. $x_{\text{trap}}(t)$ is the time dependent displacement of the optical trap from a predefined trap center. If the feedback system was instantaneous the increased trap displacement would simply create a stiffer optical trap. However due to latencies in the system this is impossible.

A variety of mechanisms are responsible for the latency of the system. In order to derive an expression for the overall latency we must take account of these factors.

Firstly, we must consider the SLMs refresh rate which happens at successive

intervals. This gives rise to low pass filtering $sinc(\omega\tau_{SLM}/2))$ of the signal as well as an effective latency of half the update period $\exp(i\omega\tau_{SLM}/2))$ (here τ_{SLM} is the update period of the SLM). We neglect aliasing given by $\sum_m \delta(\omega - 2\pi m/\tau_{SLM})$ since the power spectrum falls sharply with ω and the low pass filtering from the SLM acts as an anti-aliasing filter. The finite response time of the system, $\tau_r \approx 2ms$, can be modeled by the transfer function $1/(1 + i\tau_r\omega)$, while the additional latency in the system caused by the time taken for image acquisition and the software is represented by transfer function $exp(i\omega\tau_{lag})$.

Taking the convolution of these factors and then Fourier transforming leads to an expression for the frequency dependent trap position $\widetilde{x}_{trap}$[1] given by:

$$\widetilde{x}_{trap} \approx -\tilde{x} \times \tilde{f}(\omega)sinc(\omega/\tau_{SLM}/2)\exp^{-i\omega(\tau_{SLM}/2+\tau_{lag})}\frac{1}{1+i\tau_r\omega} \qquad (7.2)$$

Where $\tilde{f}(\omega)$ represents filtering in the control loop, the update interval of the SLM is $\tau_{SLM} = 5ms$, the response time of the SLM is $\tau_r = 2ms$ and τ_{lag} is the latency in the camera and software. Assuming that the corner frequency $f_c \ll \omega_{SLM}$ it is possible to derive an expression for the power spectrum of a bead in a closed loop holographic trap:

$$S_x = \gamma k_B T/\pi \mid -\omega^2 m + i\gamma + k + k\tilde{f}(\omega)sinc(\pi\omega/\omega_{SLM})\exp^{-i\omega(\tau_{SLM}/2+\tau_{lag})}/(1+i\tau_R\omega)\mid^{-2}$$
$$(7.3)$$

The assumption that $f_c \ll \omega_{SLM}$ however restricts us to relatively weak traps or highly viscous fluids. The spectra predicted by this equation exhibits the expected suppression of Brownian motion at low frequencies decreasing the mean squared deviation proportionally with increased gain, but has a resonance at a frequency of approximately $(\tau_{2SLM} + 4\tau_{lag} + 2\tau_r)^{-1}$ (see Fig.7.4). Due to the Bode sensitivity theorem (see Appendices) it is impossible to reduce the peak caused by the resonance of the trap, the peak may however be shifted. As a result of the above analysis we can see that the impact of the peak on the MSD is reduced as it is shifted towards

---

[1]Here tidla "~" represents the Fourier transform of a quantity.

higher frequencies. Hence the overall performance of the feedback depends on the lag time of the entire system.

7.3   Experimental Setup
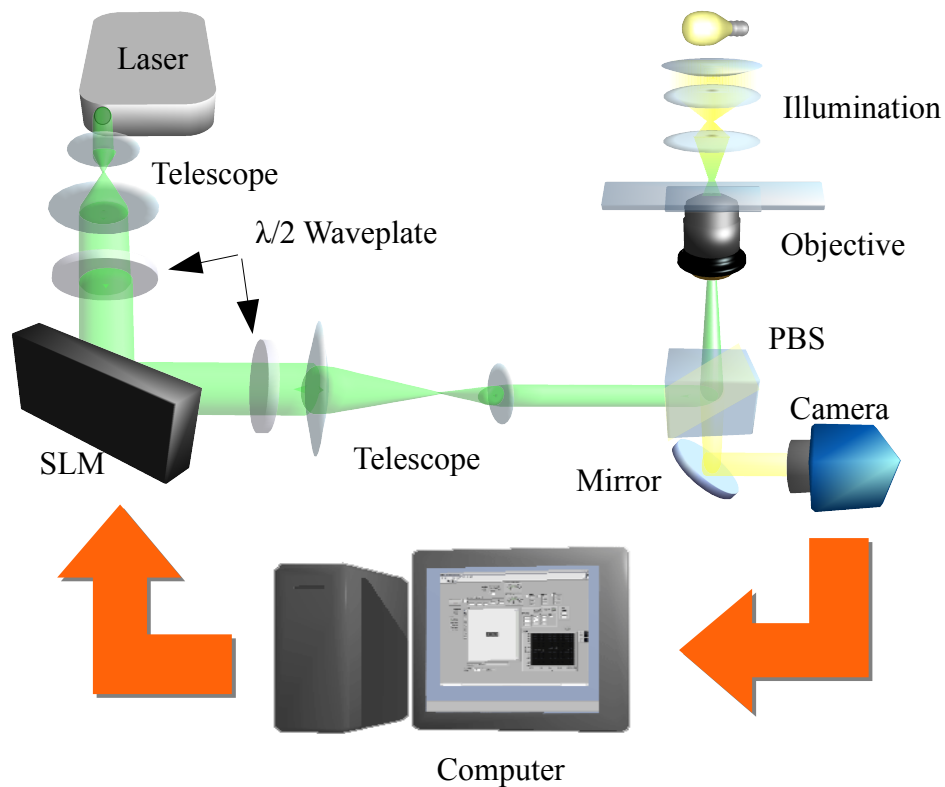
Figure 7.1: Experimental setup: A standard holographic optical tweezers set up was used. $\lambda/2$ Wave plate, Beam telescope, $\lambda/2$ Wave plate, Beam steering lenses and Condenser lens.

A 532nm frequency doubled Nd:YAG Laser (Laser Quantum) was used to generate trapping beams. The laser has a maximum power output of 3 Watts however it was generally used operating power of approximately 1 Watt. Optimization of diffraction efficiency and maximum transmission through the polarizing beam splitter was achieved with two $\lambda/2$ wave plates. The spatial light modulator used was

a BNS (XY Series) 512x512 pixels, operating at 203Hz, 16 bit. The beam is then directed into an inverted Zeiss Microscope (Axiovert 200) via a polarizing beam splitter cube. The objective lens was an oil immersion Zeiss 100X Plan-Neofluar (N.A. 1.30). Image data is collected and sent via Ethernet cable to the computer (Dell PC with Intel Xenon processor).

7.4 Software for Feedback

After acquisition of image data from the Prosilica GC640 Gigabit Ethernet Camera a center of mass algorithm [60] (see Chapter 6) was used to obtain the particle position. It was also possible to use the ratio of pixels above and below the threshold value in a similar way to [60,132]. In order to estimate the axial particle movement. In order to create a feedback system suitable for clamping a particle a PID (Proportional,Integral,Derivative) control was used [128]. The new trap position was given as:

$$x_{trap} = -(k_p x + k_i \sum_0^{n=i} x_n + k_d(x_i - x_{i-1})) \tag{7.4}$$

Here x_{trap} is the new trap position, k_p, k_i, k_d are the gains for the proportional, integral and derivative terms. In practice it was found that best results where gained by use only of the proportional and integral terms. The new position was then used to calculate a new kinoform changing the position of the optical trap to the desired trap position. Thought the PID control was done in LabVIEW in order to speed up calculation time, and minimize latency, hologram generation was done on the graphics card (NVIDIA Quadro FX 5600) via OpenGL. The system of gratings and lenses used by Lisener [55] was used for this calculation due to the simplicity and speed of the method.

Calculation of large arrays of data is a time consuming task. The use of graphics card technology is a way by which this slow operation can be sped up considerably. The parallel computing architecture of graphics cards (in the case of the nVidia Quadro FX 128 different parallel processors, each with its own RAM) makes it possible to calculate holograms extremely quickly. By efficiently optimizing the calculation algorithm such that the calculation is done over each pixel only returning

a completed hologram at the end of the algorithm and by minimizing the number of memory swaps between the graphics card and the main processor hologram calculation speeds in excess of 200Hz can be achieved. This is done by the use of the OpenGL custom shader language which allows holograms to be calculated and then displayed directly onto an external monitor or SLM. Such a system allows holograms to be calculated in less than a millisecond, significantly reducing the overall latency of the system. Though nVidia's CUDA environment had been used previously for hologram calculation it requires the resulting hologram to be re-rendered after the calculation has been returned to the CPU from the graphics card. This adds additional latency (approx. 5-15 ms for a 512x512 hologram) back into the system.

7.5 Test of the Systems Response

In order to create a system capable of position clamping it was necessary to know the latency of the system and then to reduce that latency to a minimum. In order to determine this accurately the closed loop latency was measured via a trap switching algorithm. The gratings and lenses algorithm was used to alternately switch traps between two positions. The fast camera was then used to monitor the intensity of the light in each position. The signal from the camera and the driving signal were then compared to determine the latency. It is noticeable from Fig.7.2 that the intensity profile for a single trap switched between two positions produces a waveform typical of a low-pass filtered square wave. It is plausible that this is caused by the response time of the liquid crystals aligning to the electric field as the phase of the SLM is changed. As the liquid crystal responds more quickly to the presence of an electric field than it does to the absence of one the responses are not evenly biased.

7.6 Results

Fig. 7.3 shows the position traces of three beads trapped along a line. It should be noted that trapping along a line aides the camera acquisition speed since image
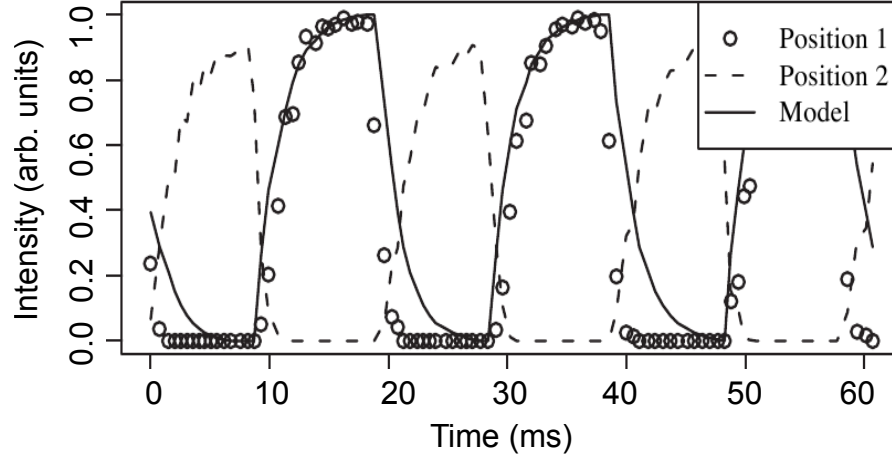
Figure 7.2: The normalized intensity of a trap as it was modulated two positions. The figure also shows the SLM response as fitted by the theoretical model of the SLM responce noted in the theory section. The parameters used to calculate this trace are the same as those used to fit the graphs in Fig.7.4.

information is read in line by line. However, similar experiments were also conducted with a triangular arrangement of beads. It can be clearly seen that in the clamped case, the beads spent significantly more time in the trap center. This demonstrates the unique ability of holographic systems to perform position clamping on multiple particles simultaneously.

The mean squared displacement of the beads from the trap center decreased by 44%±7% which corresponds to a increase in trap strength $k = k_B T/x^2$ of 77%±12%. (see Fig.7.4 (Right)) Clearly this demonstrates that effective position clamping can be achieved even in multiple optical traps. Fig.7.4(Left) shows the power spectral density of a single trapped $5\mu m$ silica bead as the feedback gain is increased. It is noticeable that although at low frequencies the MSD is indeed reduced however at higher frequencies it is increased. A trap stiffness of $k = 2.1 \times 10^{-6} Nm^{-1}$ was measured by fitting the Lorentzian power spectrum when there was no feedback.

Taking the response time as 2ms, with the update rate of the SLM being 203 Hz, we compared the results to the theoretical predictions. The experimental result gave a good fit although the resonance peak height appeared to be less than the
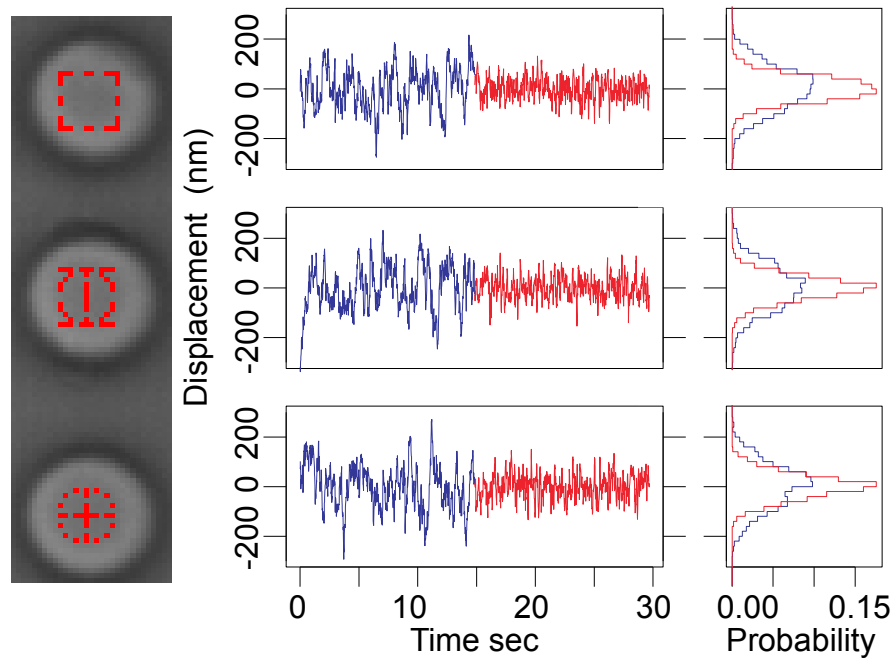
Figure 7.3: The position traces for three trapped $5\mu m$ silica beads (unclamped - blue and clamped red). The associated histograms show the likelihood of finding a bead in at a given distance from the center. The left hand images are of the three trapped silica bead the red marks indicate the COM algortihims calculation of their centers.
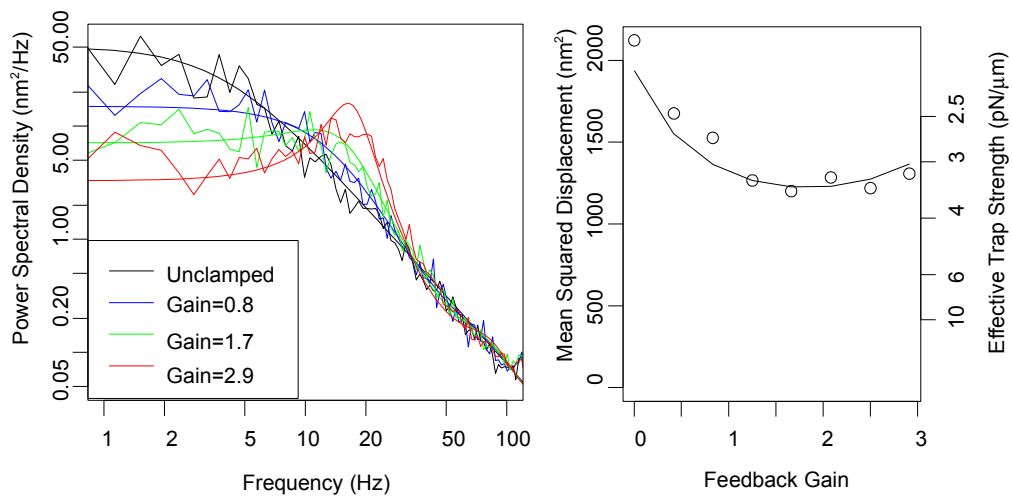
Figure 7.4: (Left) Graphs showing the the power spectral density of a trapped $5\mu m$ silica bead as the feedback gain is increased (theoretical and experimental results are shown). (Right) Graph of the mean squared displacement of the particle as the feedback gain is increased.

7th March 2011
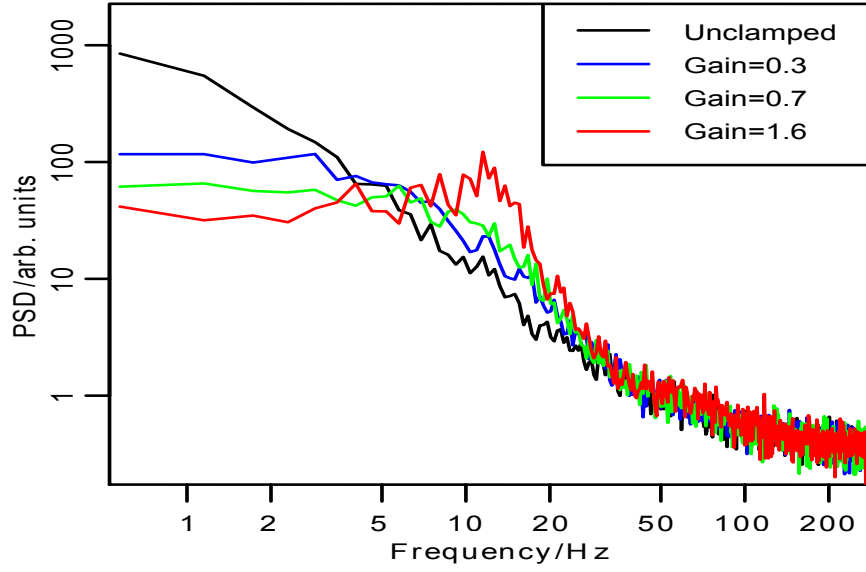
Figure 7.5: The PSD of a $5\mu m$ bead in the axial direction.

predicted value. This could be because the finite trap depth of real systems, which rather than continuing to increase in stiffness as the particle moves away from the trap, in fact disappears when $x - x_{\text{trap}} \gtrsim a$.

By using the COM algorithm and measuring the intensity fluctuations of the image of the bead (due to its movement caused by Brownian motion) with respect to the background illumination, it is possible to gauge the axial displacement of the bead from the focal plane. Using this method it was possible to implement a feedback algorithm in the axial direction. Fig. 7.5 shows the power spectral density of the axial displacement of a trapped $5\mu m$ bead. This was determined by looking at the defocusing of the bead, and is shown with arbitrary units. As the feedback gain is increased a suppression of the low frequency motion can be seen with resonance appearing at higher frequencies.

Unfortunately the magnitude of the low frequency suppression is much less than that of the transverse direction with a decrease in the MSD of only 8%. This is could be due to inaccuracy in the position detection which is a compromise to the algorithms speed.

7.7   Feed Forward Control

As a mater of interest, experiments were also carried out using closed loop control to add a suitable displacement to a particle already experiencing movement due to Brownian motion. In this case, a negative gain was applied to the instantaneous displacement of the particle causing an increased movement away from the predefined trap center. Rather than position clamping this is closer to force clamping. Which limits the total restoring force which can be applied to the particle. As an extension of this the particle could be given feedback relative to its previous position rather than to a predefined position. In this method, the particle was allowed to move across the screen in a sort pseudo-diffusion. This is only possible using camera tracking which provides a wide field of view. A photo diode system, although faster, would constrict the particle position to a restricted area thus rendering such experiments impossible. As the gain was increased the power spectrum of particle position could be seen to look as if the particle was experiencing unbounded Brownian motion. These experiments provide a basis for performing further experiments whereby the effective diffusion of particles can be controlled externally while maintaining the characteristic effects of a low Reynolds number system.

7.8   Conclusions

The limited bandwidth of the Boulder SLM (203Hz) makes it difficult to suppress Brownian motion except at very low frequencies. The system is capable of reducing the mean squared displacement of trapped $5\mu m$ silica beads positions by 44%. As SLM technology improves this situation will improve. The combination of fast camera processing and hologram calculation using the graphics card does demonstrate that such systems are both practicable in terms of information processing as well as in implementation. Unlike Photo diode and AOD systems, a SLM based system enables position clamping of multiple particles in three dimensions. This added flexibility may be very useful in a variety of biological experiments where position or force clamping of multiple particles may be helpful. It also opens the door to feedback with novel shaped beams and nanotools.

7th March 2011

Chapter 8

Wideband Microrheology

8.1 Introduction

As has been mentioned in chapter 2, one of the major uses of optical tweezers
has been for conducting micro-rheological measurements. The small scale of the
optical trap system allows for the measurement of fluctuations in the nanometer
regime, a domain where the dominant physical forces are often far different from
those at macroscopic scales. Not only does this give new insight to fundamental
physics [133], and a better understanding of the properties of materials but it also
allows rheological testing of bio-materials such as cells. [134–136].

Conventional rheology is especially interested in those materials usually liquids
or gels which depart from the conventional Newtonian principles of elasticity such as
linear viscoelastic behavior. Micro-rheology follows this approach. Since the elastic
properties of a given material are often completely unknown in a micro-rheological
experiment it is crucial not to assume a linear viscous response such as that in water.

Conventionally the viscoelastic properties of a material are measured via the
application of an oscillatory strain and the measurement of the oscillatory stress. In
a viscous material stress lags strain by a $\pi/2$ phase lag. However in a viscoelastic
material the phase lag is unknown.

We can write strain as $\varepsilon(\omega, t) = \varepsilon_0 \sin(t\omega)$ and stress as $\sigma(\omega, t) = \sigma_0 \sin(t\omega + \delta)$.
Consequently we can write the shear storage (elastic) and loss (viscous) moduli
as $G'(\omega) = \frac{\sigma_0}{\varepsilon_0} \cos\delta$ and $G''(\omega) = \frac{\sigma_0}{\varepsilon_0} \sin\delta$, respectively. It is then convenient to

represent this as the linear frequency-dependent dynamic complex modulus $G^*(\omega)$ where $G^*(\omega) = G'(\omega) + iG''(\omega)$. This provides information about both the elastic and viscous properties of the material *[137]*.

As has been mentioned earlier in this thesis the viscosity of the medium in which a trapped particle is immersed is often a key factor in the statistical distribution of the time-dependent position of the particle. For this reason measurements of the viscosity of the trapping medium are easily achieved using optical tweezers. Furthermore, effects such as Faxén's correction for the viscosity of a fluid close to an infinite wall [45, 138] have also been widely studied. However, when micro-rheological measurements of viscoelastic substances have been made the results are limited to the high end of the frequency response [139–141], either leaving out the low frequency response or taking account of the low frequency response only by the use of other techniques such as rotational rheometry [142] or passive video particle tracking micro-rheology [39]. In both cases this has been done without showing an over lapping region, leaving a significant information gap.

8.2   Wide-band Microrheolgy

In order to gather as much information as possible about the frequency dependent linear viscoelastic nature of the medium around an optically trapped particle, a method was adopted to measure both the high and low frequency responses. Firstly, a conventional "steady state" method was applied in which the thermal fluctuations were measured simply by tracking the thermal motion of a trapped particle held in a stationary optical trap. The optical trap was then moved to a new position a distance D_0 from the first trap position and the tracking repeated. Secondly, the "transient" time-dependent position of the particle was tracked. A single optical trap was switched alternately between the two predefined positions, causing the trapped particle to move with a characteristic time-dependent path between the two trapping positions.

By measuring the "steady state" behavior of the trapped particle it is possible to get information about the high-frequency viscoelastic response as well as to obtain
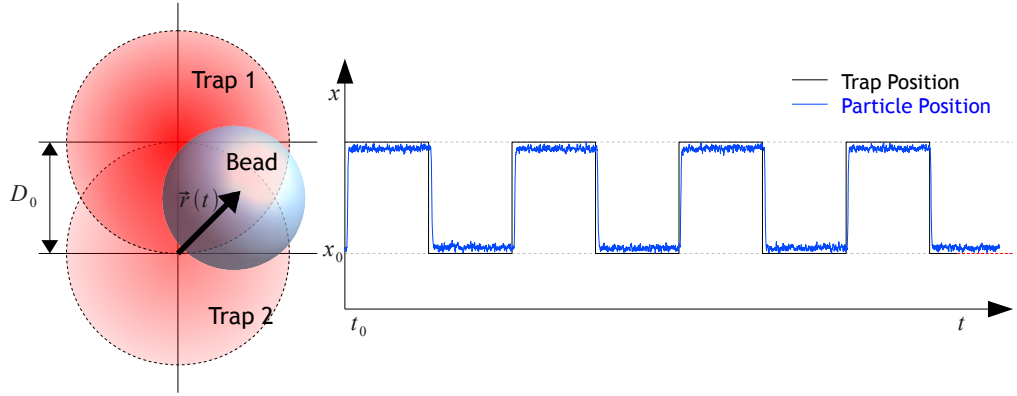
Figure 8.1: Arrangement of the optical traps and particle position as the traps are switched alternately on and off.

the trap stiffness at each trap position. By measuring the "transient" particle position it is possible to gain information about the low-frequency viscoelastic response. In principle information can be gathered about a wide range of frequencies by exerting a perfect impulse on such a system; however, this is in practice limited by a number of experimental considerations. Firstly, the fidelity of the impulse is limited both by indeterminacy in closed-loop bandwidth of the tweezers system. Also, the measured response is limited by the detector resolution and the length of the experiment. Furthermore since the particle undergoes constant Brownian motion a degree of systematic noise is to be expected. However, by combining all the information, the material's entire viscoelastic spectrum is resolvable within the limits of the experimental system.

8.3   Experimental Model

Much of the theory for the method was developed by my collaborator Manlio Tassieri [138,143,144]. However, in order to aid understanding I will recapitulate much of the theory here. A full derivation of the formulae used can be found in the appendices.

We first adopt a generalise Langevin equation Eq.8.1 in a similar way to [45]. We sum the forces in the system at a given point in time such that

$$m\vec{a}(t) = \vec{f_R}(t) - \int_{t_0}^{t} \zeta(t-\tau)\vec{v}(\tau)d\tau - \kappa_i \vec{r}(t), \qquad (8.1)$$

where m is the mass of the particle, $\vec{a}(t)$ is its acceleration, $\vec{v}(t)$ is its velocity and $\vec{f_R}(t)$ is the Gaussian white-noise term representing stochastic thermal forces acting on the particle. The integral term represents the viscous damping of the fluid, which incorporates a generalized time-dependent memory function $\zeta(t)$. The memory term can be thought of as the convolution of the time-dependent response of the material with the time-dependent impulse. This yields an output function commensurate with the drag at a given time this is explained in greater detail in [137, 143].

As has been mentioned, the method may be split into two distinct steps. The first is a measurement of the "steady state" behavior of trapped bead in each of the two trapping positions. The second is an analysis of the time-dependent path of the bead as it moves between these two positions. Let us first consider the "steady state" case where only one optical trap is on and the bead is at thermal equilibrium. In this case the traps each have an associated trap stiffness κ_1 and κ_2. The trap stiffness can be calculated for each trap via the equipartition theorem, i.e.

$$\frac{3}{2}k_B T = \frac{1}{2}\kappa_i \sigma^2, \qquad (8.2)$$

where, k_B is Boltzmann's constant, T is the sample temperature and σ^2 is the time-independent variance of the particle displacement from the trap centre.

It has been mentioned previously that there are several methods for determining the trap stiffness such as fitting the power spectrum or calculating trap stiffness via the Stokes' drag [45, 145]. The equipartition method is the only method which is independent of any assumptions about the viscoelastic properties of the material under investigation and is thus essential from a rheological viewpoint.

Apart from the trap stiffness, the high-frequency viscoelastic properties of the fluid may be analyzed at this stage, since the bead's position is subject to high-frequency thermal fluctuations via Brownian motion. It is then possible to record the high-frequency response of the fluid under test via the normalized position auto-correlation function $A(\tau)$.

$$A(\tau) = \frac{\langle \vec{r}(t_0)\vec{r}(t_0 + \tau)\rangle_{t_0}}{\langle r(t_0)^2 \rangle_{t_0}} \tag{8.3}$$

We are at this stage only limited at high frequency by the bandwidth of the position sensor. Here the time-dependent position of the trapped particle is given by the displacement vector $\vec{r}(t)$. The term $\langle r(t_0)^2 \rangle_{t_0}$ is the time-independent variance and the brackets $\langle ... \rangle_{t_0}$ denote an average over all initial times t_0. This is equivalent to σ^2 in Eqn.8.2. Taking the Laplace transform of Eq.8.1 over all time one may derive an expression relating the Laplace transform of $A(\tau)$ to the trap stiffness κ_i and the Laplace transform of the memory function $\tilde{\zeta}(s)$.

$$\tilde{A}(s) = \left(s + \frac{\kappa_i}{ms + \tilde{\zeta}(s)} \right)^{-1} \tag{8.4}$$

where $\tilde{A}(s)$ is the Laplace transform of $A(\tau)$, s is the Laplace frequency, m is the mass of the particle and $\tilde{\zeta}(s)$ is the Laplace transform of the memory function. By following Mason and Weitz [146] and substituting $\tilde{\zeta}(s) = 6\pi a\tilde{\eta}(s)$ as well as $G^*(\omega) \equiv s\tilde{\eta}(s)|_{s=i\omega}$, the following function can be derived.

$$G^*(\omega) = \frac{\kappa_i}{6\pi a} \left[\frac{i\omega \hat{A}(\omega)}{\left(1 - i\omega \hat{A}(\omega)\right)} + \frac{m\omega^2}{\kappa_i} \right] \tag{8.5}$$

where $\hat{A}(\omega)$ is the Fourier transform of $A(\tau)$ and, as mentioned before, the inertia term $(m\omega^2)$ can be neglected for frequencies $\omega \ll$ MHz. It is noteworthy that the above substitution recovers the well known relation

$$A(\tau) \rightarrow \exp\left(-\Gamma_i\tau\right) \tag{8.6}$$

Which is valid in the case of a Newtonian fluid where $\Gamma_i = \kappa_i/6\pi a\eta$ is the characteristic relaxation rate of the system and which has been used extensively in the optical tweezing community [38, 45].

The second step is the analysis of the time-dependent path of the particle as the optical trap is switched between two positions. We consider two positions to be a distance D_0 apart. When one trap is in the "on" state then we assume that

there is no light in the other and vice versa. In practice this assumption is not completely true since in a spatial light modulator the switching time of the liquid crystals is finite. However as has been shown previously this is in the region of 10 ms. Nevertheless since we are interested in determining the low frequency response with this step so it is of little consequence. Rather it is more critical that the frequency of trap switching does not exceed the characteristic relaxation time of the material under test. If the time-dependent position of the particle is expressed in terms of the distance between the two trapping positions D_0 and this distance does not exceed the region in which the particle feels a trapping force which is linear with displacement from each trap center then the same Langevin equation used in the previous step may be employed. This yields

$$G^*(\omega) = \frac{1}{12\pi a} \sum_{i=1,2} \left[\frac{\kappa_i i\omega \hat{D}(\omega)}{\left(1 - i\omega \hat{D}(\omega)\right)} + m\omega^2 \right] \tag{8.7}$$

Where $\hat{D}(\omega)$ is the Fourier transform of $D(t)$, $D(t) = |\langle \vec{r}(t) \rangle| / D_0$, and the sum takes account of transitions between traps where the particle is moving in different directions.

In steps I and II equations 8.5 and 8.7 both require a Fourier transform of the data to be performed. However the Fourier transform of real data (i.e. a non-analytic discrete data set.) for the purposes of data analysis is difficult. One reason for this is that interpolation and extrapolation of data may produce artifacts, while smoothing of the data hides unexpected effects and distorts the data. With this in mind a technique first used by Evans [143] is adopted.

Since the data sets of both the normalised position auto correlation function $A(\tau)$ and the creep compliance of the material $D(t)$ have a set of distinct characteristics i.e. They are expected to have the limits $A(0) = D(0) = 1$ and $A(\infty) = D(\infty) = 0$. Furthermore both functions are necessarily positive and real and have discreet set of unevenly spaced data points. Evans deduces via subsitution of known values into a generalsed fourier transform of the time- dependant compliance the the following equation.

$$-\omega^2 \hat{g}\left(\omega\right) = i\omega g(0) + \left(1 - e^{-i\omega t_1}\right)\frac{(g_1 - g(0))}{t_1} + \dot{g}_\infty e^{-i\omega t_N} + \sum_{k=2}^{N}\left(\frac{g_k - g_{k-1}}{t_k - t_{k-1}}\right)\left(e^{-i\omega t_{k-1}} - e^{-i\omega t_k}\right)$$

$$(8.8)$$

Here $\hat{g}(\omega)$ is the Fourier transform of any time-dependent quantity $g(t)$ sampled at a finite set of data points (t_k, g_k), where $k = 1\ldots N$. $\dot{g}_\infty$ is the gradient of $g(t)$ extrapolated to infinite time. Also $g(0)$ is the value of $g(t)$ extrapolated to $t = 0^+$. However since $\dot{g}_\infty = 0$ and $g(0^+) = 1$, the extrapolated values vanish and the formula may be simplified to:

$$-\omega^2 \hat{g}\left(\omega\right) = i\omega + \left(1 - e^{-i\omega t_1}\right)\frac{(g_1 - 1)}{t_1} + \sum_{k=2}^{N}\left(\frac{g_k - g_{k-1}}{t_k - t_{k-1}}\right)\left(e^{-i\omega t_{k-1}} - e^{-i\omega t_k}\right) \quad (8.9)$$

The use of this formula not only reduces artifacts it also eliminates the need for Laplace/inverse-Laplace transformations of experimental data [147].

8.4   Experimental Setup

Trapping is achieved using a CW Ti:Sapphire laser system (M Squared, SolsTiS) which provides up to 1 Watt at 830nm. Holographic optical traps are created via the use of a spatial light modulator (Boulder XY series) [148] in the Fourier plane of the optical traps. The tweezers are based around an inverted microscope, where the same objective lens, $100\times$ 1.3NA, (Zeiss, Plan-Neofluor) is used both to focus the trapping beam and to image the resulting motion of the particles. Samples are mounted in a motorized microscope stage (ASI, MS-2000). Particles are imaged using bright-field illumination. We use a Prosilica GC640M camera to view the trapped particle and our own suite of camera analysis software written in LabVIEW to measure the position of the trapped particle in real time at up to 2kHz.
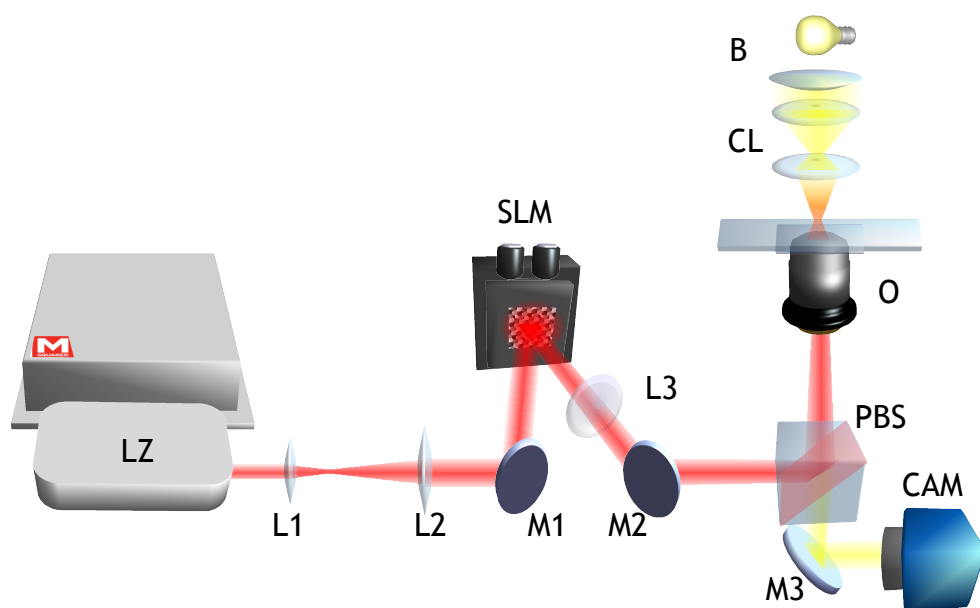
Figure 8.2: Experimental setup from left to right: (LZ) Ti:Sapphire laser system, (L1 and L2) beam telescope, (M1 and M2) folding mirrors, (SLM) Boulder fast SLM,(L3), (PBS) polarising beam-splitter cube, (M3) mirror, (CAM) Prosilica fast camera, (O) objective lens, (CL) condensing optics, (B) 250W halogen bulb.

8.5   Results

In order to test the system in the case of a simple Newtonian fluid, a sample of $5\mu m$ silica beads was suspended in water. In order to main the linearity of the gradient force to dispacement of the particle from the trap center the optical traps' separation was specified to be no more than 0.8 of the particle radius [32], setting $D_0 = 1.6\mu m$ we get $D_0/a = 0.64$. The flipping period was specified to be 20 seconds. Both steps of the experimental procedure were performed and the normalised position-autocorrelation function and normalised step response were obtained. When the "transient" portion of the experiment was carried out in order to reduce noise created by random fluctuations twenty individual flips where averaged together to produce a mean step response (see Fig.8.3). The particle position was seen to move quickly between trap centers in a characteristic simple exponential decay. This was substantiated by the normalised position auto-correlation function $A(\tau)$ of the "steady state" step which displayed the characteristic exponential relaxation rate that depends on the bead radius, fluid viscosity and trap stiffness Fig.8.6.

When a viscoelastic solution of Polyacrimide (PAM) concentration 1% w/w was used the 5 μm silica bead could be seen to move between trap positions at a slower rate (a few seconds). This can be seen in Fig.8.3 where the averages step response of both water and PAM can be seen. Twenty steps were averaged together to each with a period of 20 seconds. The normalized position auto-correlation functions $A(\tau)$ (see Fig.8.4) displayed a far more complex behavior since there is a time-dependent change in the viscous drag.

However only when the normalised transient step response $D(t) = |\langle\vec{r}(t)\rangle|/D_0$ and the normalised position auto-correlation functions $A(\tau)$ are transformed using the method of transforms shown in Eq.8.9 to give the dynamic complex modulus G^* via Eq. 8.5 and 8.7 can the overlapping regions be seen. Fig.8.5and Fig.8.6 show the values for water and PAM (concentration 1% w/w) respectively. A clear overlapping region can be seen in the data despite experimental noise. This both verifies the self consistency of the technique and provides a useful method for error analysis. The low-frequency data from flipped traps can be seen to be progressively noisier at higher frequencies, (presumably limited by the performance of the SLM), while the
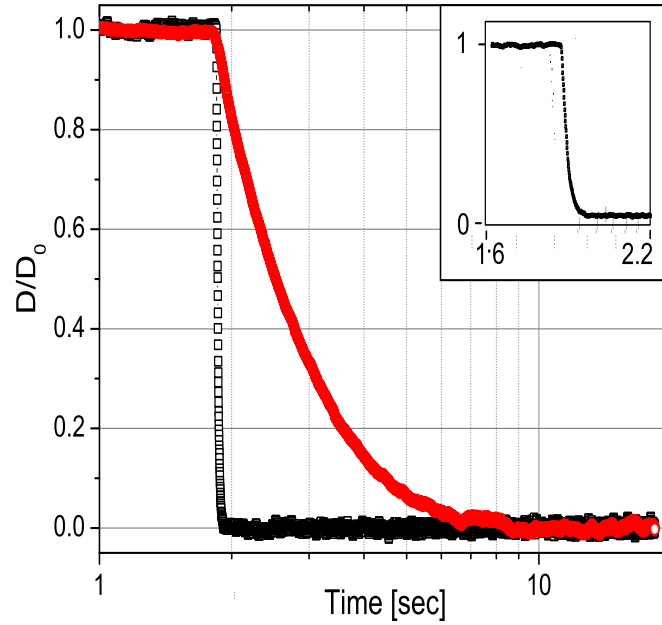
Figure 8.3: The normalised mean bead position of successive steps from shown firstly, in water (Black) and then in a water-based solution of PAM of concentrations of 1 % w/w (red). Inset shows a scaled up version of the same graph for water demonstrating the that a simple exponential decay also occurs for water though over a shorter time scale.
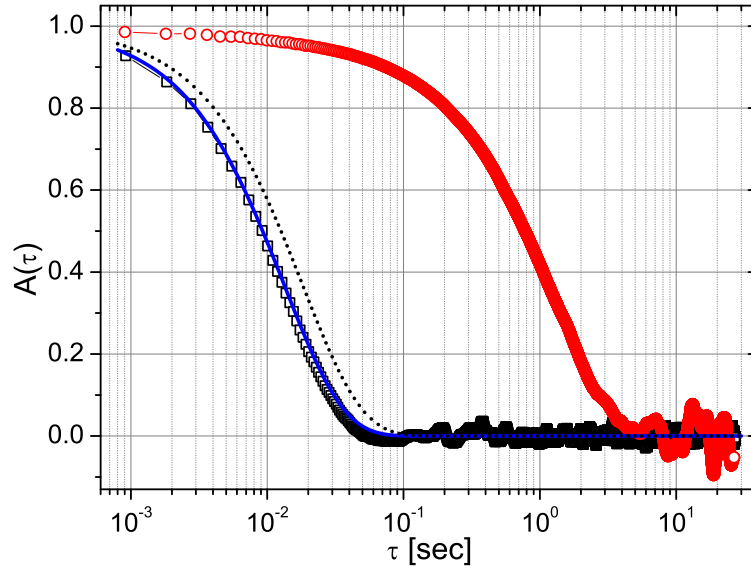
Figure 8.4: The normalised position auto-correlation function *vs.* lag-time of a $5\mu m$ diameter silica bead (squares) in water (with $\kappa = 2.7\mu N/m$) and (circles) in a water-based solution of PAM at concentrations of 1 % w/w (with $\kappa = 2.2\mu N/m$). The continuous and dotted lines represent Eq. (8.6) for a $5\mu m$ diameter bead in water at $T = 25^{o}C$ with $\kappa = 2.7\mu N/m$ and $\kappa = 2.2\mu N/m$, respectively.

7th March 2011
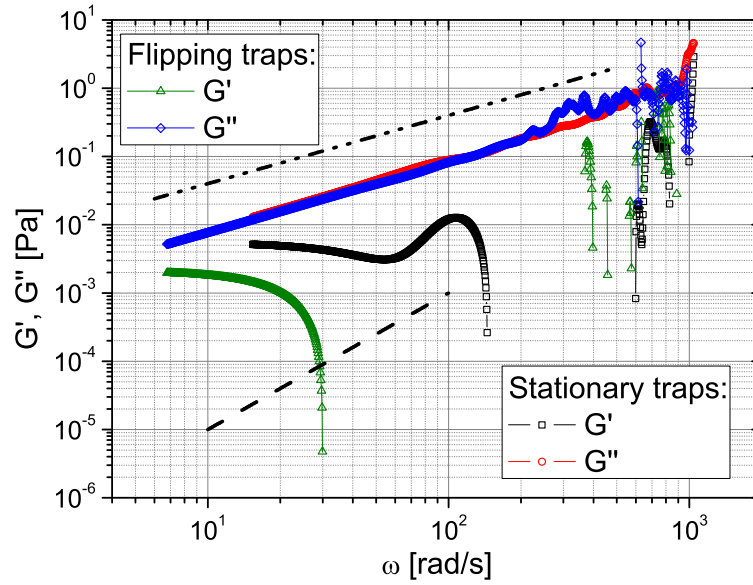
Figure 8.5: Storage (G') and loss (G'') moduli of water *vs.* frequency, analysed using both Eq. (8.5) (high frequencies) and Eq. (8.7) (low frequencies) applied directly to the experimental data presented in Fig. 8.4 and Fig. 8.3, respectively. The lines represents the expected limiting behavior of the moduli when the material reaches the terminal region: $G' \propto \omega^2$ and $G'' \propto \omega$.

higher- frequency data from "steady state" measurements maintains its noise level up until the frequency limit of the camera acquisition. As has been noted previously, the switching time of liquid crystal SLMs is not instantaneous; thus rather than displaying instantaneous kinforms the SLM fades in and out [148]. Furthermore, since the update cycle of the SLM is predetermined by its clock speed, there is a slight ambiguity in the starting time of the SLM update. In order to account for this error a simple correlation algorithm was used to eliminate time shifted step responses. Both of these factors only affect the high-frequency response of the step response.

Fig. 8.5 shows fluctuations of the Shear storage (elastic) modulus (G'). Since water is a purely viscous fluid this behavior should not be present. This error is caused by the presence of low frequency experimental noise in the system. Since a comparatively few flips were averaged together (6 above) an increased number of measurements (around 30) should eliminate this error. These errors can also be eliminated by fitting a smooth curve to the normalised position autocorrelation and normalised transient step response functions. In general the results are favorable and

7th March 2011
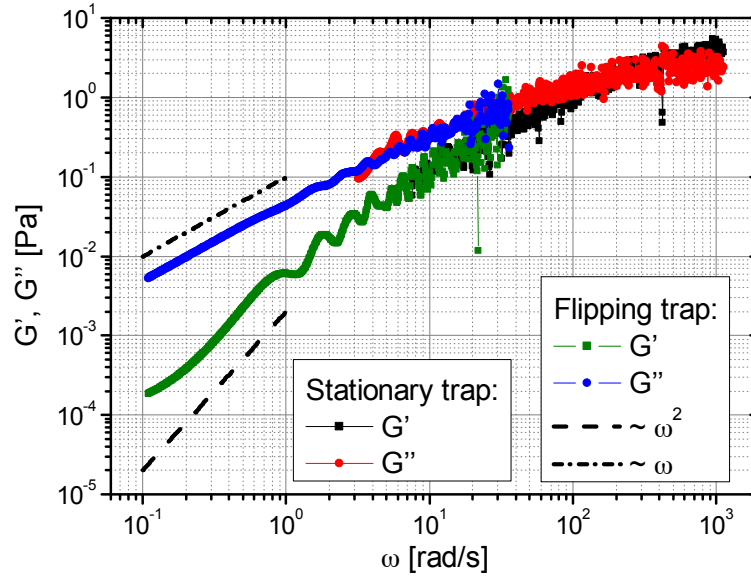
Figure 8.6: Storage (G') and loss (G'') moduli *vs.* frequency of a solution of 1% w/w of PAM in water measured by means of both Eq. (8.5) (high frequencies) and Eq. (8.7) (low frequencies) applied directly to the experimental data presented in Fig. 8.4 and Fig. 8.3, respectively. The lines represents the expected limiting behavior of the moduli when the material reaches the terminal region: $G' \propto \omega^2$ and $G'' \propto \omega$.

show the ability of the technique to clearly determine the viscoelastic properties of a fluid and give access to the terminal region (where $G' \propto \omega^2$ and $G'' \propto \omega$).

8.6 Conclusions

As has been mentioned the available frequency range is limited only by the length of the experiment. This gives access to the material's terminal region, allowing micro-rheology to be performed on fluids with very long relaxation times such as those exhibiting soft glassy rheology [149]. As SLM technology develops, SLMs capable of faster trap switching times will become available. Although this has very little value in terms of extending the measured frequency range (since high frequencies can be measured via Brownian motion), it will increase the overlapping regions of (G') and (G'') created by the differing measurement techniques. Use of photo-diodes would also increase the data sampling speed.

A range of techniques currently exist for determining the viscosity of a fluid in optical tweezers. Few exist however, which take account of viscoelastic fluids.

Fewer still are both simple and self-consistent, giving access to the entire frequency range accessible with optical tweezers. It is an advantage of spatial light modulators that optical traps can be arbitrarily created in three dimensions, making the above technique practical for investigation of micro-rheology in a variety of situations. This is of practical interest for biological experiments in which the exact behavior of the fluid may be unknown or composed of a mixture of known substances.

Chapter 9

Conclusions

The use of spatial light modulators in optical tweezers has often been maligned in the past with the accusation leveled that SLMs do not contribute significantly to experimental procedures or provide somehow flawed or insufficient optical traps. However such statements are often based on misunderstanding. Although several years ago concerns over the optical trapping abilities of holographic optical tweezers may have been justified. Accumulation of evidence has shown that most concerns are unfounded. But can the use of an SLM contribute significantly to the operation of an optical tweezers setup? The characteristics of SLMs are constantly evolving. In chapter 3 I described the design and construction of a 4 Mega-pixel spatial light modulator. The large number of line pairs (960) it can generate and its large active area (4cm x 4cm) make it ideal for the production of optical traps over a wide field of view and show that it is possible to create holographic optical tweezers which are not limited by their diffraction efficiency. Furthermore, multiplicative masks can correct the fall off in intensity with radial displacement of the optical trap. In chapter 7 we saw that the speed of the new Boulder SLM could reach 203Hz making the suppression of Brownian motion possible. Although this was limited to very low frequencies. The system was never the less (nevertheless) capable of reducing the mean squared displacement of trapped 5μm silica beads positions by 44%. Clearly, with increased development the speed of future SLMs will range into the kHz level. A number of problems thought to exist with SLMs have been shown to be resolvable with software. Aberration correction techniques have been

shown to be successful when dealing with the generation LG Beams. Computer calibration of the pixel to phase ratio of the system creates a well-defined phase response leading to more intense optical traps. With increased resolution hologram calculation might be thought of as a limiting factor, however I have shown in Chapter 7 that graphics card technology can calculate holograms at hundreds of frames per second. Combining SLMs with camera software for real time particle tracking adds a new dimension to the use of SLMs and creates the possibility of experiments involving feedback taking place in thee dimensions with multiple particles. The software used is available online providing a resource for other groups who wish to give SLMs a try. One advantage of SLMs is their ability to generate a variety of different beam types. This advantage alone makes SLMs desirable as a way of creating beams with angular momentum. In chapter 4 I described how SLMs can be used to generate beams with orbital angular momentum. Similarly, in chapter 5 I described how a split screen method could be used to give SLMs control over spin angular momentum. The split screen method can be used to independently control the polarisation state of multiple optical traps allowing the simultaneous movement and rotation of multiple vaterite particles. We also showed in chapter 4 that SLMs can be used to generate a wide range of novel optical beams which may have new and exiting applications in optical trapping. If SLMs are to prove useful for science, they must be useful for actual physical measurement. In chapter 8 I show that SLMs can be used to measure the viscoelastic properties of fluids. This is of practical interest for biological experiments in which the exact behavior of the fluid may be unknown or composed of a mixture of known substances. Clearly SLMs do have a role to play.

9.1   Future Outlook

SLM technology is a fast developing field. Optical tweezers compete with other emerging technologies for customization of SLMs to best suit the field of optical trapping. Although there has clearly been a push within the optical trapping community in recent years for faster SLMs, which are of higher efficiency and have better resolution, SLM manufactures must weigh the pros and cons of investing in research

time to develop these attributes against the profit it will bring them. Since most of the previous development of SLM technology was linked to the far more lucrative display technology market, which manufactures heads-up displays, projectors and mobile phones. The future development of phase only spatial light modulators as used in optical tweezers relies on manufactures of SLMs finding a large enough market which will be able to support future investment in the development of phase only technology. To some extent then the uptake of optical tweezers will determine its own technological development. If optical tweezers systems find a place as a standard lab tool in any biology or nanotechnology lab, then the development SLM technology must follow their success. The use of liquid crystal spatial light modulators faces a less certain future. Recent developments in MEMS technology may prove tough competition for liquid crystal micro-displays. However currently, MEMS devices are either prohibitively expensive or work only in a binary mode. One positive aspect indicating the continued use of liquid crystal technology is the large investment currently being made in development of new types of liquid crystal. This promises to yield new types of liquid crystal, which may not only have faster voltage response characteristics but also have a variety of new optical properties such as frequency modulation. While the future of SLMs is still very much up for debate, the technology used for calculating optical traps is assured. The use of graphics cards for calculation of large matrix problems has seen widespread uptake amongst the physics community. There is currently huge interest in this technology with major multinationals such as Nvidia, Ati and Intel funding research into a hybrid graphics card technologies and new parallel computing architectures. Clearly, the calculation speed of holograms will not be a limiting factor in the future. Rather the transmission of data and the response of the SLM will be key future issues to be resolved. It would be terse if I were to finish this section without saying something about the use of SLMs in the field of optical trapping as a whole. Since Ashkins discovery of the gradient force we have come a long way in applying optical trapping to a range of interesting problems. SLMs have been used along the way for a variety of experiments many of which have shed light on hitherto unexplored aspects of science. Yet SLMs have only been used by a few, possibly because of cost, possi-

bly because of a perceived learning curve in understanding how to use them. As a variety of new avenues of exploration open up for optical tweezers the SLMs ability to provide readily configurable optical potential landscapes will no doubt prove indispensable. As has been noted many times in this thesis the SLM has much to recommend it to the field of optical trapping. I have shown that the SLM has the ability to create multiple optical traps in moveable movable three dimensions. It can be updated at hundreds of Hz and be used to generate a variety of novel beams. It can be used to control both the spin and orbital angular momentum of light and be used for novel applications such as viscosity measurement. However, ultimately, the major advantage that the SLM possesses in optical tweezers setups is its adaptability. SLMs provide the ability to do what you want to do when you want to do it. SLMs give the user of an optical tweezers system a range of options, which cannot be achieved using other setups. For the experimenter their ease of use can make the difference between a good workday and a bad one. It is the user experience that will make the SLM and holographic optical tweezers in general, the future.

7th March 2011

Bibliography

[1] "Prosillica website, http://www.alliedvisiontec.com," 2011.

[2] D. Preece, S. Keen, E. Botvinick, R. Bowman, M. Padgett, and J. Leach, "Independent polarisation control of multiple optical traps," *Optics Express*, vol. 16, no. 20, pp. 15897–15902, 2008.

[3] D. McKnight, D. Vass, and R. Sillitto, "Development of a spatial light modulator: a randomly addressed liquid-crystal-over-nMOS array," *Applied Optics*, vol. 28, no. 22, pp. 4757–4762, 1989.

[4] M. Ernstoff, A. Leupp, M. Little, and H. Peterson, "Liquid crystal pictorial display," in *Electron Devices Meeting, 1973 International*, pp. 548– 551, 1973.

[5] U. Efron, J. Grinberg, P. O. Braatz, M. J. Little, P. G. Reif, and R. N. Schwartz, "The silicon liquid-crystal light valve," *Journal of Applied Physics*, vol. 57, no. 4, pp. 1356–1368, 1985.

[6] S. Bernet, A. Jesacher, S. Fürhapter, C. Maurer, and M. Ritsch-Marte, "Quantitative imaging of complex samples by spiral phase contrast microscopy," *Optics Express*, vol. 14, pp. 3792–3805, 2006.

[7] J. B. Yang and X. Y. Su, "Optical implementation of (3,3,2) regular rectangular cc-banyan optical network," *Optics Communications*, vol. 275, pp. 57–64, 2007.

[8] K. Matsuda, B. Q. Ye, N. Fukuchi, H. Okamoto, and T. Hara, "Holographic vibration measurements of rough surfaces using a LCSLM," *Optics Communications*, vol. 275, pp. 53–56, 2007.

[9] T. Inoue, N. Matsumoto, N. Fukuchi, Y. Kobayashi, and T. Hara, "Highly stable wavefront control using a hybrid liquid-crystal spatial light modulator," vol. 6306, p. 630603, 2006.

[10] T. Strzelecka, M. Davidson, and R. Rill, "Multiple liquid crystal phases of dna at high concentrations," *Nature*, vol. 331, pp. 457–460, 1988.

[11] R. S. Werbowyj and D. Gray, "Optical properties of hydroxypropyl cellulose liquid crystals," *Macromolecules*, vol. 17, no. 8, pp. 1512–1520, 1984.

[12] N. Behabtu, J. Lomeda, M. Green, A. Higginbotham, A. Sinitskii, D. Kosynkin, D. Tsentalovich, A. N. G. Parra-Vasquez, J. Schmidt, E. Kesselman, Y. Cohen, Y. Talmon, J. Tour, and M. Pasquali, "Spontaneous high-concentration dispersions and liquid crystals of graphene," *Nat Nano*, vol. 5, pp. 406–411, 2010.

[13] N. A. Clark and S. T. Lagerwall, "Submicrosecond bistable electro-optic switching in liquid crystals," *Applied Physics Letters*, vol. 36, pp. 899–902, 1980.

[14] M. Schadt and W. Helfrich, "Voltage-dependent optical activity of a twisted nematic liquid crystal," *Applied Physics Letters*, vol. 18, no. 4, pp. 127–128, 1971.

[15] N. Konforti, E. Marom, and S.-T. Wu, "Phase-only modulation with twisted nematic liquid-crystal spatial light modulators," *Optics Letters*, vol. 13, no. 3, pp. 251–253, 1988.

[16] N. Mukohzaka, N. Yoshida, H. Toyoda, Y. Kobayashi, and T. Hara, "Diffraction efficiency analysis of a parallel-aligned nematic-liquid-crystal spatial light modulator," *Applied Optics*, vol. 33, no. 14, pp. 2804–2811, 1994.

[17] "Boulder nononlinear systems, http://www.bnonlinear.com/rd/index.htm," 2011.

[18] "Holoeye photonics, http://www.holoeye.com/," 2008.

[19] "Hamamatsu, http://sales.hamamatsu.com/en/products/electron-tube-division/detectors/spatial-light-modulator.php." web, 2010.

[20] Z. He, T. Nose, and S. Sato, "Polarization properties of an amplitude nematic liquid crystal grating.," *Optical Engineering*, vol. 37, pp. 2885–2898, 1998.

[21] J. Stockley, D. Subacius, and S. Serati, "The influence of the inter-pixel region in liquid crystal diffraction gratings," *Liquid Crystal Displays II*, vol. 3635, pp. 18–29, 1999.

[22] Y. Igasaki, F. Li, N. Yoshida, H. Toyoda, T. Inoue, N. Mukohzaka, Y. Kobayashi, and T. Hara, "High efficency electrically-addressable phase only spatial light modulator," *Optical Review*, vol. 6, no. 4, pp. 339–334, 1999.

[23] J. C. Maxwell, *A treatise on electricity and magnetism*, vol. 1. Oxford : Clarendon Press, 1873.

[24] M. Padgett, J. Molloy, and D. McGloin, *Optical Tweezers: methods and applications*. Chapman and Hall/CRC, 2010.

[25] A. Ashkin, "Acceleration and trapping of particles by radiation pressure," *Physical Review Letters*, vol. 24, pp. 156–159, 1970.

[26] A. Ashkin and J. M. Dziedzic, "Optical levitation by radiation pressure," *Applied Physics Letters*, vol. 19, no. 8, pp. 283–285, 1971.

[27] A. Ashkin, J. M. Dziedzic, J. E. Bjorkholm, and S. Chu, "Observation of a single-beam gradient force optical trap for dielectric particles," *Optics Letters*, vol. 11, pp. 288–290, 1986.

[28] A. Ashkin and J. Dziedzic, "Optical trapping and manipulation of viruses and bacteria," *Science*, vol. 235, no. 4795, pp. 1517–1520, 1987.

[29] A. Ashkin and J. Dziedzic, "Optical levitation in high-vacuum," *Applied Physics L*, vol. 28, pp. 333–335, 1976.

[30] A. Ashkin and J. Dziedzic, "Feedback stabilization of optically levitated particles," *Applied Physics Le*, vol. 30, pp. 202–204, 1977.

[31] Y. Harada and T. Asakura, "Radiation forces on a dielectric sphere in the Rayleigh scattering regime," *Optics Communications*, vol. 124, no. 5-6, pp. 529–541, 1996.

[32] A. Ashkin, "Forces of a single-beam gradient laser trap on a dielectric sphere in the ray optics regime," *Biophysical Journal*, vol. 61, no. 2, pp. 569–582, 1992.

[33] T. Nieminen, N. Heckenberg, and H. Rubinsztein-dunlop, "Forces in optical tweezers with radially and azimuthally polarized trapping beams," *Optics Letters*, vol. 33, no. 2, pp. 122–124, 2008.

[34] K. Neuman, E. Chadd, G. Liou, K. Bergman, and S. Block, "Characterization of photodamage to Escherichia coli in optical traps," *Biophysical Journal*, vol. 77, no. 5, pp. 2856–2863, 1999.

[35] S. N. S. Reihani and L. B. Oddershede, "Optimizing immersion media refractive index improves optical trapping by compensating spherical aberrations.," *Optics Letters*, vol. 32, no. 14, pp. 1998–2000, 2007.

[36] A. Rohrbach, "Switching and measuring a force of 25 femtonewtons with an optical trap," *Optics Express*, vol. 13, no. 24, pp. 9695–9701, 2005.

[37] C. Mejean, A. Schaefer, E. Millman, P. Forscher, and E. R. Dufresne, "Multiplexed force measurements on live cells with holographic optical tweezers," *Optics Express*, vol. 17, no. 8, p. 6209, 2009.

[38] M. Wang, H. Yin, R. Landick, J. Gelles, and S. Block, "Stretching DNAwith optical tweezers," *Biophysical Journal*, vol. 72, no. 3, pp. 1335–1346, 1997.

[39] I. Tolić-Nørrelykke, E. Munteanu, G. Thon, L. Oddershede, and K. Berg-Sørensen, "Anomalous diffusion in living yeast cells," *Physical Review Letters*, vol. 93, no. 7, pp. 078102–078106, 2004.

[40] R. Simmons, J. T. Finer, S. Chu, and J. Spudich, "Quantitative measurements of force and displacement using an optical trap," *Biophysical Journal*, vol. 70, no. 4, pp. 1813–1822, 1996.

[41] S. Keen, J. Leach, G. Gibson, and M. J. Padgett, "Comparison of a high-speed camera and a quadrant detector for measuring displacements in optical tweezers," *Journal of Optics A*, vol. 9, pp. S264–S266, 2007.

[42] G. Stokes, "On the effect of the internal friction of fluids on the motion of pendulums," *Transactions of the Cambridge Philosophical Society*, vol. 9, pp. 8–94, 1851.

[43] S. B. Smith, Y. Cui, and C. Bustamante, "Overstretching b-dna: The elastic response of individual double-stranded and single-stranded dna molecules," *Science*, vol. 271, no. 5250, pp. 795–799, 1996.

[44] R. Brown, "A brief account of microscopical observations made in the months of June, July and August, 1827, on the particles contained in the pollen of plants; and on the general existence of active molecules in organic and inorganic bodies," *Philosophical Magazine*, vol. 4, pp. 161–173, 1828.

[45] K. Berg-Sørensen and H. Flyvbjerg, "Power spectrum analysis for optical tweezers," *Review of Scientific Instruments*, vol. 75, no. 3, pp. 594–612, 2004.

[46] G. Uhlenbeck and L. Ornstein, "On the theory of the Brownian motion," *Physical Review*, vol. 36, no. 5, pp. 823–841, 1930.

[47] K. Sasaki, M. Koshioka, H. Misawa, N. Kitamura, and H. Masuhara, "Pattern formation and flow control of fine particles by laser-scanning micromanipulation," *Optics Letters*, vol. 16, no. 19, pp. 1463–1465, 1991.

[48] K. Visscher, G. J. Brakenhoff, and J. J. Krol, "Micromanipulation by multiple optical traps created by a single fast scanning trap integrated with the bilateral confocal scanning laser microscope," *Cytometry*, vol. 14, pp. 105–114, 1993.

[49] C. Mio, T. Gong, A. Terray, and D. W. M. Marr, "Design of a scanning laser optical trap for multiparticle manipulation," *Review of Scientific Instruments*, vol. 71, no. 5, pp. 2196–2200, 2000.

[50] Y. Ogura, K. Kagawa, and J. Tanida, "Optical manipulation of microscopic objects by means of vertical-cavity surface-emitting laser array sources," *Applied Optics*, vol. 40, no. 30, pp. 5430–5435, 2001.

[51] D. Vossen, A. der Horst, M. Dogterom, and A. van Blaaderen, "Optical tweezers and confocal microscopy for simultaneous three-dimensional manipulation and imaging in concentrated colloidal dispersions," *Review of Scientific Instruments*, vol. 75, no. 9, pp. 2960–2970, 2004.

[52] J. Fournier, M. Burns, and J. Golovchenko, "Writing diffractive structures by optical trapping," *Proceedings of SPIE*, vol. 2406, pp. 101–111, 1995.

[53] E. Dufresne and D. Grier, "Optical tweezer arrays and optical substrates created with diffractive optics," *Review of Scientific Instruments*, vol. 69, pp. 1974–1977, 1998.

[54] M. Reicherter, T. Haist, E. U. Wagemann, and H. J. Tiziani, "Optical particle trapping with computer-generated holograms written on a liquid-crystal display.," *Optics Letters*, vol. 24, no. 9, pp. 608–610, 1999.

[55] J. Liesener, M. Reicherter, T. Haist, and H. Tiziani, "Multi-functional optical tweezers using computer-generated holograms," *Optics Communications*, vol. 185, no. 1-3, pp. 77–82, 2000.

[56] P. J. Rodrigo, V. R. Daria, and J. Glückstad, "Real-time three-dimensional optical micromanipulation of multiple particles and living cells.," *Optics Letters*, vol. 29, no. 19, pp. 2270–2272, 2004.

[57] R. Eriksen, V. Daria, and J. Glückstad, "Fully dynamic multiple-beam optical tweezers.," *Optics Express*, vol. 10, no. 14, pp. 597–602, 2002.

[58] C. Schmitz, J. Spatz, and J. Curtis, "High-precision steering of multiple holographic optical traps," *Optics Express*, vol. 13, no. 21, pp. 8678–8685, 2005.

[59] E. Eriksson, S. Keen, J. Leach, M. Göksor, and M. J. Padgett, "The effect of external forces on discrete motion within holographic optical tweezers," *Optics Express*, vol. 15, no. 26, pp. 18268–18274, 2007.

[60] J. Crocker and D. Grier, "Methods of digital video microscopy for colloidal studies," *Journal of Colloid and Interface Science*, vol. 179, no. 1, pp. 298–310, 1996.

[61] M. D. Summers, D. R. Burnham, and D. McGloin, "Trapping solid aerosols with optical tweezers: A comparison between gas and liquid phase optical traps," *Optics Express*, vol. 16, no. 11, pp. 7739–7747, 2008.

[62] P. Jordan, J. Leach, M. Padgett, P. Blackburn, N. Isaacs, M. Goksör, D. Hanstorp, A. Wright, J. Girkin, and J. Cooper, "Creating permanent 3d arrangements of isolated cells using holographic optical tweezers," *Lab on a Chip*, vol. 5, pp. 1224–1228, 2005.

[63] A. Jesacher, A. Schwaighofer, S. Fürhapter, C. Maurer, S. Bernet, and M. Ritsch-Marte, "Wavefront correction of spatial light modulators using an optical vortex image," *Optics Express*, vol. 15, no. 9, pp. 5801–5808, 2007.

[64] D. Preece, E. Yao, G. Gibson, R. Bowman, J. Leach, and M. Padgett, "A spatial light phase modulator with an effective resolution of 4 mega-pixels," *Journal of Modern Optics*, vol. 55, no. 18, pp. 2945–2951, 2008.

[65] M. J. Padgett and L. Allen, "Light with a twist in its tail," *Contemporary Physics*, vol. 41, pp. 275–285, 2000.

[66] T. Cižmár, V. Kollárová, X. Tsampoula, F. Gunn-Moore, W. Sibbett, Z. Bouchal, and K. Dholakia, "Generation of multiple Bessel beams for a biophotonics workstation," *Optics Express*, vol. 16, no. 18, pp. 14024–14035, 2008.

[67] S. Lee, K. Ladavac, M. Polin, and D. Grier, "Observation of flux reversal in a symmetric optical thermal ratchet," *Physical Review Letters*, vol. 94, no. 11, pp. 110601–110605, 2005.

[68] M. Friese, H. Rubinsztein-Dunlop, and J. Gold, "Optically driven micromachine elements," *Applied Physics*, 2001.

[69] J. E. Curtis, B. A. Koss, and D. G. Grier, "Dynamic holographic optical tweezers," *Optics Communications*, vol. 207, pp. 169–175, 2002.

[70] E. O. Eriksson, D. Engström, J. Scrimgeour, and M. Goksör, "Automated focusing of nuclei for timelapse experiments on single cells using holographic optical tweezers," *Optics Express*, vol. 17, no. 7, pp. 5585–5594, 2009.

[71] G. Knöner, S. Parkin, T. Nieminen, V. Loke, N. Heckenberg, and H. Rubinsztein-Dunlop, "Integrated optomechanical microelements," *Optics Express*, vol. 15, no. 9, pp. 5521–5530, 2007.

[72] G. Sinclair, P. Jordan, J. Leach, M. J. Padgett, and J. Cooper, "Defining the trapping limits of holographical optical tweezers," *Journal of Modern Optics*, vol. 51, pp. 409–414, 2004.

[73] E. Carcole, J. A. Davis, and D. M. Cottrell, "Astigmatic phase correction for the magneto-optic spatial light modulator," *Applied Optics*, vol. 34, pp. 5118–5120, 1995.

[74] R. W. Gerchberg and W. O. Saxton, "A practical algorithm for the determination of phase from image and diffraction plane pictures," *Optik*, vol. 35, pp. 237–246, 1972.

[75] J. Leach, G. Gibson, M. Padgett, E. Esposito, G. McConnell, A. Wright, and J. Girkin, "Generation of achromatic Bessel beams using a compensated spatial light modulator," *Optics Express*, vol. 14, no. 12, pp. 5581–5587, 2006.

[76] J. Leach, M. Dennis, J. Courtial, and M. J. Padgett, "Laser beams – knotted threads of darkness," *Nature*, vol. 432, p. 165, 2004.

[77] J. Leach, M. R. Dennis, J. Courtial, and M. J. Padgett, "Vortex knots in light," *New Journal of Physics*, vol. 7, pp. 55.1–55.11, 2005.

[78] G. Spalding, J. Courtial, and R. Di Leonardo, *Holographic Optical Trapping in Structured Light and its Applications: An Introduction to Phase-Structured Beams and Nanoscale Optical Forces.* Elsevier Press, 2008.

[79] J. Nye and M. Berry, "Dislocations in wave trains," *Proceedings of the Royal Society A*, vol. 336, no. 1605, pp. 165–190, 1974.

[80] S. Barnett and L. Allen, "Orbital angular momentum and nonparaxial light beams," *Optics Communications*, vol. 110, no. 5-6, pp. 670–678.

[81] R. Beth, "Mechanical detection and measurement of the angular momentum of light," *Physical Review*, vol. 50, pp. 115–125, 1936.

[82] J. Crichton and P. Marston, "The measurable distinction between the spin and orbital angular momenta of electromagnetic radiation," *Electronic Journal of Differential Equations*, vol. 04, pp. 37–50, 2000.

[83] L. Allen, S. Barnett, and M. Padgett, *Optical angular momentum.* Institute of Physics Publishing, 2003.

[84] M. Vasnetsov and K. Staliunas, *Optical vortices.* Nova Science Publishers, 1999.

[85] V. Y. Bazhenov, M. V. Vasnetsov, and M. S. Soskin, "Laser beams with screw dislocations in their wavefronts," *JETP Letters*, vol. 52, pp. 429–431, 1990.

[86] M. Beijersbergen, L. Allen, H. Van Der Veen, and J. Woerdman, "Astigmatic laser mode converters and transfer of orbital angular momentum," *Optical angular momentum*, vol. 96, pp. 123–132, 2003.

[87] P. Coullet, L. Gil, and F. Rocca, "Optical vortices," *Optics Communications*, vol. 73, pp. 403–408, 1989.

[88] M. Padgett, J. Courtial, and L. Allen, "Light's orbital angular momentum," *Physics Today*, vol. 57, no. 5, pp. 35–40, 2004.

[89] M. Beijersbergen, "Helical-wavefront laser beams produced with a spiral phase-plate," *Optics Communications*, vol. 112, pp. 321–327, 1994.

[90] R. Oron, R. Davidson, A. Friesem, and F. Hasman, "Efficient formation of pure helical laser beams," *Optics Communications*, vol. 182, pp. 205–208, 2000.

[91] J. Courtial and M. Padgett, "Performance of a cylindrical lens mode converter for producing Laguerre-Gaussian laser modes," *Optics Communications*, vol. 159, pp. 13–18, 1999.

[92] N. Heckenberg, R. McDuff, C. Smith, H. Rubinsztein-Dunlop, and M. Wegener, "Laser beams with phase singularities," *Optical and Quantum Electronics*, vol. 24, no. 9, pp. 951–962, 1992.

[93] K. Gahagan and G. Swartzlander Jr, "Optical vortex trapping of particles," *Optics Letters*, vol. 21, no. 11, pp. 827–829, 1996.

[94] L. Marrucci, C. Manzo, and D. Paparo, "Optical spin-to-orbital angular momentum conversion in an inhomogeneous anisotropic media," *Physical Review Letters*, vol. 96, p. 163905, 2006.

[95] J. E. Curtis and D. Grier, "Modulated optical vortices," *Optics Letters*, vol. 28, pp. 872–874, 2003.

[96] Y. Roichman and D. Grier, "Projecting extended optical traps with shape-phase holography," *Optics Letters*, vol. 31, pp. 1675–1677, 2006.

[97] M. Friese, J. Enger, H. Rubinsztein-Dunlop, and N. Heckenberg, "Optical angular-momentum transfer to trapped absorbing particles," *Physical Review A*, vol. 54, no. 2, pp. 1593–1596, 1996.

[98] A. I. Bishop, T. A. Nieminen, N. R. Heckenberg, and H. Rubinsztein-Dunlop, "Optical application and measurement of torque on microparticles of isotropic nonabsorbing material," *Physical Review A*, vol. 68, p. 033802, 2003.

[99] J. Johnston, H. Merwin, and E. Williamson, "The several forms of calcium carbonate," *The American Journal of Science*, vol. 61, no. 246, pp. 474–512, 1916.

[100] M. E. J. Friese, T. A. Nieminen, N. R. Heckenberg, and H. Rubinsztein-Dunlop, "Optical alignment and spinning of laser-trapped microscopic particles," *Nature*, vol. 394, pp. 348–350, 1998.

[101] H. He, M. Friese, N. Heckenberg, and H. Rubinsztein-Dunlop, "Direct observation of transfer of angular momentum to absorptive particles from a laser beam with a phase singularit," *Physical Review Letters*, vol. 75, no. 5, pp. 826–829, 1995.

[102] N. Simpson, K. Dholakia, L. Allen, and M. Padgett, "Mechanical equivalence of spin and orbital angular momentum of light: an optical spanner," *Optics Letters*, vol. 22, no. 1, pp. 52–54, 1997.

[103] J. Courtial, "Limit to the orbital angular momentum per unit energy in a light beam that can be focussed onto a small particle," *Optics Communications*, vol. 173, no. 1-6, pp. 269–274, 2000.

[104] M. Berry, "Optical vortices evolving from helicoidal integer and fractional phase steps," *Journal of Optics A: Pure and Applied Optics*, vol. 6, no. 2, pp. 259–268, 2004.

[105] J. Götte, K. O'Holleran, D. Preece, F. Flossmann, S. Franke-Arnold, S. Barnett, and M. Padgett, "Light beams with fractional orbital angular momentum and their vortex structure.," *Optics Express*, vol. 16, no. 2, pp. 993–1006, 2008.

[106] N. Heckenberg, R. McDuff, C. Smith, and A. White, "Generation of optical phase singularities by computer-generated holograms," *Optics Letters*, vol. 17, no. 3, pp. 221–223, 1992.

[107] C. Alonzo, P. Rodrigo, and J. Glückstad, "Helico-conical optical beams: a product of helical and conical phase fronts," *Optics Express*, vol. 13, no. 5, pp. 1749–1760, 2005.

[108] S. Lee, Y. Roichman, and D. Grier, "Optical solenoid beams.," *Optics Express*, vol. 18, no. 7, pp. 6988–6993, 2010.

[109] G. Siviloglou, J. Broky, A. Dogariu, and D. Christodoulides, "Observation of accelerating Airy beams," *Physical Review Letters*, vol. 99, no. 21, pp. 23–26, 2007.

[110] A. Bishop, T. Nieminen, N. Heckenberg, and H. Rubinsztein-Dunlop, "Optical microrheology using rotating laser-trapped particles," *Physical Review Letters*, vol. 92, no. 19, pp. 14–17, 2004.

[111] S. Sato, M. Ishigure, and H. Inaba, "Optical trapping and rotational manipulation of microscopic particles and biological cells using higher-order mode Nd:YAG laser beams," *Electronics Letters*, vol. 27, pp. 1831–1832, 1991.

[112] A. O'Neil, I. MacVicar, L. Allen, and M. J. Padgett, "Intrinsic and extrinsic nature of the orbital angular momentum of a light beam," *Physical Review Letters*, vol. 88, no. 5, p. 53601, 2002.

[113] L. Paterson, M. MacDonald, J. Arlt, W. Sibbett, P. Bryant, and K. Dholakia, "Controlled rotation of optically trapped microscopic particles," *Science*, vol. 292, no. 5518, pp. 912–914, 2001.

[114] Z. Luo, Y. L. Sun, and K. An, "An optical spin micromotor," *Applied Physics Letters*, vol. 76, pp. 1779–1781, 2000.

[115] V. Bingelyte, J. Leach, J. Courtial, and M. J. Padgett, "Optically controlled three-dimensional rotation of microscopic objects," *Applied Physics Letters*, vol. 82, pp. 829–831, 2003.

[116] K. Ladavac and D. Grier, "Microoptomechanical pumps assembled and driven by holographic optical vortex arrays," *Optics Express*, vol. 12, no. 6, pp. 1144–1149, 2004.

[117] A. Jesacher, S. Fürhapter, C. Maurer, S. Bernet, and M. Ritsch-Marte, "Holographic optical tweezers for object manipulations at an air-liquid surface," *Optics Express*, vol. 14, no. 13, pp. 6342–6352, 2006.

[118] C. Maurer, A. Jesacher, S. Fürhapter, S. Bernet, and M. Ritsch-Marte, "Tailoring of arbitrary optical vector beams," *New Journal of Physics*, vol. 9, pp. 78–98, 2007.

[119] S. Parkin, R. Vogel, M. Persson, M. Funk, V. Loke, T. Nieminen, N. Heckenberg, and H. Rubinsztein-Dunlop, "Highly birefringent vaterite microspheres:

production, characterization and applications for optical micromanipulation," *Optics express*, vol. 17, no. 24, pp. 21944–21955, 2009.

[120] M. Funk, S. J. Parkin, T. Nieminen, and N. Heckenberg, "Microrheology with aom controlled optical tweezers," *Proceedings of SPIE*, vol. 7227, pp. 72270D–1, 2009.

[121] G. Knöner, S. Parkin, N. Heckenberg, and H. Rubinsztein-Dunlop, "Characterization of optically driven fluid stress fields with optical tweezers," *Physical Review*, vol. 72, p. 031507, 2005.

[122] R. Gerchberg and W. Saxton, "Phase determination from image and diffraction plane pictures in electron-microscope," *Optik*, vol. 34, no. 3, pp. 275–284, 1971.

[123] J. R. Fienup, "Phase retrieval algorithms: a comparison," *Applied Optics*, vol. 21, no. 15, pp. 2758–2769, 1982.

[124] G. Sinclair, J. Leach, P. Jordan, G. M. Gibson, E. Yao, Z. J. Laczik, M. J. Padgett, and J. Courtial, "Interactive application in holographic optical tweezers of a multi-plane gerchberg-saxton algorithm for three-dimensional light shaping," *Optics Express*, vol. 12, pp. 1665–1670, 2004.

[125] R. D. Leonardo, F. Ianni, and G. Ruocco, "Computer generation of optimal holograms for optical trap arrays," *Optics Express*, vol. 15, no. 4, pp. 1913–1922, 2007.

[126] G. Wuite, R. Davenport, A. Rappaport, and C. Bustamante, "An integrated laser trap/flow control video microscope for the study of single biomolecules," *Biophysical Journal*, vol. 79, no. 2, pp. 1155–1167, 2000.

[127] K. D. Wulff, D. G. Cole, R. L. Clark, R. Di Leonardo, J. Leach, J. Cooper, G. Gibson, and M. J. Padgett, "Aberration correction in holographic optical tweezers.," *Optics Express*, vol. 14, no. 9, pp. 4170–4175, 2006.

[128] A. E. Wallin, H. Ojala, E. Haeggstrom, and R. Tuma, "Stiffer optical tweezers through real-time feedback control," *Applied Physics Letters*, vol. 92, no. 22, pp. 224104–224107, 2008.

[129] J. Molloy, J. Burns, J. Kendrick-Jones, R. Tregear, and D. White, "Movement and force produced by a single myosin head," *Nature*, vol. 378, pp. 209–212, 1995.

[130] O. Otto, C. Gutsche, F. Kremer, and U. F. Keyser, "Optical tweezers with 2.5 kHz bandwidth video detection for single-colloid electrophoresis," *Review of Scientific Instruments*, vol. 79, no. 2, pp. 023710–023716, 2008.

[131] G. M. Gibson, S. J. Leach, A. J. W. Keen, and M. J. Padgett, "Measuring the accuracy of particle position and force in optical tweezers using high-speed video microscopy," *Optics Express*, vol. 16, no. 19, pp. 14561–14570, 2008.

[132] Z. Zhang and C. Menq, "Three-dimensional particle tracking with subnanometer resolution using off-focus images," *Applied Optics*, vol. 47, no. 13, pp. 2361–2370, 2008.

[133] D. M. Carberry, J. C. Reid, G. M. Wang, E. M. Sevick, D. J. Searles, and D. J. Evans, "Fluctuations and irreversibility: An experimental demonstration of a second-law-like theorem using a colloidal particle held in an optical trap," *Physical Review Letters*, vol. 92, no. 14, p. 140601, 2004.

[134] P. Negulescu, T. Krasieva, A. Khan, H. Kerschbaum, and M. Cahalan, "Polarity of T cell shape, motility, and sensitivity to antigen.," *Immunity*, vol. 4, no. 5, pp. 421–430, 1996.

[135] K. Svoboda, C. Schmidt, D. Branton, and S. Block, "Conformation and elasticity of the isolated red blood cell membrane skeleton," *Biophysical Journal*, vol. 63, no. 3, pp. 784–793, 1992.

[136] S. Tolić-Nørrelykke, E. Schäffer, J. Howard, F. Pavone, F. Jülicher, and H. Flyvbjerg, "Calibration of optical tweezers with positional detection in the back focal plane," *Review of Scientific Instruments*, vol. 77, no. 10, p. 103101, 2006.

[137] J. Ferry, *Viscoelastic properties of polymers.* Wiley, 3rd ed., 1980.

[138] A. Yao, M. Tassieri, M. Padgett, and J. Cooper, "Microrheology with optical tweezers.," *Lab on a Chip*, vol. 9, no. 17, pp. 2568–75, 2009.

[139] L. Starrs and P. Bartlett, "One- and two-point micro-rheology of viscoelastic media," *Journal of Physics: Condensed Matter*, vol. 15, no. 1, pp. S251–S256, 2003.

[140] M. Atakhorrami, D. Mizuno, G. H. Koenderink, T. B. Liverpool, F. C. MacKintosh, and C. F. Schmidt, "Short-time inertial response of viscoelastic fluids measured with brownian motion and with active probes," *Physical Review E*, vol. 77, no. 6, pp. 061508–061521, 2008.

[141] N. Nijenhuis, D. Mizuno, J. Spaan, and C. Schmidt, "Viscoelastic response of a model endothelial glycocalyx.," *Physical biology*, vol. 6, no. 2, p. 25014, 2009.

[142] G. Pesce, A. De Luca, G. Rusciano, P. Netti, S. Fusco, and A. Sasso, "Microrheology of complex fluids using optical tweezers: a comparison with macrorheological measurements," *Journal of Optics A: Pure and Applied Optics*, vol. 11, no. 3, pp. 34016–34026, 2009.

[143] R. M. L. Evans, M. Tassieri, D. Auhl, and T. A. Waigh, "Direct conversion of rheological compliance measurements into storage and loss moduli," *Physical Review E*, vol. 80, no. 1, pp. 012501–012505, 2009.

[144] M. Tassieri, G. Gibson, R. Evans, A. M. Yao, R. Warren, M. Padgett, and J. Cooper, "Measuring storage and loss moduli using optical tweezers: Broadband microrheology," *Physical Review E*, vol. 81, no. 2, pp. 026308–026313, 2010.

[145] K. Neuman and S. Block, "Optical trapping.," *The Review of Scientific Instruments*, vol. 75, no. 9, pp. 2787–2809, 2004.

[146] T. Mason and D. Weitz, "Optical measurements of frequency-dependent linear viscoelastic moduli of complex fluids," *Physical Review Letters*, vol. 74, no. 7, pp. 1250–1253, 1995.

[147] T. Mason, K. Ganesan, J. van Zanten, D. Wirtz, and S. Kuo, "Particle tracking microrheology of complex fluids," *Physical Review Letters*, vol. 79, no. 17, pp. 3282–3285, 1997.

[148] D. Preece, R. Bowman, A. Linnenberger, G. Gibson, S. Serati, and M. J. Padgett, "Increasing trap stiffness with position clamping in holographic optical tweezers.," *Optics Express*, vol. 17, no. 25, pp. 22718–25, 2009.

[149] S. M. Fielding, P. Sollich, and M. E. Cates, "Aging and rheology in soft materials," *Journal of Rheology*, vol. 44, no. 2, pp. 323–369, 2000.

[150] C. Feng, "Synthesis of spherical calcium carbonate crystals," project report, The University Queensland, 2005.

[151] M. Persson, "Materials and methods for optical micromanipulation of single DNA molecules," Master's thesis, University of Gothenburg, 2008.

[152] K. D. Wulff, D. G. Cole, and R. L. Clark, "Servo control of an optical trap," *Applied Optics*, vol. 46, no. 22, pp. 4923–4931, 2007.

Appendix A

On the Preparation of Functionalized Vaterite

A.1 Introduction

We note the basic preperation method for the preperation of vaterite along with the chemicles needed and the process for functionalisation. The fuctionalisation process creates vaterite crystals which may be used for biological experiments and attached to biochemicals. The following gives a simple guide for the uniform production of functionalised vaterite from its basic constituent parts and brings together knowledge accumulated over time at the University of Queensland micro-manipulation group where I was sent for one month in February 2009.

A.2 Basic Preparation

The basic method for the creation of vaterite crystals is that set out in [98].

We combine six drops of 0.1 mol K_2CO_3 with a solution of 1.5 ml of 0.1 mol $CaCl_2$together with four drops of 0.1 mol $MgSO_4$. As is set out in the above paper the solution is then agitated by pipetting. The solution forms a white precipitate which slowly clears as crystals of vaterite form. After several minutes large vaterite crystals form of the order of 3 microns.

The results of this crystallization process are variable and often large rhombo-

hedral calcite crystals form along with the spherical vaterite crystals. Birefringence may also vary among the vaterites created . A practical solution to this is to create several solutions in parallel and to then use the best of these to create seed solution for later refinement.

It should also be noted that vaterite crystals are inherently metastable and though the spherical polymorph is favored at room temperature the solution will degrade over a period of days without some means of stabilization.

To this end vaterite my be stabilized both by the replacement of the solute with ethanol and by the addition of the surfactant solution agepon. The addition of agepon to the solution after the initial formation of crystals also allows some control over the size of the vaterite crystals created, since the agepon quickly coats the already formed crystals and ceases crystal growth. Thus size control my be achieved by adding the agepon after a given time.

A.3 Refinement

Once a seed solution has been prepared this may then be used to create further generations of vaterite. The "Quality" i.e. the sphericity and uniformity of the vaterites produced, may be improved using Chow Fengs method [150]. This involves the production of vaterite created in a solution with the following ratio (0.5 ml $CaCl_2$, 2 drops $MgSO_4$, 2 drops K_2CO_3) The solution is seeded with a few drops of seed solution discussed earlier, before addition of the final two drops K_2CO_3. Experiments have shown that a wait time of 3 minutes 20 seconds minutes is sufficient to produce vaterite spheres of approximately 5 microns after 3 minutes 20 seconds Agepon is added to stop crystal formation. This process is tends improve the quality of the resultant vaterites. However the process should be repeated 3 times or more to get the best quality vaterite spheres. Each time the previous solution is used as the seed for the next.

A.4   Functionalisation

A.4.1   Washing

Before fuctionalisation the vaterites they need to be thoroughly washed this is done by first centrifuging 1.5ml eppendorf tubes at 8000rpm for 100 seconds till the vaterite forms a small clump at the bottom of the tube the solution is then removed and replaced with ethanol the vaterite can then be separated again by sonication. This not only helps to stablise the vaterites but also washes the spheres of excess chemicals. Before functionalisation this washing process should be repeated at least three times.

A.4.2   APS Coating

After washing the solid vaterite should be suspended in a solution of 15μl 3-aminopropyltrimethox 940μl ethanol and 50 μl ammonia in a 1.5ml eppendorf tube. This should be incubated of two hours if not longer. After the process is completed the vaterite should be rewashed as above with ethanol.

A.4.3   TEOS Coating

The procedure for coating with TEOS is very similar to the APS coating procedure however with the substitution of 25 μl TEOS instead of 15 μl APS. The solution may be washed and further APS coating applied if necessary.

A.5   Notes

- It should be noted that the above experimentation was largely done using plastic pipettes, beakers, test tubes etc. It has been suggested that crystal formation can be affected by the material in which the crystallization process takes place however little variation in crystal growth was noticed when glass apparatus was used.

- A careful check should be made of the state of the chemicals used to make

vaterite. Degradation of either chemicals or seed solution will contribute negatively to the production of stable vaterite.

- The use of a microscope in the production process may aid the production of vaterite crystals with given characteristics this can be used not only establish a timing regime which will give good sizing but also to select for traits and quality control.

A.6 Chemicals

- (3-Aminopropyl)trimethoxysilane 97% (ALDRICH)

- Tetraethyl orthosilicate 99.999% (ALDRICH)

- Agepon wetting agent (AGFA)

- Ammonia 0.1 mol

- $CaCl_2$ solution 0.1 mol

- MgSO solution 0.1 mol

- K_2CO_3 solution 0.1 mol

Further details can be found in [110, 150, 151].

Appendix B

Derivation on key formula for trap switching in optical tweezers

Step I, Derivation of the equation for a bead held in a static trap.

Starting with the Langevan equation.......:

$$m\vec{a}(t) = \vec{f_R}(t) - \int_{t_0}^{t} \zeta(t - \tau)\vec{v}(\tau)d\tau - \kappa_i\vec{r}(t) \tag{B.0.1}$$

Where m is the mass of the particle, $\vec{a}(t)$ is its acceleration, $\vec{v}(t)$ is the bead velocity and $\vec{f_R}(t)$ is a stochastic Gaussian white noise term. The integral term represents the viscous damping of the fluid, which incorporates a generalized time-dependent memory function $\zeta(t)$.

From Laplacian identities we know: (LT Laplace transforms is Laplace frequency)

$$a = r(t)'' \Rightarrow L.T. \Rightarrow s^2\tilde{r} - sr_0 - v_0 \tag{B.0.2}$$

$$v = r(t)' \Rightarrow L.T. \Rightarrow s\tilde{r} - r_0 \tag{B.0.3}$$

Also,

$$(f * g)(t) \Rightarrow L.T. \Rightarrow F(s) \cdot G(s) \tag{B.0.4}$$

the integral tern inB.0.1 may be rewritten in its laplacian form

$$\int_{t_0}^{t} \zeta(t-\tau)\vec{v}(\tau)d\tau \Rightarrow \mathcal{L}(\zeta(t)).\mathcal{L}(v(t)) = \mathcal{L}(\zeta(t)).(s\tilde{r}-r_0) \tag{B.0.5}$$

B.0.1 as a whole can be expressed as:

$$ms^2\tilde{r} - msr_0 - mv_0 = \tilde{f}_R - \widetilde{\zeta}(s)(s\tilde{r}-r_0) - \kappa_i\tilde{r} \tag{B.0.6}$$

multiply both sides of B.0.6by r_0 then averaging r over time we get

$$ms^2 <r_0\tilde{r}> -ms<r_0^2> -m<r_0v_0> =<r_0\tilde{f}_R> -\zeta(s)s<r_0\tilde{r}> -\zeta(s)<r_0^2> -\kappa_i<r_0\tilde{r}> \tag{B.0.7}$$

We assume that over many sample averages ; $<r_0\tilde{f}_R>$ becomes 0 and $m<r_0v_0>$ also becomes 0.

Substituting this into the above formulae we get.

$$ms^2 <r_0\tilde{r}> -ms<r_0^2> = -\zeta(s)s<\tilde{r}r_0> -\zeta(s)<r_0^2> -\kappa_i<\tilde{r}r_0> \tag{B.0.8}$$

Note $<r_0^2>$is equivalent to the variance.

We now reorder the terms of the equation.

$$ms^2 <r_0\tilde{r}> +\zeta(s)s<\tilde{r}r_0> +\kappa_i<\tilde{r}r_0> = ms<r_0^2> +\zeta(s)<r_0^2> \tag{B.0.9}$$

taking out the constant $<r_0\tilde{r}>$on the LHS and $<r_0^2>$on the RHS.

$$<r_0\tilde{r}>(ms^2+\zeta(s)s+\kappa_i) =<r_0^2>(ms+\zeta(s)) \tag{B.0.10}$$

we then further rearrange to get an expression for $\frac{<r_0\tilde{r}>}{<r_0^2>}$which is equivalent to the autocorrelation function.

$$\frac{<r_0\tilde{r}>}{<r_0^2>} = \frac{(ms+\zeta(s))}{(ms^2+\zeta(s)s+\kappa_i)} = \tilde{A}(s) \tag{B.0.11}$$

7th March 2011

the inverting the formula we get

$$\tilde{A}(s)^{-1} = \frac{(ms^2 + \zeta(s)s + \kappa_i)}{(ms + \zeta(s))} \tag{B.0.12}$$

we take out a factor of s from the numerator.

$$\tilde{A}(s)^{-1} = \frac{s(ms + \zeta(s) + \kappa_i)}{(ms + \zeta(s))} \tag{B.0.13}$$

then rearranging the fraction and inverting we get

$$\tilde{A}(s) = \left(s + \frac{\kappa_i}{ms + \zeta(s)}\right)^{-1} \tag{B.0.14}$$

Where $\tilde{A}(s)$is the Laplace transform of the normalized position auto correlation function.

We assume via Mason and Weitz that the microscopic memory function is proportional to the bulk frequency dependent viscosity of the fluid$\tilde{\zeta}(s) = 6\pi a\tilde{\eta}(s)$. Though this is an approximation which is true only at the limits of the frequency range. It is valid for $ms \ll \tilde{\zeta}(s)$ (which is a good approximation up to MHz frequencies for micron sized beads with density of order $1g/cm^3$ in aqueous suspension). We are then able to rearrange by substituting $6\pi a\tilde{\eta}(s)$ in place of $\tilde{\zeta}(s)$.

$$\tilde{A}(s) = \left(s + \frac{\kappa_i}{ms + 6\pi a\tilde{\eta}(s)}\right)^{-1} \tag{B.0.15}$$

Inverting the formula and subtracting s we get.

$$\frac{1}{\tilde{A}(s)} - s = \frac{\kappa_i}{ms + 6\pi a\tilde{\eta}(s)} \tag{B.0.16}$$

multiplying both sides by $\tilde{A}(s)$ we get

$$1 - s\tilde{A}(s) = \tilde{A}(s)\left(\frac{\kappa_i}{ms + 6\pi a\tilde{\eta}(s)}\right) \tag{B.0.17}$$

we then rearranging the formula to have $\tilde{A}(s)$ on the same side.

$$\frac{1 - s\tilde{A}(s)}{\tilde{A}(s)} = \frac{\kappa_i}{ms + 6\pi a\tilde{\eta}(s)} \tag{B.0.18}$$

7th March 2011

Inverting the formula one more

$$\frac{\tilde{A}(s)}{1 - s\tilde{A}(s)} = \frac{ms + 6\pi a\tilde{\eta}(s)}{\kappa_i} \tag{B.0.19}$$

Separating into two fractions.

$$\frac{\tilde{A}(s)}{1 - s\tilde{A}(s)} = \frac{ms}{\kappa_i} + \frac{6\pi a\tilde{\eta}(s)}{\kappa_i} \tag{B.0.20}$$

we rearrange for to get the viscosity term on the LHS.

$$\frac{6\pi a\tilde{\eta}(s)}{\kappa_i} = \frac{\tilde{A}(s)}{1 - s\tilde{A}(s)} - \frac{ms}{\kappa_i}$$

We then extract other terms onto the RHS.

$$\tilde{\eta}(s) = \frac{\kappa_i}{6\pi a} \left[\frac{\tilde{A}(s)}{1 - s\tilde{A}(s)} - \frac{ms}{\kappa_i} \right] \tag{B.0.21}$$

We know again from Mason and Weitz [146] $G^*(\omega) \equiv s\eta(s)\mid_{s=i\omega}$

Multiplying both sides by s we get

$$s\tilde{\eta}(s) = \frac{\kappa_i}{6\pi a} \left[\frac{s\tilde{A}(s)}{1 - s\tilde{A}(s)} - \frac{ms^2}{\kappa_i} \right] \tag{B.0.22}$$

Substituting in $G^*(\omega)$ we at last arrive at an expression for G^* .

$$G^*(\omega) = \frac{\kappa_i}{6\pi a} \left[\frac{i\omega\tilde{A}(\omega)}{1 - i\omega\tilde{A}(\omega)} - \frac{m\omega^2}{\kappa_i} \right] \tag{B.0.23}$$

where $m\omega^2$ is the inertial term and can be neglected at frequencies $< MHz$ for micron sized beads with density of order$1g/cm^3$

Step II, Derivation of the equation for a bead flipping between two optical traps a distance D_0 apart.

We can define the time dependent position the particle just after a flip in terms of the trap separation D_0. In a exactly the same way as in step I, we can then arrive at and expression for $G^*(\omega)$ however this time using D rather than r.

7th March 2011

$$ms^2\tilde{D} - msD_0 - mv_0 = \hat{f}_R - \zeta(s)(s\tilde{D} - D_0) - \kappa_i\tilde{D} \qquad \text{(B.0.24)}$$

Letting $D(t) = r(t)/D_0$ and similarly,$< D_0\hat{f}_R >=0$ and $m < D_0v_0 >=0$,

this lead in a similar way to Step 1 to:

$$\tilde{\eta(s)} = \frac{\kappa_i}{6\pi a}\left[\frac{\tilde{D}(s)}{1 - s\tilde{D}(s)} - \frac{ms}{\kappa_i}\right] \qquad \text{(B.0.25)}$$

However since the trap position is effectively a square wave. We must average over both up and down strokes.

Thus:

$$G^*(\omega) = \frac{\sum_{i=1,2}\left(\frac{\kappa_i}{6\pi a}\left[\frac{i\omega\tilde{A}(\omega)}{1-i\omega\tilde{A}(\omega)} - \frac{m\omega^2}{\kappa_i}\right]\right)}{2} \qquad \text{(B.0.26)}$$

$$G^*(\omega) = \frac{\kappa_i}{12\pi a}\sum_{i=1,2}\left[\frac{i\omega\tilde{A}(\omega)}{1 - i\omega\tilde{A}(\omega)} - \frac{m\omega^2}{\kappa_i}\right] \qquad \text{(B.0.27)}$$

Appendix C

Bode Sensitivity Theorem

It is worth recapitulating Bode sensitivity theorem [152]. Let $L(s)$ be the loop-gain such that $sL(s) \to 0$ as $s \to 0$. If the sensitivity $S = (1 + L(s))^{-1}$ is stable, then:

$$\int_0^\infty | \ln(S(j\omega) | \, d\omega = \pi \sum_i p_i \qquad \text{(C.0.1)}$$

where p_i are the right-half plane poles of $L(s)$, $Re\, p_i > 0$. If $L(s)$ has no right-half plane poles then the right hand side is zero. The consequence of the Bode sensitivity theorem is that the natural log of the sensitivity must be conserved; that is, good disturbance rejection in one frequency range is causes increased disturbance in another.

Appendix D

List of Commercial LCSLM Manufactures

Boulder Nonlinear Systems

450 Courtney Way, #107 Lafayette,

CO 80026, USA

Phone: 303.604.0077

Toll Free: 866.466.0506

Fax: 303.604.0066

Web:http://www.bnonlinear.com/

Hamamatsu Photonics UK Limited

2 Howard Court, 10 Tewin Road Welwyn Garden City,

Hertfordshire, AL7 1BW,

United Kingdom

Phone: 44-(0)1707-294888

Fax: 44-(0)1707-325777

Web:http://jp.hamamatsu.com

Holoeye Photonics AG

Albert-Einstein-Str. 14 12489

Berlin-Adlershof, Germany

Phone: +49 (0)30 63 92 36 60

Fax: +49 (0)30 63 92 36 62

Web:http://www.holoeye.com

Meadowlark Optics

Inc. P.O. Box 1000 Frederick,

CO 80530, USA

Phone: 303-833-4333

Fax: 303-833-4335

Cambridge Correlators

Cedars Business Incubation Centre,

Wakefield, West Yorkshire,UK

Email: nicknew@cambridgecorrelators.com

Phone: +44 (0)7764 754786

Web:http://www.cambridgecorrelators.com

Displaytech

2602 Clover Basin Drive,

Longmont, CO 80503

USA

Fax: (303) 772-2193

Web:http://www.displaytech.com

Appendix E

Glossary

Words/Terms	Meaning
Allan variance	Also known as two-sample variance is a measure of frequency stability in clocks, oscillators and amplifier.
amorphous	(of a solid) Noncrystalline; Having neither definite form nor apparent structure.
angular momentum	The momentum imparted by a light beam around the direction of beam propagation.
AODs	Acousto-Optic Deflectors
AOM	Acousto-Optic Modulator
API	(Application Programming Interface) prewritten software for a given programming task.
azimuth	The horizontal angle or direction of a compass bearing.
birefringent	Having two different refractive indices.
Blue Tweezers	A software package created at Glasgow University for the generation of holograms.
Brownian Motion	The erratic random movement of microscopic particles in fluid as a result of molecular collisions.
Brownian Walk	The path a particle takes while under the influence of Brownian motion.

Words/Terms	Meaning
CMOS	Complementary metal dioxide semiconductor is a technology for constructing integrated circuits.
coaxial	Having a common axis.
Colloid science	The study of the suspension of small particles in liquids.
CUDA	A programming language developed by video for the purpose of programming graphics cards.
dichroic	(of a crystal) Showing different colours when viewed from different directions, or (more generally) Having different absorption coefficients for light of different frequencies.
dielectric	Having the property of transmitting electric force without conduction; Insulating.
dipole	A molecule in which a concentration of positive electric charge is separated from a quantity of negative electric charge.
Faxen's correction	A mathematical correction to the calculation of fluid viscosity next to a boundary.
ferroelectric	A substance exhibiting permanent electric polarisation that varies in strength with the applied electric field.
Fire wire camera	Camera using a firewire cable for fast data transmission.
fractional orbital angular momentum (FOAM)	Type of angular momentum where the value of the winding number is non integer.
Fuselli	Twisty pasta.
Gaussian	Having the form of a Gaussian function.
Gaussian process	Any stochastic process resulting in a Gaussian probability density function.

Words/Terms	Meaning
Gerchberg Saxton algorithm	An error reduction algorithm useful for retrieval of phase information from intensity information in two planes.
Ghost Orders	Unwanted spots of light caused by aliasing in diffractive optics.
Gigabit Ethernet	Term describing various technologies for transmitting ethernet frames at a rate of a gigabit per second.
Gouy Phase	A phase change in a focused beam caused by an uncertainty in the transverse momentum.
Hermite-Gaussian	Laser mode formulated a by Hermite polynomials.
Kinoform	An image representing phase information.
LabVIEW	A visual programming language used extensively at Glasgow optics group.
Laguerre Gaussian	Laser mode formulated a by Laguerre polynomials.
lattice	A regular repeated three-dimensional arrangement of atoms, ions, or molecules in a metal or other crystalline solid.
LUT	Look up table used for looking up one value given another.
micro-machine	A machine or mechanism operating at the microscale.
micro-scale	In the size range 1-1000 micrometers.
microrheology	The study of rheology on the micron scale.
MSD	(Mean Squared Displacement) usually used with respect to a particles postion with respect to an optical trap over time.
nematic	Relating or denoting a state of a liquid crystal in which the molecules are originated in parallel but not arranged in well-defined planes.

Words/Terms	*Meaning*
orthogonal	Of or involving right angles; At right angles / Statistically independent; Having variants that can be treated as statistically independent.
parabolic	Of or like a parabola or part of one.
paraxial	Situated alongside, or on each side of, an axis. In the case of light referring to rays traveling parallel to each other.
piezoelectricity	Electric polarisation in a substance (esp. certain crystals) resulting from the application of mechanical compression/stretching.
Polyacrimide (PAM)	A polymer (-CH2CHCONH2-) formed from acrylamide subunits with viscoelastic properties.
polymerize	Combine or cause to combine to form a polymer.
polymorph	An inorganic object or material that takes various forms.
raster	A rectangular pattern of parallel scanning lines followed by the electron beam on a television screen or computer monitor.
ROI	Region of Interst (ROI) extracted area of an image displayed on a computer.
smectic	Denoting or involving a state of liquid crystal in which the molecules are oriented in parallel and arranged in well-defined planes.
SNR	(Signal to Noise Ratio) measure of signal quality with respect to the noise in the system.
spherulite	A small spheroidal mass of crystals (esp. of a mineral) grouped radially around a point.

Words/Terms	*Meaning*
stochastic	Randomly determined; Having a random probability distribution or pattern that may be analyzed statistically but may not be predicted precisely.
uni-axial	(of crystals) Having one optic axis, as in the hexagonal, original, and tetragonal systems.
vaterite	A birefringent polymorph of calcium carbonate with spherical structure.
viscoelasticity	The property of a substance (usually a fluid) exhibiting both elastic and viscous behavior.
vortex	A mass of whirling fluid or air, used in this case for light. At a vortex all light is canceled out by a superposition of waves.
white-noise	Noise containing many frequencies with equal intensities